CZECH TECHNICAL UNIVERSITY IN PRAGUE

Faculty of Civil Engineering
Department of Material Engineering and Chemistry

Thermal Resistance of Calcium Aluminate Cement Based Composites

DOCTORAL THESIS

Ing. Dana Koňáková

Doctoral study program: Civil Engineering
Branch of study: Physical and Material Engineering

Doctoral thesis tutor: doc. Ing. Eva Vejmelková, Ph.D.

Prague, 2018

CZECH TECHNICAL UNIVERSITY IN PRAGUE

Faculty of Civil Engineering
Department of Material Engineering and Chemistry

DECLARATION and ACKNOLEDGEMNT

Ph.D. student's name: Ing. Dana Koňáková

Title of the doctoral thesis: Thermal Resistance of Calcium Aluminate Cement Based Composites

I hereby declare that this doctoral thesis is my own work and effort written under the guidance of the tutor doc. Ing. Eva Vejmelková, Ph.D.

All sources and other materials used have been quoted in the list of references.

The doctoral thesis was written in connection with research on the project: GAP104/12/0791 – Vláknové kompozity na bázi cementu pro vysokoteplotní aplikace.

I would like to express my sincere gratitude to my tutor doc. Ing. Eva Vejmelková, Ph.D. for the continuous support of my study, for her help, kindliness and motivation. My sincere thanks also goes to my husband, my sons, and my whole family and friends for all the patience and comprehension during my studies.

In Prague on .....

.....
signature

Abstrakt:

Stavební konstrukce mohou být během své životnosti vystaveny extrémním podmínkám. Jednou z těchto extrémních situací je požár, respektive zatížení vysokou teplotou, kdy je velká pravděpodobnost, že dojde k poškození jednotlivých stavebních materiálů. Toto poškození může v konečném důsledku vést až k porušení a kolapsu celé konstrukce. Běžně používané betony na bázi Portlandského cementu jsou málo odolné tepelnému namáhání. Při optimálním navrženém složení jsou vhodné pro aplikace do teplot kolem 400°C, při zvýšených teplotách dochází k rozkladu portlanditu a úplné dehydrataci CSH gelů. Cílem této práce je navrhnout cementový kompozit s lepší tepelnou odolností, vhodný pro použití na konstrukce s vyšším rizikem vzniku požáru (např. ostění tunelu, tepelně-izolační obkladové desky,…). První část této práce je věnována navržení cementového kompozitu, výběru vhodných surovin, jejich charakterizaci a optimalizaci složení výsledné směsi. Suroviny byly vybírány s ohledem na jejich tepelnou odolnost. Z těchto důvodů byl použit hlinitanový cement, čedičové kamenivo a čedičová vlákna, která byla použita i v kombinaci různých délek. Druhá část této práce je zaměřena na stanovení tepelné odolnosti navrženého kompozitu. Ta byla charakterizována pomocí experimentálního měření residuálních fyzikálních vlastností kompozitních směsí, tak aby bylo možné popsat i vliv jednotlivých vstupních surovin. Jednotlivé charakteristiky byly stanoveny na směsích vystavených různému teplotnímu zatížení (konkrétně teplotám 105 °C, 400 °C a 1000 °C). Ve třetí části je následně stanoven optimální poměr délky čedičových vláken, a to pomocí stejného principu stanovení residuálních vlastností. Pomocí dosažených vlastností byla prokázána zvýšená teplotní odolnost navrženého kompozitu složeného z hlinitanového cementu, čedičového kameniva a čedičových vláken s ideálním poměrem dlouhých ke krátkým vláknům v poměru 90:10.

Klíčová slova: *Hlinitanový cement, čedičové kamenivo, čedičová vlákna, residuální vlastnosti*

Abstract:

Building structures can be exposed to extreme conditions during their lifetime. One of these extreme situations is fire, or more precisely, exposure to extreme temperatures. In this case, there is a high likelihood of damage occurring to building materials, which could lead to the final collapse of a whole structure. Ordinary concrete, based on Portland cement, does not resist high temperatures very well; it is suitable for temperatures up to 400 °C. However, when exposed to higher temperatures decomposition of portlandite and dehydration of CSH gel will show. The aim of this thesis is to develop of such cement-based composites with better thermal resistance in regard to the application to structures with higher fire hazard i.e. boards for a tunnel lining or as face panel for improving thermal resistance. The first step was research into an optimization of material composition, which takes into account a choice of raw materials, their characterizations and setting of their amounts. For better thermal stability calcium, aluminate cement was chosen as a binder. The remaining components were basalt aggregate and basalt fibres; furthermore, the combination of different lengths of basalt fibres was investigated also. The second step was an assessment of a thermal resistance of these designed composites. This was performed by virtue of experimental measurement of physical properties. The particular characteristics of concrete were determined after being exposed to three different temperatures; specimens were pre-treated by three thermal loadings (105 °C, 400 °C, and 1000 °C). In the third part, the issue of optimal length fibres combination was investigated with the employment of similar approach of determining the residual properties. From the achieved results were concluded, that designed fibre reinforced, calcium alumina cement based composites with basalt aggregate proved its applicability in civil structures, and the optimal basalt fibres combination of longer: shorter fibres was found in the ratio of 90:10.

Keywords: *Calcium aluminate cement, basalts aggregates, basalt fibres, residual properties*

Content

1 Introduction

Concrete, in regards to its surroundings, is a highly resistant material widely used in the building industry. There is a high probability of damage likely to occur when commonly used building materials are exposed to extreme conditions. A typical example of the extreme situations is fire and the exposure to high temperatures. Due to the effects of heating, mechanical properties, as well as physical parameters and durability of material, are significantly deteriorated, which can lead to the collapse of a whole building structure. As time has gone many kinds of materials and improvements have been developed, these materials need to meet demanding requirements on better thermal resistance. Cement composites fibre-reinforced by asbestos were the most successful (if not the only) solution in the history of technology of concretes sufficiently resistant to high temperatures. The use of the asbestos-cements composites dates back to the end of 19th century. Due to the excellent properties of asbestos, such as for example good acid and resistivity, electrical non-conductivity, high strength and flexibility, great thermal resistance and non-combustibility, asbestos-cement, led to its very widespread use in the second half of 20th century. From the most common applications, it can be named for example production of roof covering, facing panels, thermal and acoustic insulating boards, or spray coatings. However, later it was proved harmful to health and in 1984 asbestos was put on the list of proved carcinogenic agents; which lead to being prohibited in 1997 (in the Czech Republic). Even though there has been considerable effort and investment to finding substitute to asbestos, very few substitutes have been found. The main purpose of this thesis is to contribute to the development of cement-based fibre-reinforced composites for high-temperature applications. These composites should have the same beneficial properties as asbestos composites, although with no risk to human health.

Preparation of cement composite materials resistant to high temperatures is a complex, and in-depth, process with two main aspects; firstly, the temperature resistance of utilized components, which involves the matrix, aggregates and fibres, secondly their compatibility both in ordinary and especially in high temperature conditions. Specific components of studied composites were chosen in conformity with thermal resistance of raw materials. Regarding the matrix, hydrated Portland cement (PC) does not resist high temperatures very well; therefore, it is beneficial to use calcium aluminate cement (CAC) rich in alumina oxide (Al_2O_3). Despite losing its long-term strength, depending on its amount of alumina oxide (Al_2O_3), calcium aluminate

cement is suitable for production of concrete elements and composites exposed to temperatures even above 1000 °C. A second main component of concrete is aggregate. Silica aggregate is commonly used for ordinary concrete. Nevertheless, it is not appropriate for high temperature application due to crystal transformation of the quartz at 573 °C, which is consequently accompanied by big volumetric changes. On the other hand, basalt aggregate, as one of the most thermal resistant natural aggregates, seems to be an acceptable alternative for the preparation of thermal resistant concrete. Due to its origin from volcanic rocks basalt aggregate is stable up to about 900 °C. Another enhancement of composites can be realized by reinforcing its matrix with fibres. Nowadays there are many kinds of materials applicable for fibres preparation, the most common are steel, glass, polymer, or organic fibres. For need of this doctoral thesis, basalt fibres were chosen from wide scope of fibre-reinforcement kinds. This choice was performed also with respect to compatibility of all raw-materials. Basalt fibres are, in comparison with asbestos fibres, environmentally friendly and non-hazardous. They have many functional properties, such as biological and chemical stability, thermal resistance, high strength and durability, which make them advantageous for the general purpose of concrete reinforcement.

In this doctoral thesis, the cement based composites composed of calcium aluminate cement, basalt aggregate and basalt fibres were studied. The first part of the work was focused on material design. Primarily the appropriate raw materials were chosen, then their detailed characterization was performed and finally the particular composition of cement based composite was optimized. The main emphasis of the second part of this thesis was focused on thermal resistance of designed material, which is determined by virtue of a variety of physical properties measured after three different thermal exposure conditions. Basic physical properties, mechanical characteristics, hydric transport parameters, and thermal characteristics belong among the studied properties. Before experimental measurements the specimens were exposed to two different temperature loadings (400 °C and 1000 °C). Reference measurements with no temperature pre-treatment were also carried out. In the experimental program, the aim was not only to describe thermal resistance of designed fibre-reinforced cement-based composite but also to determine the influence of particular raw materials on thermal resistivity of concrete. Furthermore, the effect of combination of basalt fibres length was also investigated.

2 Conception of high temperatures

2.1 Thermal transport

Thermal transport is the fundamental phenomena dealing with behaviour of materials affected by temperature loading. When speaking about materials for application in structures with higher fire hazard, or thus with higher temperature loading, it is obligatory to understand to this issue. Also in the case of ordinary building materials this theme should be well-known, because of still increasing demands of thermal energy management. Thermal transport can be divided into three categories according of the system of transportation: conduction, convection and radiation. For the building materials which are generally solid, the conduction is the most dominant transport system in common temperatures. Conduction in combination with convection generally acts jointly in the case of fluids. Therefore, in the case of building materials, convection could act inside pores, and its impact would be growing with increasing dimensions of pores. While radiation is transportation system when talking about gases. Therefore, radiation should act in the case of highly porous materials on opposite sides of pores walls and in the case of the other solid materials at high temperatures.

2.1.1 Elementary thermodynamic model

Elementary thermodynamic equation was proposed in 1811 by Fourier. It was formulated on the ground of experimental results and proposed the basis for the analysis of heat conduction [1]. It is called Fourier's law and can be noted as:

$$\overrightarrow{J_q} = -\lambda(T).\,\mathrm{grad}T \tag{1}$$

j_q …	heat flow	[W m^{-2}]
$\lambda(T)$ …	thermal conductivity	[W m^{-1} K^{-1}]
T…	temperature	[K]

However, Fourier's law describes dependency of heat flow on position; however, in its basic form do not takes into the account the dependency on time. Such equation could be thus employed just in the case of stationary thermal transport. When speaking about nonstationary thermal transport, the necessary equation is derived from balance equation of internal energy:

$$\frac{\partial(\rho U)}{\partial t} = -\mathrm{div}\overrightarrow{J_q} \quad \Rightarrow \quad \rho\frac{\partial U}{\partial t} = -\mathrm{div}\overrightarrow{J_q} - U\frac{\partial \rho}{\partial t} \tag{2}$$

U …	internal energy	[kg m^{-2}]
t …	time	[s]
ρ…	bulk density	[kg m^{-3}]

Because building materials are in general porous, and inside the pores some other medium (generally water) can be transported, also the mass balance will be of need:

$$\frac{\partial(\rho_c)}{\partial t} = \frac{\partial(\rho c)}{\partial t} = -\mathrm{div}\overrightarrow{J_c} \quad \Rightarrow \quad \rho\frac{\partial c}{\partial t} = -\mathrm{div}\overrightarrow{J_c} - c\frac{\partial \rho}{\partial t} \tag{3}$$

ρ_c …	bulk density of transported medium	[kg m^{-3}]
c …	concentration of transported medium	[-]
j_c…	mass flux	[kg m^{-2} s^{-1}]

For future deriving (based on the information from [2, 3, 4]), the first thermodynamics law will be needed as well. It is defined as follows, and it can be rewritten in the form of Gibbs equation:

$$\mathrm{d}U = \delta Q + \delta P = T\,\mathrm{d}S - p\,\mathrm{d}V + \mu\,\mathrm{d}c = T\,\mathrm{d}S + \frac{p}{\rho^2}\mathrm{d}\rho + \mu\mathrm{d}c \tag{4}$$

$$\frac{\partial U}{\partial t} = T\frac{\partial S}{\partial t} + \frac{p}{\rho^2}\frac{\partial \rho}{\partial t} + \mu\frac{\partial c}{\partial t} \tag{5}$$

Q …	heat	[J]
P …	work	[J]
S…	entropy	[J kg^{-1}]
p …	pressure	[Pa]
V …	volume	[m^3]
μ…	chemical potential	[J kg^{-1}]

Entropy production, which has to be determined, can be formulated as:

$$\frac{\partial \mathrm{S}}{\partial t} = \frac{\partial}{\partial t}\int_V \rho s\,\mathrm{d}V \tag{6}$$

$$\frac{\partial(\rho s)}{\partial t} = \rho\,\frac{\partial s}{\partial t} + s\frac{\partial \rho}{\partial t} \tag{7}$$

Now by substituting of balances equations (2, 3) and the first thermodynamics law (4) into the equation of entropy (7) it is possible to get:

$$\frac{\partial(\rho s)}{\partial t} = \frac{\rho}{T}\left(\frac{\partial U}{\partial t} - \frac{p}{\rho^2}\frac{\partial \rho}{\partial t} - \mu\frac{\partial c}{\partial t}\right) + s\frac{\partial \rho}{\partial t} = -\frac{1}{T}\mathrm{div}\overrightarrow{J_q} - \frac{U}{T}\frac{\partial \rho}{\partial t} - \frac{p}{\rho T}\frac{\partial \rho}{\partial t} + \frac{\mu}{T}\mathrm{div}\overrightarrow{J_c} + \frac{\mu c}{T}\frac{\partial \rho}{\partial t} + s\frac{\partial \rho}{\partial t} =$$

$$= -\frac{1}{T}\mathrm{div}\overrightarrow{J_q} + \frac{\mu}{T}\mathrm{div}\overrightarrow{J_c} - \frac{1}{T}\left(U + \frac{p}{\rho} - \mu c - sT\right)\frac{\partial \rho}{\partial t} \tag{8}$$

Taking to the account the equation the first thermodynamics law (4), the bracket term is equal to zero and therefore:

$$\frac{\partial(\rho s)}{\partial t} = -\frac{1}{T}\mathrm{div}\overrightarrow{J_q} + \frac{\mu}{T}\mathrm{div}\overrightarrow{J_c} = -\frac{1}{T}\,\mathrm{div}\left(\overrightarrow{J_q} - \mu\overrightarrow{J_c}\right) + \left(\overrightarrow{J_q} - \mu\overrightarrow{J_c}\right)\mathrm{grad}\left(\frac{1}{T}\right) - \frac{1}{T}\overrightarrow{J_c}\mathrm{grad}\mu \tag{9}$$

Which when substituted back to the entropy leads to the form:

$$\frac{\partial S}{\partial t} = -\int_V \mathrm{div}\,\frac{1}{T}\left(\overrightarrow{J_q} - \mu\overrightarrow{J_c}\right)\mathrm{d}V + \int_V \left(\overrightarrow{J_q} - \mu\overrightarrow{J_c}\right)\mathrm{grad}\left(\frac{1}{T}\right)\mathrm{d}V - \int_V \frac{1}{T}\overrightarrow{J_c}\mathrm{grad}\mu\,\mathrm{d}V =$$

$$= -\int_S \vec{n}\cdot\frac{1}{T}\left(\overrightarrow{J_q} - \mu\overrightarrow{J_c}\right)\mathrm{d}S + \int_V \frac{1}{T^2}\left(\overrightarrow{J_q} - \mu\overrightarrow{J_c}\right)\mathrm{grad}T\,\mathrm{d}V - \int_V \frac{1}{T}\overrightarrow{J_c}\mathrm{grad}\mu\,\mathrm{d}V \tag{10}$$

Taking into account the closed system, the first term should be zero and the equation can be simplified as:

$$\frac{\partial S}{\partial t} = \int_V \frac{1}{T^2}\left(\overrightarrow{J_q} - \mu\overrightarrow{J_c}\right)\mathrm{grad}T\,\mathrm{d}V - \int_V \frac{1}{T}\overrightarrow{J_c}\mathrm{grad}\mu\,\mathrm{d}V \tag{11}$$

Production entropy can be also formulated in the form of particular flux caused by thermodynamic forces or in combination with kinetic coefficient:

$$\frac{\partial S}{\partial t} = \overrightarrow{J_\iota}\,\overrightarrow{X_\iota} = L_{ik}\overrightarrow{X_\iota}\overrightarrow{X_k} \tag{12}$$

So for their identification, let's assume following:

$$\overrightarrow{J_1} = \overrightarrow{J_c} \tag{13}$$

$$\overrightarrow{J_2} = \overrightarrow{J_q} - \mu\overrightarrow{J_c} \tag{14}$$

$$\overrightarrow{X_1} = -\frac{1}{T}\mathrm{grad}\mu \tag{15}$$

$$\overrightarrow{X_2} = \frac{1}{T^2}\mathrm{grad}T \tag{16}$$

$$L_{11} = \alpha T \tag{17}$$

$$L_{12} = L_{21} = \beta T^2 \tag{18}$$

$$L_{22} = \gamma T^2 \tag{19}$$

Particular flux can then be written in the form of:

$$\overrightarrow{J_c} = -\alpha \mathrm{grad}\mu - \beta \mathrm{grad}T \tag{20}$$

$$\overrightarrow{J_q} - \mu\overrightarrow{J_c} = -\beta T \mathrm{grad}\mu - \gamma \mathrm{grad}T \tag{21}$$

Chemical potential depends on concentration, pressure and temperature, it gradient can be rewritten as:

$$\mathrm{grad}\mu = \left(\frac{\partial \mu}{\partial c}\right)_{p,T} \mathrm{grad}c + \left(\frac{\partial \mu}{\partial p}\right)_{c,T} \mathrm{grad}p + \left(\frac{\partial \mu}{\partial T}\right)_{p,c} \mathrm{grad}T \tag{22}$$

Therefore, the equations (20) and (21) look like:

$$\overrightarrow{J_c} = -\alpha \left(\frac{\partial \mu}{\partial c}\right)_{p,T} \mathrm{grad}c - \alpha \left(\frac{\partial \mu}{\partial p}\right)_{c,T} \mathrm{grad}p - \left[\alpha \left(\frac{\partial \mu}{\partial T}\right)_{p,c} + \beta\right] \mathrm{grad}T \tag{23}$$

$$\overrightarrow{J_q} - \mu\overrightarrow{J_c} = -\beta T \left(\frac{\partial \mu}{\partial c}\right)_{p,T} \mathrm{grad}c - \beta T \left(\frac{\partial \mu}{\partial p}\right)_{c,T} \mathrm{grad}p - \left[\beta T \left(\frac{\partial \mu}{\partial T}\right)_{p,c} + \gamma\right] \mathrm{grad}T \tag{24}$$

For now, the following definitions are needed:

$$D = \frac{\alpha}{\rho}\left(\frac{\partial \mu}{\partial c}\right)_{p,T} \tag{25}$$

$$\varphi = \frac{\alpha}{\rho}\left(\frac{\partial \mu}{\partial p}\right)_{c,T} = \frac{D\Theta}{p} \tag{26}$$

$$\delta_s = \frac{1}{\rho}\left[\alpha \left(\frac{\partial \mu}{\partial T}\right)_{p,c} + \beta\right] = \frac{D\Theta}{T} \tag{27}$$

$$k_c = \beta T \left(\frac{\partial \mu}{\partial c}\right)_{p,T} \tag{28}$$

$$k_p = \beta T \left(\frac{\partial \mu}{\partial p}\right)_{c,T} \tag{29}$$

$$\lambda^* = \beta T \left(\frac{\partial \mu}{\partial T}\right)_{p,c} + \gamma \tag{30}$$

D…	diffusion coefficient	[$m^2\ s^{-1}$]
φ…	barodiffusion coefficient	[$m^3\ s\ kg^{-1}$]
δ_s…	thermodiffusion coefficient (Soret coef.)	[$m^2\ s^{-1}\ K^{-1}$]
k_c…	diffusion-thermo coefficient (Dufour coef.)	[$kg\ m^{-1}\ s^{-1}$]
k_p…	diffusion-baro coefficient	[s]
λ^*…	generalized thermal conductivity	[$kg\ K^{-1}\ m^{-1}\ s^{-1}$]

Therefore, the equation for mass flux can be simplified:

$$\overrightarrow{J_c} = -\rho(D\mathrm{grad}c + \varphi\mathrm{grad}p + \delta_s\mathrm{grad}T) \tag{31}$$

$$\overrightarrow{J_q} - \mu\overrightarrow{J_c} = -k_c\mathrm{grad}c - k_p\mathrm{grad}p - \lambda^*\mathrm{grad}T \tag{32}$$

For interpretation of heat flux in comparison with Fourier's law, let's go back to the equations (19) and (20), which together by excluding the term of gradient of chemical potential can be written as:

$$\overrightarrow{J_q} - \left(\frac{\beta T}{\alpha} + \mu\right)\overrightarrow{J_c} = \left(\frac{\beta^2 T}{\alpha} - \gamma\right)\mathrm{grad}T \tag{33}$$

Taking into account the Fourier's law, when the mass flux is zero, for the thermal conductivity it must be valid following:

$$\overrightarrow{J_q} = \left(\frac{\beta^2 T}{\alpha} - \gamma\right)\mathrm{grad}T \quad \Leftrightarrow \quad \overrightarrow{J_q} = -\lambda(T)\mathrm{grad}T \quad \Rightarrow \quad \lambda(T) = \left(\gamma - \frac{\beta^2 T}{\alpha}\right) \tag{34}$$

Right now, the particular fluxes are determined adequately. Therefore, let's go back to the balance equations. When formulation (6) is substituted into the equation (10), it can be modified as:

$$T\frac{\partial(\rho s)}{\partial t} + \mathrm{div}\left(\overrightarrow{J_q} - \mu\overrightarrow{J_c}\right) + \overrightarrow{J_c}\mathrm{grad}\mu = 0 \tag{35}$$

For most of the real application, the following simplifications can be performed:

$$\rho = konst \ \Rightarrow \ \frac{\partial\rho}{\partial t} = 0 \tag{36}$$

$$\overrightarrow{J_c}\mathrm{grad}\mu \ll \mathrm{div}\left(\overrightarrow{J_q} - \mu\overrightarrow{J_c}\right) \ \Rightarrow \ \overrightarrow{J_c}\mathrm{grad}\mu \cong 0 \tag{37}$$

$$P = konst \ \Rightarrow \mathrm{grad}p = 0 \tag{38}$$

$$\mathrm{d}Q = mc_p\mathrm{d}T \;\Rightarrow T\mathrm{d}s = \mathrm{d}Q = c_p\mathrm{d}T \tag{39}$$

m…	mass	[kg]
c_p…	specific heat capacity at specific process	[J kg^{-1} K^{-1}]

Thus, the final balance equations of coupled heat and mass transfer, derived from (3) and (35), can be written in the forms:

$$\frac{\partial c}{\partial t} = \mathrm{div}(D\mathrm{grad}c + \delta\mathrm{grad}T) \tag{40}$$

$$c_p\rho\frac{\partial T}{\partial t} = \mathrm{div}(k_c\mathrm{grad}c + \lambda^*\mathrm{grad}T) \tag{41}$$

Further simplification can be done by consideration of simple heat transport, when mass transport is zero. Therefore, the balance equation can be formulated as:

$$c_p\rho\frac{\partial T}{\partial t} = \mathrm{div}(\lambda^*\mathrm{grad}T) \tag{41}$$

In the elementary thermodynamic model there is neglected several things. The most important is the phase changes of water (liquid water X water vapour). This issue has been studied e.g. by Philip and de Vries in 1957 [5], who derived their convection models of coupled heat and moisture transport from the Darcy's equation, Fick's law and Fourier's law. This was modified by de Vries in 1987 [6] by covering also heat flux caused by convection of gaseous phase and phase transition of water to water vapour. Another similar interpretation of coupled heat and moisture transport was proposed by Milly in 1982 [7], however his convectional models was based directly on Darcy's equation and he used Kelvin equation for definition of relation between relative humidity and pressure head. Krischer in 1963 [8] proposed the first diffusion models, which take into account the phase changes of water, but there is no mutual intersecting impact of moisture and heat transport. More sophisticated diffusion model was derived by Lykov [9], where the cross effects of heat and moisture transport were somehow included. On the basis of Kircher and Lykov models so-called German school was developed. Kiessl, [10] Häupl and Stopp [11] and Künzel [12] belong among the representatives of this school.

2.1.2 Thermal transport in high temperatures

When considering the high temperature transport, the previous elementary thermodynamic model cannot be simplified by the final assumptions of constant bulk density, pressure (equations (36) and (38)). Therefore, the final heat and moisture balance equations can be written in the following forms:

$$\frac{\partial \rho c}{\partial t} = \mathrm{div}[\rho(D\mathrm{grad}c + \varphi \mathrm{grad}p + \delta \mathrm{grad}T] \tag{42}$$

$$c_p \rho \frac{\partial T}{\partial t} + Ts\frac{\partial \rho}{\partial t} = \mathrm{div}\left(k_c \mathrm{grad}c + k_p \mathrm{grad}p + \lambda^* \mathrm{grad}T\right) \tag{35}$$

However, this model deals with heat conduction and diffusion only. The impact of radiation is neglected. The simplest way to include radiation is adding radiation flux in the equation of heat flux [13]:

$$\overrightarrow{J_{qt}} = \overrightarrow{J_q} + \overrightarrow{J_{qr}} \tag{36}$$

j_{qt} …	total heat flow	[W m^{-2}]
j_{qr} …	heat flow caused by radiation	[W m^{-2}]

Heat flow caused by radiation can be defined with employing of Stefan-Boltzman law for black body:

$$E_b = \int_0^\infty E(\lambda, T)\mathrm{d}\Lambda = \frac{C_1}{\lambda^5(\exp\frac{C_2}{\Lambda T}-1)} = \sigma_0 T^4 \tag{37}$$

E_b…	emissivity power	[W m^{-2}]
Λ…	wavelength	[m]
C_1…	first radiation constant	[W m^{-2}]
C_2…	second radiation constant	[m K]
σ_0…	Stefan-Boltzman constant	[W m^{-2} K^{-4}]

Taking into account the pores system of building materials, radiation can act on the opposite sides of pores surface. For simplification let's assume the pores are in the form of parallel walls. When the wall is irradiated, the fraction of electromagnetic waves is absorbed, reflected and transmitted. Transmitted fraction can be in the case of solid material neglected. Thus spectral emissivity defines ratio of emissive power of a specific material to that of blackbody at the same temperature. Therefore, the radiation

heat flow of one wall is equal to the sum of radiation heat flow caused by the wall emission and the reflected emission caused by the other wall [14].

$$\overrightarrow{J_{qr}} = \mathrm{F}_{12}(E_{\mathrm{b}1} - E_{\mathrm{b}2}) = \frac{\varepsilon_1 \varepsilon_2 \sigma_0 (\varepsilon_1 {T_1}^4 - \varepsilon_2 {T_2}^4)}{\varepsilon_2 + \varepsilon_{1-\varepsilon_1 \varepsilon_2}} \quad (38)$$

F_{12}…	apparent shape factor	[-]
ε…	spectral emissivity at particular temperature	[-]

Despite adding the member of radiation, this form of the thermal transport model is applicable only for those conditions, where no phase transition occurs, and so gradient of chemical potential can be neglected. Except for already mentioned chemical and physical changes of particular components of building materials, the other most limiting factors of these models are the phase changes of water and changes of pore system. Water phase changes within the scope of capillary's evaporation or condensation can be covered by applying the sorption isotherms. Nevertheless, the temperature range of applicability of the elementary thermodynamic model is, thanks to these limitations, approximately 5-90 ºC [2]. For description of thermal transport in high temperatures modified models are of need. Lykov in 1956 [9] presented such a model, which included phase change of water to vapour by applying liquid-vapour phase change coefficient. Even though this model seems to be adequate, this coefficient is not possible to determine experimentally. Another possibility proposed Černý and Venzmer [15] by replacing the liquid-vapour phase change coefficient by evaporation coefficient together with drying curves. Černý [16] further described a modification by application of discontinuity surface theory. Bažant and Thonguthai [17] derived more complicated model based on general thermodynamic relations. Federov and Pilon [18] studied this issue of thermal transport at high temperatures also, they studied on glass foams and they included also the part of radiation transfer. Another approach in the case of radiation employment was presented in study of Cheng and Fan [19]; they derived their model based on the following assumption: matrix isotropy, neglecting of volumetric changes due to the moisture gradient, local thermal equilibrium of particular phases, and equilibrium of moisture content on matrix surface.

2.2 Legislation dealing with fire safety

As well as the previous chapter describing the thermal transport, another related theme which should have been paid attention to, when focused on thermal resistant materials, is indisputably legislation of fire safety. The basic European standards dealing with fire safety of construction products is presented in the regulation No. 305/2011 [20], where are defined seven essential requirements for construction works, and the second one is the safety in the case of fire. However, the specific satisfaction of these requirements is up to the particular members of the European Union. This regulation replaced previously valid council directive 89/106/EEC [21]. Regarding the Czech Republic, there are quite big scope of valid laws, subordinate regulations (decrees, government regulations), Czech technical standards (dealing with projects, values, subjects, tests, classifications) and European design standards (Eurocodes), which are jointly known as a Fire Code. The basic document is ČSB 73 0810 Fire protection of buildings – general requirements [22], which provides the necessary connections between European standards and other standards of the Fire Code. The basic project standards are ČSN 73 0802 Fire protection of buildings - Non-industrial buildings [23] and ČSN 73 0804 Fire protection of buildings – Industrial buildings [24]. The main laws dealing with fire protection are The Building Act no. 225/2017 [25] and The Fire Protection Act no. 133/1985 [26] which are currently being amended by the Building Act. As it was mentioned, the content of Fire Code is huge and it is not the question of this work to enumerate and interpret it all particulars documents. However, there are three basic issues that will be gone through: Classification of construction products according to reaction to fire, fire resistance of building structure and fire scenarios.

Classification of construction products and building elements is defined in standard ČSN EN 13501-1+A1 [27]. There are seven basic classes (A1, A2, B, C, D, E, F) that correspond to the reaction to fire, which means how the particular material, due to its flammability, contributes to progress and intensity of fire. Class F is composed of materials and products, which cannot be classified in any other classes, and those, which have not been documented yet. Class E includes such products, which are able to resist to the small flame for a short time without significant progress of fire. Another class D is described as having acceptable contribution to the fire. These products must confirm the requirements of class E, but for longer periods. They also have to withstand a thermal attack of a single burning thing with significant delay and

reduction of heat releasing. Class C is described as limited contribution to fire; products have to fulfil the same requirements as for previous class D but with stricter demands. Furthermore, these products also have to show a limited subsequent spread of flame, when exposed to single burning item. Same but much more stringent requirements are placed on class B. These products are defined as having very limited contribution to fire. In the case of class A2, which contains materials which in the case of fully developed fire will not contribute caloric load and fire progress. The last class A1 composes of non-combustible materials, which are defined as such materials, which do not contribute to the fire in any of its phases. For each class there are defined standards for its examinations. They are summarized in Table 1 as well as some examples of class members. Additional classifications deal with smoke production and divides building products into three groups (S1-S3), and flaming droplets/particles, which has also three classes (D0-D2).

Table 1 Classes of reaction to fire (PCS = gross calorific potential, FS = flame spread, FIGRA = fire growth rate index, THR = total heat release, LFS = lateral flame spread)

Class	Standards	Requirements	Examples
A1	ČSN EN ISO 1182 [28]	Heat attack: 60 kW m^{-2} Temperature rise < 30 ºC Mass loss < 50% Flaming duration: 0 s	Natural stones Concrete Bricks Ceramics Glass Steel
	ČSN EN ISO 1716 [29]	PCS < 2 MJ kg^{-1}	
A2	ČSN EN ISO 1182 [28]	Heat attack: 60 kW m^{-2} Temperature rise < 50 ºC Mass loss < 50% Flaming duration: 20 s	Materials of A1 with minor content of organic materials
	ČSN EN ISO 1716 [29]	PCS < 3 MJ kg^{-1}	
B	ČSN EN ISO 11925-2 [30]	Flame height: 20 mm Time: 30 s FS < 150 mm within 60 s	Vinyl floors Cement-splinter boards Fire retardant woods products
	ČSN EN ISO 13823 [31]	Heat attack: 40 kW m^{-2} FIGRA < 120 W s^{-1} THR_{600} < edge of sample LFS < 7.5 MJ	

C	ČSN EN ISO 11925-2 [30]	Flame height: 20 mm Time: 30 s FS < 150 mm within 60 s	Phenolic foam Gypsum boards
	ČSN EN ISO 13823 [31]	Heat attack: 40 kW m^{-2} FIGRA < 250 W s^{-1} THR_{600} < edge of sample LFS < 15 MJ	
D	ČSN EN ISO 11925-2 [30]	Flame height: 20 mm Time: 30 s FS < 150 mm within 60 s	Construction wood Wood based products
	ČSN EN ISO 13823 [31]	Heat attack: 40 kW m^{-2} FIGRA < 750 W s^{-1}	
E	ČSN EN ISO 11925-2 [30]	Flame height: 20 mm Time: 15 s FS < 150 mm within 20 s	Plastic based insulation products
F	ČSN EN ISO 11925-2 [30]	Flame height: 20 mm Time: 15 s FS > 150 mm within 20 s	Non tested products ESP without fire-retardant

Another important thing when dealing with fire safety is fire resistance of building structures, which is defined in standard ČSN EN 13501-2. Fire resistance means the ability of building structures to withstand the effect of fully developed fire. There are several defined limit states, describing specific function of building structures. The first four are the most important states. Primarily, there is Loadbearing Capacity R, which says that all loadbearing structures have to fulfil its loadbearing function in the case of fire. The second state deals with Integrity E, and it is obligatory for all fire-splitting structures. Integrity of structure means that during the fire no cracks or holes, which allow passing through flames or hot gases appear. Insulating ability is the third most important limit state. Also this state deals with fire-splitting structures, and say that during the fire no temperature growth (higher than 140 °C) can occur on the side of wall which is not exposed to fire. The fourth state is called Radiation, and it restricts the thermal flux (maximal 15 kW m^{-2}) from the wall to place without fire exposure. Other limited states are Mechanical Action M, Self-closing C, Smoke Leakage S, Soot Fire Resistant G, Dire Protection Ability K etc. The limit states are followed by the time, of how long the structure is able to withstand. The time of fire resistance is set in minutes

and basic time classifications are 15, 30, 45, 60, 90, 120 and 180 minutes. The last specification which is valid in the Czech Republic is the definition of structure type; three valid groups are DP1 – Non-combustible construction, DP2 – Mixed construction, DP3 – Flammable construction. The structure type is set according to used building material, respectively according to their classes of reaction to fire. For specific building structures there are defined specific demands for particular state, time, and type which determine the degree of fire safety from I to VII.

In both previous paragraphs the term fully developed fire was mentioned several times. In a real situation, fire can be divided into three or four basic phases, defined by its temperature and time. The first stage ignition starts by the occurrence of fire as a consequence of chemical reaction of oxygen, fuel, and heat. The temperatures are usually quite low, also the fire is very small. The second smouldering phase is sometimes joint with the first stage and then its so-called incipient or growth phase. Temperatures during the incipient phase are increasing according to many factors such caloric loading near the beginning of fire, ceiling height, ventilation system, temperature of the structure, and its time is really variable. It can take from a few minutes up to several hours. Most of the released heat is usually consumed by flaming up of other fuels. This part generally finishes by flashover, and the phase of fully developed fire begins. The most of the flammable materials in the fire section are burning and the maximal temperature of fire is reached. The last phase of decay is usually the longest stage of fire. For better clarity the fire development is drawn in Figure 1. [32, 33]

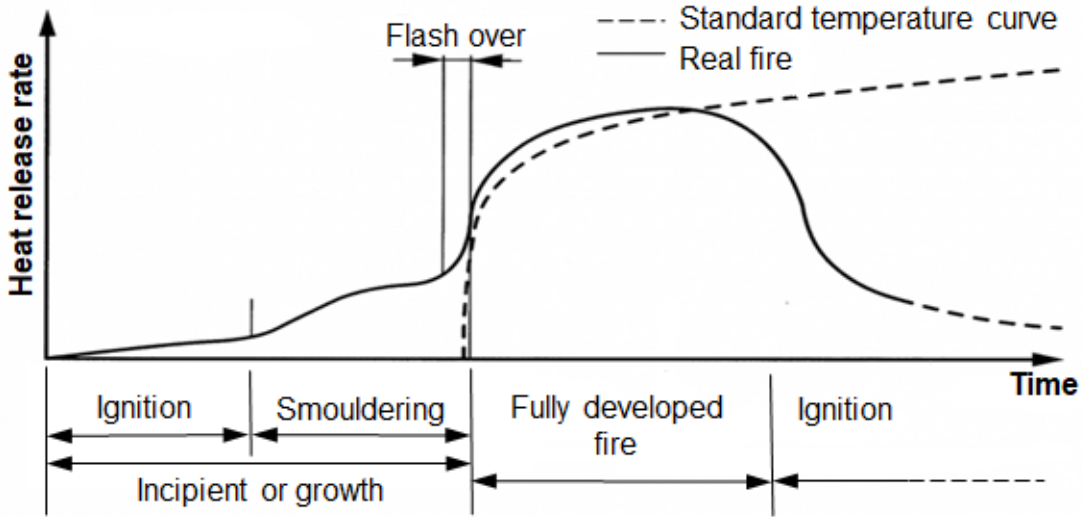

Figure 1 Typical development of fire

As it seems despite the similar course of fire all particular fires will work somewhat differently, act for different temperature and for varying time, etc. Therefore, for practical reasons, specifically e.g. assessment of fire safety of construction, it is favourable to define something like standard fire. This is included in the standard ČSN EN 1365-2. Standards temperature curve was developed based on statistics and its definition is as follows:

$$T = 345 \log(8t + 1) + 20 \tag{39}$$

T …	temperature in a furnace	[ºC]
t …	time from beginning of test	[min]

Except for standard curve also the fire scenario was developed, which are more relevant for particular situation. Some examples are shown in Figure 2 and fire resistance can be determined both for the standards curve or for parametric theoretical course of fire.

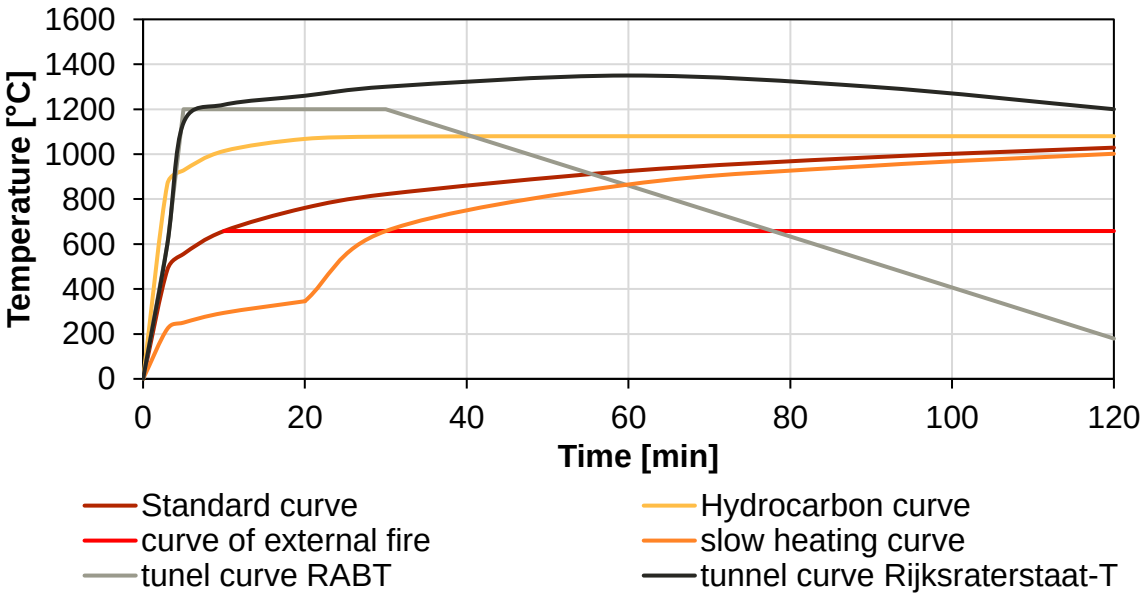

Figure 2 Fire scenarios

3 Materials for high temperature application

Refractory materials are defined as those, which are able to resist high temperatures, usually to 1500 °C [34], without any physical or chemical reaction. Moreover, these materials have to resist the contact of the meltage, the abrasion by other solids and chemical attacks. Other demands can be placed on their insulating properties and resistivity to the thermal shocks. For broader applications, another necessary requirement is the good availability of raw-materials. When focused on physical properties, the most important is good mechanical strengths at elevated temperatures, high melting point and low thermal strain. Temperature resistance is expressed as a temperature up to which materials fulfil hereinabove mentioned requirements. Specific methods for its examination are described in standards for particular kinds of refractories.

Generally, the materials, which are considered as temperature resistance, are non-metallic inorganic materials; however, they are a huge scope of different kinds of materials. The basic division is according to the production process to shaped products and unshaped monolithic refractories. Another sorting can be done according to raw-materials to acid, neutral, and basic refractories. The main components for production of thermal resistant materials can be summarized as follows: alumina, silica, calcium or magnesium oxides and their compounds, silicon carbide and various form of carbon. Dividing according to the porosity is also possible; based on these criteria; the dense and insulating materials can be recognized. The main production processes are as follows: sintering, fused casting, hand moulding and bonding.

The most of refractories (over 73%) are used in iron and steel industry, followed by cement and lime sector (over 13%) [35]. According to the specific application of thermal resistant materials, particular refractory with adequate temperature resistance are chosen. Some examples of industrial processes with their temperature ranges are presented in [35]. Therefore, it can be concluded that the most common refractories should have the temperature resistance in the range of 1300 °C – 1800 °C. However, the aim of this thesis was not such a high temperature. The main goal was to improve the temperature resistance of cement composites with temperature applicability up to 1000 °C. Despite this fact, the general review of thermal resistant materials should be done due to the better understanding of this issue.

Table 2 Temperature ranges of some industrial processes

Industrial process	**Temperature range [°C]**
Industrial drying	50 – 300
Petrochemical industries	100 – 1100
Hydroxide calcination	400 – 800
Glass annealing	400 – 800
Carbon combustion	400 – 900
Steam boiler	400 – 1000
Heat treatment and annealing of metals	500 – 1300
Aluminium and magnesium industry	800 – 1100
Carbonate calcining	800 – 1300
Sulphate decomposition	800 – 1400
Foundry industry and rolling mills	900 – 1400
Salt glazing of conventional ceramics	1000 – 1300
Fusion process	1000 – 2200
White ware industries	1100 – 1500
Glass making	1300 – 1500
Iron and steel making	1300 – 1800
Baking of carbon	1300 – 1800
Oxide sintering	1300 – 1800
Refractories	1300 – 1850
Portland cement	1350 – 1700
Carbides sintering	1500 – 1900
SiC industries	1800 – 2200
Refractory metals	1900 – 2200

3.1 Shaped products

Shaped products are products from plastic paste or semi-solid production mixture and usually they are created by melting. According to standard [36] they are divided into four groups to alumina-silicates products, alkaline products contains less than 7% of residual carbide, alkaline products contains from 7% to 50% of residual carbide and special products.

Alumina-silicates contain wide scope of materials. They can be further divided according to the amount of basic oxides into three categories. The aluminates contain

more than 90% of aluminium oxide (Al_2O_3), and as a representative Corundum, with temperature resistance about 1600 °C – 1750 °C [34, 37], can be mentioned. This material is extremely hard, therefore it is usually used as an abrasive material and its good thermal resistance is less employed. Alumina-silicates composed of 28 – 73% of silicate oxide (SiO_2) and 20 – 77% aluminium oxide (Al_2O_3). The most common product is fireclay with temperature applicability 1480 °C [34, 35]. This is the most common refractory, which is widely used in high temperature applications lining furnaces and firebricks. The last categories are silicates, based on silica oxide (SiO_2) in amount higher than 90%. The representatives are dinas with temperature resistance up to 1680 °C [34] or fused silica applicable up to 1000 °C [34]. These materials show worse resistance in lower temperatures (below 600 °C) due to the silica recrystallization, connected with volumetric expansion, and thus they are usually used for such application with permanent high temperatures.

Alkaline products are as it was mentioned divided into two categories according to the amount of residual carbon. These categories are based on magnesium oxide (MgO) or calcium oxide (CaO). The first subgroup is composed of magnesium carbonates based products with amount of magnesium oxide (MgO) over 80%. They are more temperature stable than alumina-silicate. No modification occurs in the case of magnesium. On the other hand, they are less resistant to the temperature shocks due to the quite high thermal expansion coefficient. Thermal stability of these materials ranges from 1600 °C to 1680 °C [34, 35] and they are mostly used in the field of iron metallurgy. Another two subgroups are magnesia-lime products and magnesia-dolomite, with temperature resistance up to 1650 °C [34, 35] and are usually employed as lining materials in converters.

Special products cover a big scope of varying materials, which are used in much reducing volume and only in some special cases. They can be divided into the oxidic, combined and non-oxidic. As a representative of oxidic materials, zircon ($ZrSiO_4$) or chrome oxides (CrO_3) based materials can be mentioned. Zirconia refractories have an excellent chemical resistance to the action of melts, alkalis, and most of the acids, temperature resistance is above 2000 °C [35] but they are quite expensive. Due to their excellent chemical resistance, they are usually used as glass tank furnaces. Chromite refractories can be applicable in the temperature ranges from 1500 °C to 1900 °C [35], according the amount of impurities and other components. The most common application is reheating furnaces in rolling mills. Another group of special

products are materials based on carbon, which can be used only in a non-oxidizing environment. In such condition, its temperature resistance is above 1700 °C [35]. They are employed in aluminium industry. Silicon carbide refractories should also be mentioned, as they show one of the highest temperature resistance. They can be stable up to 2200 °C [35] in the case of reducing atmosphere, while in the air they can serve up to 1400 °C [37]. Due to the high hardness, these products are primarily used as an abrasive. Other applications are metallurgical additives, electrical heating elements, etc.

3.2 Unshaped monolithic refractories

The basic definition of unshaped refractories is that they are not defined by its size or shape. Primarily this group covered materials such as mortars or adhesive binders, utilized for placing or fixing shaped refractories. However, later the necessity of more complicated shapes of refractories led to their widespread utilization. Currently unshaped refractories contain not only mortars and adhesive binders but also groups of plastic and castable refractories. Generally, these materials are not fired and they are composed of several gradings of aggregates homogeneously mixed in a specific ratio with some binder materials. Usually there is a need of some other mixing liquid (mostly water). Nowadays there are also many kinds of property-enhancing additives that are increasingly employed. The production process is, as it can be assumed, quite easy and less demanding, and larger products with various shapes can be made from monolithic refractories. Another advantage is the possibility of jointless performance; joints are usually the weak points of structure, simply undergoes to corrosion. Also the repairing process of thermal resistant structure from unshaped refractories is easier than in the case of shaped ones. Unshaped materials can usually be fixed without previous disposing, just with some minor treatment; while the shaped products have to be demounted completely.

Regarding the classification of monolithic refractories, in contrast to previous case of shaped one, where the most common dividing is based on the components nature, this division is inapplicable in the case of unshaped materials. The components nature is mostly alumina or aluminium silicates. The others are not used or their application is limited to certain special occasions. Therefore, the dividing of unshaped refractories is usually done according to application technique; for example, casting, ramming, gunning, pasting, spraying or vibration. However, because the main issue of this work

is not an application technique, but the material itself, in the following chapters will be described possibilities of raw-materials divided according to its function.

3.2.1 Binders

Binders have in the case of high temperature resistant materials several main interconnected functions. Primarily they serve as a connecting material (same as in the case of ordinary products) which retains the shape of the structure. Moreover, they are essential for the strength development at both ordinary and high temperatures. The basis of the binder performance is some kind of bond, which predicts the behaviour and applicability of final products.

The first used binder for production of thermal resistant materials was plastic clays. The ceramic bond is suitable for temperature over 1000 °C [34], when it gives rise due to the sintering process. Sintering is physical process, when due to the diffusion and viscosity of the material (at higher temperatures) materials start to agglomerate. Consequently, the porosity of the product sharply decreases, and whole process is campaigned by volumetric changes. Therefore, these kinds of materials show low strengths in ordinary temperatures, and also big shrinkage (due to the higher water requirement) during the heat treatment. They are usually used for production of refractory mortars, sealant, and paste.

Another possibility of kind of binder is an application of cement. Refractory concretes are based on a hydraulic bond, which is applicable up to about 600 °C. The most common Portland cement is less suitable, because its higher amount of calcium oxide; about 60 – 65% [35]. Hydraulic bond of PC collapsed up to 625 °C [35], and in the case of cycling loading even at 400 °C. However, in appropriate combination of raw-materials, e.g. fireclays or shales, it is possible to design thermal resistant concrete based on PC with applicability up to 1000 °C. Most suitable and in fact most common binder is calcium aluminate cement (CAC). According to other raw-materials, the CAC based composites can be applicable up to 1700 °C, when the hydraulic bond is at higher temperature replaced by ceramic bond. More detailed description of this material is provided in chapter 4.1.

Inorganic chemical bond is the newest possibility. The strengthening is based on some chemical reaction except for hydraulic one. The main issue of these materials is to find such system without calcium oxide, which is detrimental for refractoriness. Temperature range of its applicability depends on particular materials, but in general it

can be suitable up to 1400 °C [34]. The most common representatives are colloidal silica, hydratable alumina phosphate or liquid glass.

3.2.2 Aggregates

The problem with refractory concrete is not only binder degradation but also thermal resistance of aggregate as the most chemical and physical changes during the heating are negligible and have significant impact on possible applicability of aggregate. Some examples of processes in various aggregates are presented in Table 3. As it can be seen, one of the most determining properties for aggregate suitability is thermal expansion; which should be as low as possible, or better corresponding to the used binder. In Figure 3 and Figure 4 there are presented some values of thermal strain for natural aggregate and for the artificial respectively. For temperatures up to 700 °C, natural rocks are acceptable. However, they have to exhibit appropriate properties (stable mechanical characteristic and the lowest possible thermal expansion). Basalt, greenstone and andesite belong among viable natural rocks. For higher temperatures, up to 1000 °C, aggregates such as ground basalt, ceramics, and blast furnace slag have to be used. In the case of temperature over to 1000 °C, artificial aggregates are the only possible solutions.

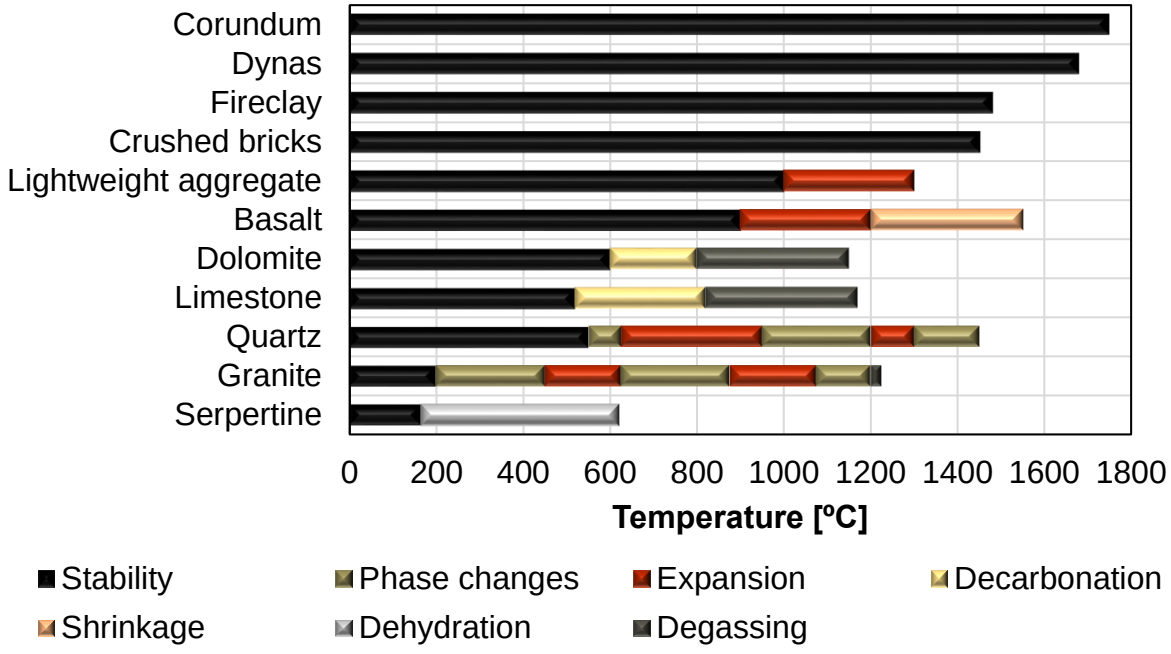

Table 3 Processes in various aggregates during heating [38, 39]

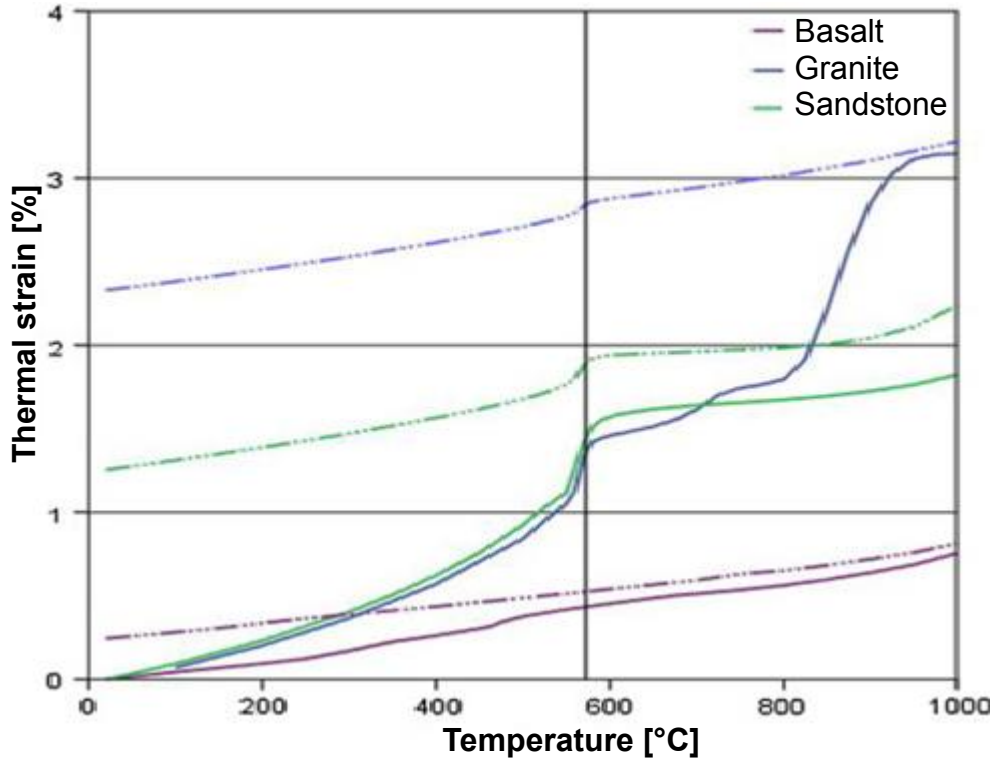

Figure 3 Thermal expansions of some natural aggregates [40]

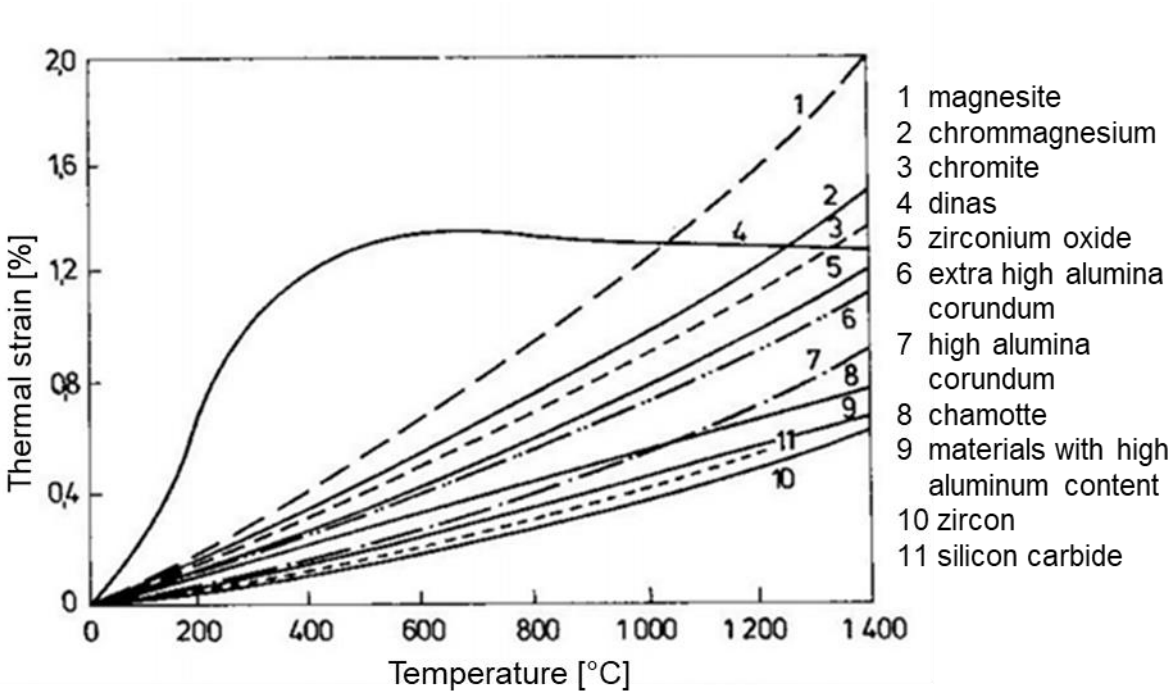

Figure 4 Thermal expansions of some artificial aggregates [41]

3.2.3 Reinforcement

Fibres are added to concrete for several reasons, such as increasing the toughness of concrete, tensile, flexural and shear strength, impact resistance, frost resistance, restraining the shrinkage, etc. The choice of fibres (metalic, glass, synthetic, organic fibres etc.) depends on the desired properties, and where the improvement is desired. For fire resistant concretes or composites, an important characteristic is the ability of fibres to lessen the spalling of the surface layer, and to increase the fracture energy after heating.

The first group of fibres are employed for the mentioned elimination of spalling effect. This phenomenon is caused by presence of water in the material structure. During the heating, the water (especially free water, but also physically and chemically bonded) is evaporated in the pores. On the surface, water vapour can freely release and thus only drying shrinkage usually occurs. Bigger problems arise inside the structure. Without a simple way for its releasing (as it can be observed on the surface), the internal water vapour pressure significantly grows and can easily exceed the strength of materials. This causes explosive breakage or shatter, where the flayed fragments of materials can cause further damage on surroundings. For the reason of lessen this effect, fibres with low melting temperature (below 250 – 300 ºC) are employed. The most common representatives on this field are organic fibres. The decomposition temperature of organic-chemical bond is below 250 ºC [34]. During the heating, these fibres are decomposed and create “channels” in the structure for vapour releasing without growing of pressure. Usually these fibres should be the length of about 10 mm and diameter about 20 μ [35]. Their amount is in the range from 0.02 to 0.1%.

The second group of fibres helps to improve the performance of thermal resistant materials in their nature, similar as in the case of composites without the temperature loading. These fibres are usually bigger in comparison with previous; length is up to 30 mm and diameter up to 0.4 mm [35]. In addition, their amount is usually higher, up to 6%. The particular choice of fibres depends on their mechanical properties as well as about their temperature of applicability. For the high temperatures about 1200 ºC, usually chromium or nickel containing steel alloys are used.

Some typical examples of most common used fibres with their basic physical properties are summarized in the following Table 4 [35, 42, 43, 44].

Table 4 Properties of some fibres used as concrete reinforcement

Fibres	Density [kg m^{-3}]	Average tensile strength [GPa]	Elastic Modulus [GPa]	Linear thermal expansion coefficient [10^{-6} K^{-1}]	Elongation at break [%]	Softening Temp. [ºC]
E-glass	2580	3.445	76.0	5.4	4.8	846
S2-glass	2460	4.890	97.0	2.9	5.4	1056
Basalt	2700	4.840	110.0	8.0	3.1	1260
Steel	7800	0.620	207.0	10.8	23.0	1440
Carbon	1760	3.500	235.0	0.36	1.2	3500
PP	910	0.475	4.1	150.0	25.0	160
PVA	1260	1.250	22.0	0.1	7.5	225
Nylon	1140	0.470	3.0	80	30.0	241
PET	1500	1.200	14.0	60	8.5	260
PE	920	0.103	130	180	45	120
Hemp	1250	0.255	9.5	-	2.2	150
Coir	150	0.174	2.3	-	32.0	200
Bagasse	550	0.230	1.7	-	8.7	180
Flax	1450	0.700	6.7	0.5	2.0	165

3.3 Special properties of refractories

Except for ordinary properties (such as bulk and matrix density, porosity, mechanical strengths…) there are some special characteristics dealing with materials for high temperature application. The most common is refractoriness or pyrometric cone equivalent [45], which characterize softening temperature of materials. This temperature means that the materials start to soften under the action of heat without any external loading under only its own weight. It is usually quite lower than the melting point and softening can take place in quite wide range. The scope of softening range depends on chemical nature of the impurity of refractory, amount of impurities, the lowest melting point of component and the capacity of this component to react and dissolve other constituents. Measurements method is based on comparative principle, when the performance of studied material is compared with reference one of the known behaviour. For this reason, reference etalons with the shape of triangular pyramid are prepared and they are so-called pyrometric cone [46]. Each one is labelled by number,

which means a specific temperature when the cone will soften. During the experiments, the standard cones and the studied one of the same shape are placed in the oven with temperature rate 3°C per min. Due to the temperature loading, the top of the pyrometric cone becomes bent and the point when the top of the cone touches the base is defined as a softening temperature.

Softening temperature in fact proposed quite inapplicable information, because in real utilisation at high temperatures, materials are always loaded by some external loading. Therefore, refractoriness-under-load (RUL) [47] is defined as a property combining the effect of temperature and mechanical loading. During the measurement on the cylindrical specimens (with height and diameter of 50mm) are loaded by external pressure of 0.2 MPa (0.05 MPa in the case of insulating materials) jointly with continuously growing temperature 4.5 – 5.5 K min^{-1}. The decrease of the samples height is measured and the RUL is defined as a temperature when the falls reached 5% of the initial value.

Another important property, when speaking about materials for high temperature application, is thermal shock resistance [48]. Thermal shock resistance is property-describing degradation of material due to the cyclic changes of temperature. This fatigue resistance is of higher importance especially in such application when the repeated heating and cooling occurs. Thermal shock resistance is influenced by thermal expansion of particular constituencies of refractories, their thermal conductivity, mechanical strengths, elastic modulus and porosity. From the external impacts, it can be named especially temperature range of cycle, the rate of heating and cooling period, and the environment of the process. The experiment method is based on the determination of how many cycles material can withstand without damage. One cycle includes heating of prismatic samples (114 x 64 x 64 mm) to temperature 950 ºC, and 5 minutes of airflow cooling to the ambient temperature. Then the bending strength is determined. The damage is defined as a decrease of bending strength below one third of the initial value, or when the visible cracks on the surface occur.

The last described property is permanent linear changes of heating (PLC) [49]. This is of great importance especially in the case of the furnace lining, when joints between refractories can significantly grow and thus undesirable leakage of heat can occur, or in the case of positive changes, the increasing stress in lining can lead to its deformation, with same results of heat releasing. The first step of experimental

measurement is drying of rectangular specimens and determination of their dimension. Then samples are exposed to the thermal loading by prescribed rate and then for the five (in some special occasion up to twelve hours) hours persists at the required temperature. Then the specimens are cooling spontaneously in the furnace and the dimension in the cooled state is measured. Refractories should fulfil the specific requirements for the maximal PLC: 1.5% for thermal resistant concrete, 2% for plastic refractories and insulating refractories.

4 Selected raw-materials for composite design

4.1 Calcium aluminate cement

As it was mentioned above, regarding refractory concrete, it is beneficial to use calcium aluminate cement, rich in Al_2O_3, as it performs beneficially when in contact with fire and high temperatures. There is a detailed summary of the development of calcium aluminate cement covering over 150 years as presented by Kopanda and MacZura [50]. This type of binder was developed in 1865 in France. Calcium aluminate cement was originally developed for its chemical resistance, but saw rapid growth because of its high early strength development. However, the extensive use of calcium aluminate cements as binders did not occur until the 1920's [50]. In the Czech Republic calcium aluminate cement was widely used between 1930 and 1960, especially for construction with demands of high initial strength growth or casting in winter period. Widespread use of calcium aluminate cement was interrupted due to many defects and failures that occurred in constructions. Afterwards it was proven that concrete based on calcium aluminate cements strength deteriorates during time because of mineralogical conversion [51]. Because this calcium aluminate cement for load-bearing constructions was forbidden in 70's throughout the world. In the Czech Republic it was prohibited in 1984 after the collapse of a factory building in Uherské Hradiště [34]. However, its utilisation as a binder for refractory concrete is still possible and has its advantages. For prevention of negative conversion's effects (increasing of porosity and decreasing of strengths) it is recommended to use higher amounts of calcium aluminate cement (more than 400 kg m^{-3}) and the water-cement ratio should not exceed the value of 0.40 [52].

The basic raw materials for the manufacture of calcium aluminate cement are limestone and bauxite in ratio 1:1. Limestone is sedimentary rock composed mainly of calcium carbonate ($CaCO_3$), while bauxite is residual rock composed of alumina minerals (böhmit, gibbsite, diaspor) and oxygen. The content of silica (SiO_2) must be minimal (lower than 6%) because it prevents formation of gehlenite (C_2AS) and dicalcium silicate (C_2S) [52]. A variety of processes has been used for the manufacture of calcium aluminate cements. There are two main production processes: melting procedure and sintering procedure. Melting cement is usually manufactured in an electric-arc furnace at temperatures of about 1600 °C, while the sintering process is performed in a rotary kiln in temperature around 1350 °C. Sintering leads to the

formation of very pure cement with higher aluminate content [52]. The mineralogical composition of the final product depends mainly on the purity of the raw material, composition of the stack, the firing procedure, and the cooling process. In Table 5 [52] a different composition of calcium aluminate cements is presented.

In comparison with Portland cement, calcium aluminate cement fundamentally differs in its phase composition. As it was mentioned above calcium silicates are ineligible. The main phase of calcium aluminate cement is monocalcium aluminate (CA), which in the case of higher alumina cement is accompanied by calcium dialuminates (CA_2) and dodecacalcium heptaaluminate ($C_{12}A_7$) [53]. Minor phases which calcium aluminate cement can contain are gehlenite (C_2AS), brownminillerrite (C_4AF) and dicalcium silicate (C_2S) [51].

Table 5 Composition ranges for calcium aluminate cements [%]

Grade	**Al_2O_3**	**CaO**	**SiO_2**	**Fe_2O_3, FeO**	**TiO_2**	**MgO**	**Na_2O**	**K_2O**
Standard low alumina	36-42	36-42	3-8	12-20	<2	1	0.1	0.15
Low alumina, low iron	48-60	36-42	3-8	1-3	<2	0.1	0.1	0.05
Medium alumina	65-75	25-35	<0.5	<0.5	<0.05	0.1	<0.3	0.05
High alumina	>80	<20	<0.2	<0.2	<0.05	<0.1	<0.2	0.05

The hydration process is, of course, widely influenced by phase composition. However, in contrast to the hydration of calcium silicate compounds (the formed hydrates remain broadly similar with time and temperatures up to about 100 °C), the process of hydration in calcium aluminate cements is strongly dependent on temperature. The hydration process is faster in comparison with Portland cement, therefore the setting time (time between initial and final set) is shorter [52]. It is also connected with a higher heat of hydration. The total evolved heat range between 545 J g^{-1} and 650 J g^{-1} (while in the case of Portland cement it is approximately from 375 J g^{-1} up to 525 J g^{-1}) [54]. In Table 6 different hydration processes of calcium aluminate (CA) are presented [55, 56], while in Table 7 the basic properties of hydration products are presented [55, 56, 57, 58]. Hydration of dodecacalcium heptaaluminate ($C_{12}A_7$) is analogous, however due to the higher C/A ration the formation of C_2AH_8 is

predominant also at lower temperatures. In comparison with reaction of mococalcium aluminate (CA) the hydration is more reactive and very exothermic, which leads to the shortening of cement setting time [52]. The last main component calcium dialuminate (CA_2) shows the lowest reactivity but proposed good temperature resistance. Its hydration is slow and it usually occurs at higher temperatures.

Table 6 Hydration products depending on temperature of hydration

Temperature range [°C]	**Hydration reaction (dominant / *coexisting*)**	**Product of hydration (dominant / *coexisting*)**
< 15	CA + 10 H	CAH_{10}
15 – 27	2 CA + 11 H *CA + 10 H*	C_2AH_8 + AH_3 (amorph.) *CAH_{10}*
27 – 30	2 CA + 11 H *3 CA + 12 H*	C_2AH_8 + AH_3 (amorph.) *C_3AH_6 + 2 AH_3 (amorph.)*
30 – 35	3 CA + 12 H *2 CA + 11 H*	C_3AH_6 + 2 AH_3 (cryst./amorph.) *C_2AH_8 + AH_3 (cryst./amorph.)*
> 35	3 CA + 12 H	C_3AH_6 + 2 AH_3 (cryst.)

Table 7 Properties of crystalic hydration products

Hydrates	**Chemical composition [%]**			**Structure**	**Specific gravity [kg m^{-3}]**
	CaO	**Al_2O_3**	**H_2O**		
CAH_{10}	16.6	30.1	53.3	Hexagonal	1743
C_2AH_8	31.3	28.4	40.3	Hexagonal	1950
C_3AH_6 - Katoite	44.4	27.0	28.6	Cubic	2520
C_4AH_{13}	40.0	18.2	41.8	Hexagonal	2046
C_2ASH_8 - Strätlingite	27.4	24.9	33.0	Hexagonal	1936
AH_3 - Gibbsite	-	65.4	34.6	Hexagonal,	2420
AH_3 - Bayerite	-	65.4	34.6	Monoclinic	2530
AH_3 - Norstrandite	-	65.4	34.6	Triclinic	2420

Calcium aluminate hydrates are metastable; only tricalcium aluminate hexahydrate (C_3AH_6) is thermodynamically stable. All metastable products eventually transform into stable hydrates [58, 59]. This process is called conversion, and it is inevitable. The time of this conversion depends on many aspects i.e. temperature, humidity, w/c ratio of mixture, tress and the presence of ‘releasable’ alkalis in the aggregate [58, 60]. Due to the strong dependence on temperature and high hydration heat, the conversion

process can appear even during hydration process thanks to self-heating of large samples [61]. Conversion process is described in following equations [61, 62].

$$2\ CAH_{10} \rightarrow C_2AH_8 + AH_3 + 9\ H \tag{40}$$

$$3\ C_2AH_8 \rightarrow 2\ C_3AH_6 + AH_3 + 9\ H \tag{41}$$

Concrete based on calcium aluminate cement has, thanks to its fast hydration, high initial strength development. It is usually connected with the formation of metastable hydrates and, on account of the conversion; it has to be regarded simply as transient strength [52]. During the conversion the low-density metastable hydrates are transformed into stable hydrates with a higher density, which is succeeded by an increase in porosity and a decrease in strength. In addition, water release occurs during the conversion process [60]. Long-term strength results mainly from stable tricalcium aluminate hexahydrates, and the strength is lower than its initial strength. In the case of mixtures with a low water cement ratio in the matrix anhydrous cement remains. This cement can afterwards react with released water. This can lead to a later strength increase [52]. Effectively, a continuous strength increase can be reached in the case of rapid formation of stable hydrates (large elements or elevated temperature). Mechanical stability of the concretes can also be affected by adding pozzolanic materials; for example, silica fume helps to reduce a decrease in strength, while utilisation of fly ash is not seen to be really advantageous [63]. By adding slag to the mixtures of concrete mechanical strength can be improved [64]. Generally, it can be concluded that the application of such materials, which contains higher amounts of silica, leads to the formation of strätlingite (C_2ASH_8) or calcium silicate hydrates (CSH) and thus avoid the conversion process. Another researches deal with alkali-activation [65] or phosphate modification [66], which caused direct creation of stable hydrates and therefore they prevent negative conversion process. Typical curves of strength development are shown in Figure 5 and Figure 6.

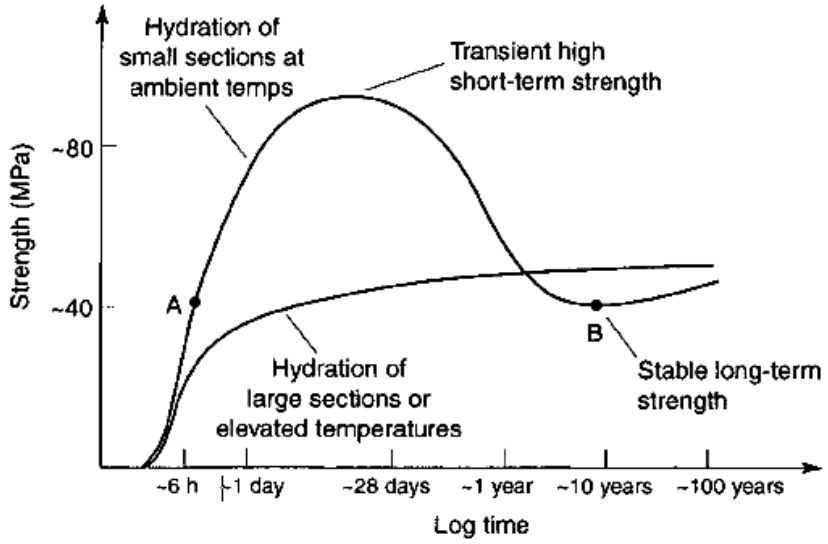

Figure 5 Schematic strength development of concretes based on calcium aluminate cement [63]

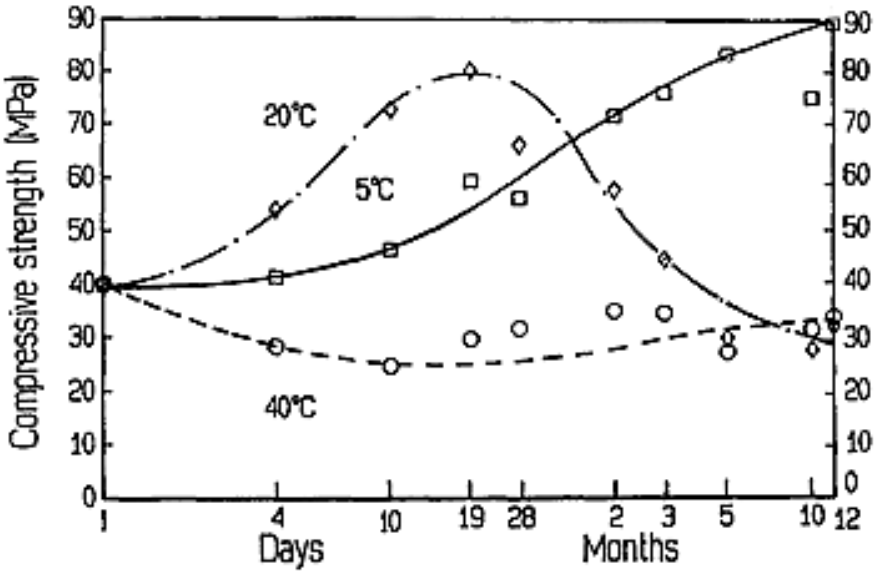

Figure 6 Schematic strength development of concretes based on calcium aluminate cement depending on temperatures [63]

Except conversion, another important process dealing with calcium aluminate cement is carbonation. Due to the impact of carbonate dioxide (CO_2) calcium aluminate hydrates are decomposed with formation of calcium carbonate ($CaCO_3$) and alumina hydroxide (AH_3), and separation of water [52]. In fact, primarily the vaterite or aragonite are created [67], while calcite occurs later due to the recrystallization at higher moisture content. The structure of alumina hydroxide is in most cases amorphous, rarely

bayerite or norstrandite can occur [67]. Chemical reactions of partial calcium aluminate hydrates can be summarized as follows [52]:

$$CAH_{10} + CO_2 \rightarrow CaCO_3 + AH_3 + 7\,H \quad (42)$$

$$C_2AH_8 + 2\,CO_2 \rightarrow CaCO_3 + AH_3 + 5\,H \quad (43)$$

$$C_3AH_6 + 3\,CO_2 \rightarrow 3\,CaCO_3 + AH_3 + 3\,H \quad (44)$$

Similar to PC carbonation leads primarily to the strength growth, but only in the absence of alkalis [52, 68, 69]. Their presence can lead to alkaline hydrolysis, which is described hereinafter. In fact, controlled carbonation curing can serve as a prevention for conversion process, because the metastable hydrates are transformed during hydration and thus no changes and porosity increase further occur [68, 70], however the formation of calcium carbonate ($CaCO_3$) is not beneficial from the point of thermal resistance of CAC. The most affecting factors of carbonation rate are the amount of carbonate dioxide, diffusion permeability, high moisture content or humidity, and temperature. Also alkalinity can play important roles. Due to the high alkalinity (caused e.g. by feldspar or mica in aggregate, or in mixing water) dissolution of calcium aluminate hydrate (CAH) as well as of aluminium hydrate (AH_3). However, this was observed when the pH was 14, lower values show no significant impact on mechanical properties or weight loss [52]. In the presence of alkalis, the decomposition of calcium aluminate hydrates is much faster. This process is so-called alkaline hydrolysis and leads to the dramatic decrease of mechanical strength [52]. Tricalcium aluminate hexahydrate (C_3AH_6) is the most susceptible to decomposition, while calcium aluminate decahydrate (CAH_{10}) is generally more resistant [69]. As an example, the reaction in the presence of potassium carbonate can be presented:

$$CAH_{10} + K_2CO_3 \rightarrow CaCO_3 + K_2O.Al_2O_3 + 10\,H \quad (45)$$

$$K_2O.Al_2O_3 + CO_2 \rightarrow K_2CO_3 + Al_2O_3 \quad (46)$$

In comparison with the conversion, carbonation respectively alkaline hydrolysis is much faster process. The effect can be observed even after one week. Moreover, both conversion and alkaline hydrolysis have synergic effects. Due to the conversion the porosity increases which leads to the permeability growth and thus alkaline hydrolysis goes up. In the case of alkaline hydrolysis, the amount of tricalcium aluminate

hexahydrate (C_3AH_6) is significantly lowered, thus the equilibrium of the system is changed and consequently the conversion process is accelerated [69].

When hydrated calcium aluminate cement is exposed to elevated temperatures following changes occurs [56]: Temperature about 110 °C is necessary for the evaporation of surface and unbound moisture and also weakly bond water of amorphous AH_3 gel is removed. At 200 °C dehydration process of calcium aluminates hydrates begins, and at 300 °C decomposition of crystalline gibbsite AH_3 starts. When the temperature is increased to 500 °C formation of dodecacalcium heptaaluminate $C_{12}A_7$ is initiated. With growing temperature, its converting to renovated calcium aluminate CA and further also calcium dialuminate CA_2 occurs. Over temperature of 1400 °C monocalcium hexaaluminate CA_6 arises. Basic decomposition reactions of amorphous alumina hydrate (AH_x) [71], calcium aluminate hydrates [56, 71] and gibbsite (γ-$Al(OH)_3$) [72] can be written in following form:

$$AH_x \rightarrow A + xH \tag{47}$$

$$2\ CAH_{10} \rightarrow C_2AH_8 + AH_3 + 9\ H \tag{48}$$

$$3\ C_2AH_8 \rightarrow 2\ C_3AH_6 + AH_3 + 9\ H \tag{49}$$

$$7\ C_3AH_6 \rightarrow C_{12}A_7H + 9\ CH + 32\ H \rightarrow C_{12}A_7 + 42\ H + 9\ C \tag{50}$$

$$C_{12}A_7 + 5\ A \rightarrow 12\ CA \tag{51}$$

$$2\ \gamma{-}Al(OH)_3 \rightarrow 2\ \gamma - ALOOH + 2\ H_2O \rightarrow Al_2O_3 + 3\ H_2O \tag{52}$$

When focused on the strength development in temperature loading, at about 300 °C the mechanical strength starts to decrease due to phase dehydration. This fall continues up to 1000 ºC when the sintering process becomes, which leads to the progressive growth of mechanical strength. Applicability of CAC ranges from 1300 ºC to 1550 ºC [35] according to the specific compositions and purity of cement.

4.2 Basalt aggregates

Basalt is natural volcanic rock from the tertiary period with the amplest sources available (it comprises about 90% of volcanic rocks [73]) in the ground. Its colour is black (weather-worn rock blends into grey). Basalt was created from eruptive magma, which rapidly cooling on the surface, and belongs to the group of extrusive igneous

volcanic rock. The mineralogical and chemical composition varies depending on the source of location. Its crystal structure can be modified by the rate of cooling after the lava is taken off the Earth's surface. On average fine-grounded minerals are composed mainly of pyroxene (about 50%), plagioclase feldspar (about 30%), and other minerals (especially olivine) [74]. From the chemical point of view its main components are silica dioxide SiO_2 (about 50%) which is succeeded by aluminium oxide Al_2O_3 (about 16%), calcium oxide CaO (about 10 %), and magnesium oxide MgO (about 6.8%) [75].

Furthermore, basalt aggregate is one of the most thermal stable natural rocks. It is stable up to about 900 °C [38]. The melting process occurs in a wide range of temperature i.e. from 1000 °C to 1260 °C [75]. Basalt aggregate is advantageous for utilisation in high temperature application, also for its quite low value of linear thermal strains coefficient (3.6 – 9.7 10^{-6} K^{-1}) [76]. Other important mechanical and physical properties (from five different quarries) are summarized in Table 8 [76, 77].

Table 8 Basic physical and mechanical properties of basalt aggregate

Characteristic	**Value**
Specific gravity [kg m^{-3}]	2500 – 2915
Los Angeles Coefficient [% mass losses]	14 – 18
Compressive strength [MPa]	141 – 172
Water absorption [%]	0.163 – 18
Freeze – thaw resistance [% mass losses]	7.2 – 8.5

Basalt aggregate is widely used in the civil engineering industry as filler in concrete, asphaltic concrete, ballast for highways or road-metal, rock fill for dams etc. [77]. Basalt rock is twice as hard (measured by Mohs hardness test) as limestone. Therefore its good wear resistance makes it a suitable material for concrete asphalt surface layers [78]. Regarding its application in concrete, the high bulk density of these volcanic rocks and their inclination to create angular pieces during crushing, can lead to the segregation of fresh concrete mixture and worsening of workability. On the other hand, particles with this type of shape interlock with one another, and produce denser concrete. The texture and mineralogy of basaltic rocks determine its physical and mechanical properties which are very good in relation to the final concrete strength and fire resistance. Unlike limestone and quartzite, the basalt-cement paste interfacial bond strengths increase consistently with the increasing surface roughness

of the aggregate. Basalt rock has either a firmer or stronger crystalline texture with no zones of weakness causing the high “apparent” interfacial bond strength achieved by its fractured surface [79]. Mechanical strengths of concretes with coarse basalt aggregate are somewhat higher than in the case of utilisation of limestone or gravel [80] (especially in the case of high strength concretes).

4.3 Basalt fibres

As it was already mentioned basalt fibres are a very suitable choice for reinforcing thermal resistant concrete due to their high resistance to a wide range of temperatures from -260 °C to +750 °C [81]. Moreover, they are environmentally friendly and non-hazardous, possess high modulus, good resistance to chemical attack, excellent interfacial shear strength, and are currently commercial available. All of which makes them advantageous for the general purpose of concrete reinforcement [82].

The origins of development of basalt fibre production dates back to the early 20th century. Production technology was patented in 1920, but an industrial boom in technology of basalt fibre manufacturing occurred after the Second World War (the First factory in the Czech Republic was opened in 1952) [83]. The manufacturing process of basalt fibres is similar to that of glass fibres, however, basalt consumes less energy and does not need any additives for melting. Production is thus cheaper compared to glass fibres or carbon fibres [84]. The raw material (basalt rock which should be as pure as possible and without unfamiliar minerals) is melted in a furnace at temperatures of about 1450 °C – 1500 °C [74]. There are two possible ways to process molten material – blowing technology and the technology of continuous spinning. Blowing technology uses a horizontal shaft spinning device with one accelerating and two fibrillating centrifugal cylinders. The molten is blown off by the centrifugal force in the form of droplets, which are then, during the flow, moulded into shape of fibres. This technology is used for production of short and cheap fibres. Unfortunately, these fibres have poor mechanical properties. The second one is the spinneret method, which produces continuous fibres of better quality. In essence continuous spinning forces, the molten through platinum or rhodium crucible bushings which shapes the material into long continuous fibres. These can then be cut in order to obtain a specific length of fibres. The diameter of basalts fibres ranges from 10 μm to 20 μm [84] according to the production process and quality of raw material. This can also affect the chemical compositions of basalt fibres. Similarly, to basalt, the fibres

are composed mainly of silica dioxide SiO_2 (43 – 47%), succeeded by aluminium oxide Al_2O_3 (11 – 13%), calcium oxide CaO (about 10 – 12%), and magnesium oxide MgO (8 – 11%) [30]. Even though basalt fibres have similar composition as asbestos fibres, basalt fibres are non-hazardous to human health [85, 86]. They have different morphology and surface properties. These characteristics are important variables which suppress any carcinogenic or toxicity effects presented by asbestos [87]. Most of non-polymeric fibres are breaking up into thin and long pieces, which leads to its emission during handling. In contrast, basalt fires show the same fibre fragment diameter as diameter of fibres, thus no splitting of fibres occurred during the fracture and therefore even from this perspective basalt fibre are non-hazardous to human health [88].

Basalt fibres have many advantages which make them a perspective material for engineering purposes. The chief physical properties of basalt fibres are summarized in Table 9 [74, 84, 89, 90]. They are well resistant to abrasion and have high biological and chemical stability (good resistance to weather, and acids exposure). The fibres can withstand a wide range of temperatures; their thermal stability depends not only on the composition of raw material but also on the presence of a large amount of micro-pores [91]. Figure 7, where thermal gravimetric analysis of glass and basalt fibres are presented, shows good thermal stability of basalt fibre.

Table 9 Basic physical and mechanical properties of basalt fibres

Characteristic	**Value**
Density [kg m^{-3}]	2700 – 2900
Water absorption [%]	0.5
Softening temperature [°C]	960
Sustained operating temperature [°C]	1093
Melting temperature [°C]	1720
Elastic modulus [GPa]	75 – 100
Tensile strength [GPa]	0.99 – 2.5
Compressive strength [MPa]	300
Elongation at fracture [%]	1.8 – 3.2
Thermal conductivity [W m^{-1} K^{-1}]	0.027 – 0.038
Thermal expansion coefficient [K^{-1}]	8.0 10^{-6}

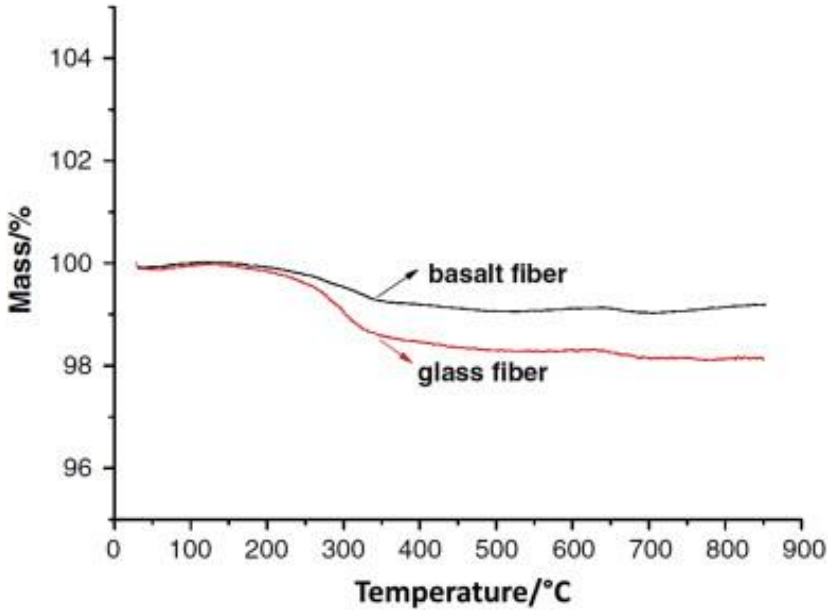

Figure 7 TGA curves [92]

In civil engineering basalt fibres are chosen as insulating materials for their excellent sound and thermal properties. Their good mechanical properties predestine them to be a suitable reinforcement of concrete. Although basalt fibres somehow reduce workability of fresh concrete, they improve bending and tensile strength, toughness, abrasion resistance, fatigue strength, deformation capability, and load bearing capacity after cracking [93]. It was recorded that the presence of basalt fibres significantly reduced the drying shrinkage of cement paste or mortar and increase the strength and bond properties of cement paste in early ages [94]. Enhancement of mechanical properties is higher when longer fibres are used [93]. As they do not lose their properties under high temperatures [95], an advantageous behaviour of basalt fibres in concrete arises also in fire-resistant concrete applications.

Despite many advantageous properties of basalt fibres, it has to be mentioned that similarly to glass fibres they are somehow subjected corrosion in alkaline environment. Its degradation is similar as in the case of glass. However, the degradation process is strongly influenced by the particular environment. Typical evaluation of alkali resistance is performed in NaOH solution, in which loosely bound peeling corrosion shell is created on the surface of basalt fibres [84, 96]. Therefore, the mass changes in first steps could not be observed despite the strength loss and basalt fibres seem to have good alkali resistivity. In contrast when basalt fibres in its natural form were subjected to the cement solution, the corrosion pattern is significantly different. Holes of different sizes and depths become occurs [97]. Similar solution as in the case of

glass fibre can be used also for basalt fibres; by sizing of fibre by appropriate material the alkali resistance (together with other properties) can be significantly improved. Particular sizing agents depend on desired properties of final products. Protective film forming sizing agents are based on polymers (polyurehtased, epoxides, polyether, polyvinyl acetate…) [98]. Zirconyl chloride octahydrate ($ZrOCl_2.8H_2O$) slow down corrosion of fibres [96], while saline based coupling agent can further improve interfacial adhesion of fibre to polymer based matrix (epoxy resin, HDPE) [99], or cement matrix [100] and thus improved also the mechanical performance of final composites [101] [102].

5 State of the art

Current research of thermal resistant materials can be divided into two groups. The first is focused on behaviour of structural elements under fire or higher temperature exposure, and the second group deals with residual properties of building materials. From the first group, it can be named for example work of Wei et al. [103] whose studied fire resistance of concrete-filled steel plate composite walls. Shekastehband et al. [104] investigated the fire performance of stiffened concrete filled double skin steel tubular columns and Song et al [105] investigated blind bolted composite beam to column joints. However, because in this work mostly residual properties are measured for determination of temperature resistance, the presented list of current research is focused primarily on the articles from the second group.

5.1 Cements

Practical application of CAC is mainly connected with designing refractory constables. Wang et al. [106] investigated material composed of tabular alumina, reactive alumina, CAC and dispersant agent up to 1500 °C. They reported the mechanical strengths decrease in temperature range from 110 °C to 800 °C. However, exceeding the temperature 900 °C the mechanical performance growth due to the recrystallization of dodecacalcuim heptaaluminate ($C_{12}A_7$). In temperatures range between 1100 °C to 1200 °C they observed slight decrease, caused by volume expansion of rising calcium (C) and calcium di-aluminate (CA_2). And finally creation and sintering of calcium hexaaluminate (CA_6) caused another improvement at temperatures about 1400 °C.

Khaliq et al. [62] studied the difference between behavior of concrete based on CAC and PC (CEM I 42.5R). As aggregate they used natural sand and crushed limestone. Measurements of particular mechanical properties were performed at high temperatures and after air cooling as well. They confirmed better mechanical performance of CAC based concrete, as well as lower mass loss and microstructural damage in temperature range 20 °C – 800 °C, as well as better elastic modulus and compressive toughness. When compared the residual and heated samples, the residual properties were generally lower. This was caused by further deterioration of material during the cooling.

Ogrodnik and Szulej [107] dealt with the PC (CEM I 32,5R) and CAC at high temperatures also. Moreover, they studied the applicability of waste sanitary ceramics

and the impact of concrete aeration. They determined mechanical strength of studied mixtures in three different loading condition: samples were not treated, exposed to temperature of 1049 °C, or primarily water saturated and then exposed to the temperature loading. They reported beneficial impact of aerating admixture on lessening the spalling and improvement of residual properties in both moisture states.

Another research focused on thermal resistance of CAC and PC was performed by Baradaran-Nasirt and Nematzadeh [108], whose studied the impact of recycled aggregate up to the 1000 °C. Specifically they used PC (CEM I 42.5 N), CAC, natural aggregate (unfortunately not specified) and crushed refractory bricks. Several temperature loading was performed: none (24 °C and 110 °C) and then with the step of 200 °C up to 1000 °C. They presented wide scope of physico-mechanical properties, and proved the applicability of recycled aggregate and CAC, which at higher temperatures improved the behaviour of concretes.

5.2 Aggregates

Regarding the varying aggregate, there were found just few of the studies dealing with varying natural aggregates for high temperature application. Hager et al. [39] studied impact of different coarse aggregate on the physical and mechanical properties of high-performance concrete subjected to high temperatures. Specifically, they studied granite, basalt, quartz sandstone and dolomite in combination with Portland cement. The fine aggregate was in all cases silica sand. They measured residual properties up to temperature exposure to 1000 °C, with the 200 °C of temperature step. Due to used cement (CEM I 42.5) and silica sand they can observe the influenced of varying aggregate below 600 °C. Over this temperature, the decomposition of cement paste is the most significant, also silica transformation occurs, and thus the impact of different aggregate cannot be properly judged. They presented that dolomitic aggregate is not usable for high temperature because of the higher content of carbonates. During heating their decomposition leads to lime creation, which rehydration during cooling is accompanied by high volumetric changes.

Coarse quartzite, granite and basalt aggregates were investigated also by Masood et al. [109]. They prepared mixture based on ordinary Portland cement (OPC 43) and with employing of fine river sand. Temperature loading was up to 600 °C, with the 200 °C of temperature step. Surprisingly, they presented the best performance of

quartzite aggregate, while basalt showed the worst. They assumed that it was caused probably by the presence of ferro-magnesium minerals in their basalt aggregate.

Hartlieb et al. [40] also performed study dealing with different aggregates. For their research they chose basalt, granite and sandstone, however they study thermal properties of the rocks in its nature up to 1000 °C. They confirmed that content of quartz has a significant role in thermal resistance of the aggregate.

5.3 Reinforcement

One of the most common possibility how to improved concrete and cement composites performance is reinforcing them by fibres. As it was mentioned hereinabove, there are two different issues when choosing appropriate material for reinforcements, lessen of sapling effect and improvement of the mechanical performance. However only few studies dealing with fibre reinforcement of CAC were performed. It can be named study of Frantsis et al. [110] dealing with steel fibres and its bonding ability in CAC. However, this study was more focused on the new experimental technology than on the specific material compositions.

Boris et al. [111] studied applicability of carbon fibres up to 0.6% by mass in combination with CAC based paste. They presented positive effect of fibres on compressive and bending strengths at ambient temperature. However, regarding the higher temperature, the studied mortars only by virtue of thermal analysis. At about 600 ºC, these fibres burnt out, and thus they can provide no beneficial effect exceeding this temperature.

Garcés et al. [41] investigated also carbon fibres, but as reinforcement for CAC blended mortars. As a binder, they used CAC cement in combination with silica fume. Aggregate was silica sand, and amounts of fibres were up to 5% of binder mass. According to their results, 0.5% of carbon fibres improved the mortars strength but at the same increased porosity. However, in this research no evaluation of the temperature impact can be found.

More investigations were focused on reinforcing of PC based concrete. In this case, several studied dealt also with residual properties. Bodnárová et al [112] investigated behaviour of blended cement (PC with blast furnace slag, or in addition of limestone) based composites with steel and polypropylene fibres, and basalt or lightweight clay based aggregate. Temperature loadings were 200 °C, 400 °C, 660 °C and 800 °C and the scope of investigated parameters covered mechanical properties.

They reported positive effect of dispersed reinforcement and basalt aggregate, while application of lightweight aggregate led to deterioration of mechanical properties.

Cementitious composites based on blended cement (PC with fly ash) with hybrid PVA and steel fibres were examined in study performed by Liu et al. [113]. They presented decrease of compressive strength by about 50% due to 800 °C temperature exposure. Despite they used silica sand and Portland cement, they reached great results of residual compressive strength; it was probably by positive effect of pozzolanic fly ash and PVA fibres. Unfortunately, they studied only one mixture, so no conclusion dealing with impact of particular component can be derived.

Carbon fibres were examined for example by Tanyildzi [114]. He employed these fibres in amount up to the amount of 8 kg m^{-3}. Presented mixture were based on Portland cement (CEM I 42.5) combined with silica fume up to 20% of replacement level. As an aggregate, he used pumice lightweight aggregate. Specimens were exposed to 400 °C, 600 °C and 800 °C of temperature loading and among studied properties belonged compressive and flexural strength. The best ratio of carbon fibres was found to be 0.5% for pure PC, and 1% for blended cement.

Regarding the application of basalt fibres, Jalasutram et al. [115] investigated mechanical properties of fibre-reinforced concrete and found out, that the basalt fibres up to 2% of volume lead to almost no different of compressive strength, or to just minor reduction. However, the splitting strength and flexural strength was improved due to the reinforcement and flexural toughness as well. The problem in this study was reduction of workability during the mixing, which authors did not correctly improve (higher w/c ratio, plasticizer utilization…). Thus, samples with higher fibres dosage were probably not properly mixed and could not provide adequate improvement.

Ren et al. [116] dealt with the influence of basalt fibers on concrete based on blended cement exposed to elevated temperatures. Mixtures presented in their study contain PC, fly ash, silica fume, crushed limestone, and basalt fibers up to 0.3% of volume. The temperature loading was performed up to 800 °C, with the 200 °C of temperature step, and in contrast with previous studied the cooling was done by water spraying. They reported that their application led to improvement of strength performance, deformation capacity and energy absorption of concrete also after temperature exposure up to 800 °C. The optimal volume fraction was found out to be 0.2%.

6 Experimental methods

6.1 Material characterization

6.1.1 Technological properties

For measurement of granulometric curve of cements the laser diffraction method was used. This method is based on the Mie or Fraunhofers theory, which put into the relation the laser diffraction angle of the particle with its size. Specifically, “Analysette 22 NanoTec” from Fritsch GmbH [117] was employed. The range of measurement of this equipment is from 0.1 μm to 2100 μm of particle size. Time of measurement is by about 2 minutes and the evaluation is automatic and done by special software "MaS control". As a result, the cumulative particle size distribution curves are obtained. Finesses of cement were also described by specific surface area. This property was measured by applying so called Blaine permeability methods in accordance with standard [118].

Setting times are one of the most important technological properties. “Automatic Vicat Nedle Device” from FORM+TEST Seidner&Co. GmbH [119] was used. This equipment automatically performs plunges in predefined intervals and records depths of needle penetration. Final initial and setting times were determined in accordance to standard [120]. Intervals of penetration are 10 minutes. Initial setting time is defined as time interval from the mixing of cement with water to the point when the distance between the mould’s bottom and needle penetration is 6±3mm. Final setting time is reached when the penetration depth is less than 0.5 mm. Measurements for particular cements were performed three times and the average value was presented as a final setting time.

Consistency of fresh mixture is described by employment of flow. For the determination, standard method for mortars [121] was used, since it is applicable also for those mixtures with fine aggregate. Fresh mixture is put in the special mould with the shape of a truncated cone and it is compacted. Then the mould is given away and the flow table is lifted up and dropped 15 times (approximately 1 fall per second). Two orthogonal diameters (of flowed mixtures) characterize the mixture flow.

Granulometric curves of aggregates were determined by grading test according to standard [122]. This experiment is based on distribution of studied material by sifting the material through a set of sieves. The set of sieves are prescribed according to

nominal size of square sieve mesh as follows: 0.063 mm, 0.125 mm, 0.250 mm, 0.5 mm, 1 mm, 2 mm, 4 mm, 8mm, 16 mm, 32 mm, 64 mm and 125 mm. After sifting, the partial residues on every sieve are weighed and then cumulative passing are counted. Then granulometric curve is delineated. For the need of this study, the utilised sieve was set up to 8 mm, because just fine aggregate was used in mixture design. Partial gradings were measured separately with weight portion of 0.6 kg. The difference between weight portion and sum of partial residues were less than 1% in all cases, as it is defined in the standard [122]. Finally, the combination of curves according to partial results were counted.

6.1.2 Chemical analysis

The phase composition of calcium aluminate cement pastes was studied by X-ray diffraction (XRD) by means of a "PANalytical X´Pert PRO" from Malvern Panalytical Ltd [123]. The conception of XRD is the application of monochromatic x-ray emission on studied polycrystalline powder material, with generation of diffraction patterns based on Bragg's diffraction law, which are recorded and analyzed. In the case of powder methods, the obtained result is a graph with dependency of the input emission position (angle 2θ) on the intensity of the diffraction one. The quantification of the present phases was performed by Rietveld analysis with internal standard (20 % of ZnO); the evaluation was done by the TOPAS software.

The elementary composition was measured by X-ray fluorescence spectrometry. Similar to previous XRD method, high-energy monochromatic X-ray acts on a studied material, however in this method the characteristic emissions are excited and measured. The final result is fluorescence spectra; dependency of fluorescence intensity on wavelength of emission. Based on Moseley's law the atomic numbers of particular elements can be derived from the wavelength of emitted X-ray emission and its intensity is in correlation with the amount of the element. Specifically, device Thermo ARL 9400 XP made by Thermo Fisher Scientific Inc was used. The acquired data were evaluated by software UniQuant 4.

6.1.3 Thermal analysis

Simultaneous thermal analysis (STA), consisting of differential scanning calorimetry (DSC) and thermogravimetry (TG), was used for the purpose of better characterization of raw-materials behaviour in higher temperatures and for determination of particular temperatures for thermal pre-treatment. Specifically,

measurement device “LABSYS EVO DTA/DSC” from SETARAM Inc [124] was employed. The measurement is based on comparative method, where heat effects on studied samples (heat flows and mass changes) are determined through the view of comparison with reference samples. Two samples (the reference one and the studied one) are put in one cell but each has its own thermal sensor. They are connected by thermal bypass and so the temperatures of both samples are maintained isotherm by heat inputs. Thermal loading is programme-controlled and was set as follows: After temperature stabilization (at 30 °C), temperature increased with heating rate of 5 °C / min up to reaching 1000 °C. An argon atmosphere in cell was set, with the heat flow rate of 40 mL min^{-1}.

6.2 Basic physical characteristic

6.2.1 Basic physical properties

Vacuum water saturation [125] was used as one of the methods for determination of the basic physical properties. Three samples with dimensions of 50 × 50 × 50 mm were measured. Water vacuum saturation is based on Archimedes law. To remove physically bounded water and determination of dry mass, specimens are dried in a drying box kept at the temperature of 105 ˚C. The second state is the water saturation. Samples are put into a desiccator with boiled distilled water and air is evacuated with vacuum pump. After removing samples from desiccator, their mass in the saturated state is measured. Finally, the mass of saturated samples under the water, so called the Archimedes mass is determined. The basic physical characteristics are calculated from the equations:

$$V = \frac{m_s - m_d}{\rho_{H_2O}} \tag{53}$$

$$\rho = \frac{m_d}{V} \tag{54}$$

$$\psi_0 = \frac{m_s - m_d}{V \cdot \rho_{H_2O}} \tag{55}$$

$$\rho_{mat} = \frac{m_d}{V(1 - \Psi_0)} \tag{56}$$

V …	volume	[m^3]
m_s …	saturated mass	[kg]

m_d …	dry mass	[kg]
ρ_{H2O} …	density of water	[kg m^{-3}]
ρ …	bulk density	[kg m^{-3}]
Ψ_0 …	open porosity	[-]
m_a …	Archimedes mass	[kg]
ρ_{mat} …	matrix density	[kg m^{-3}]

The matrix density was determined also by the helium pycnometry. This experiment was carried out by the device “Pycnomatic ATC” from Thermo Fisher Scientific Inc [126]. This device has analogous principle as a classic pycnometry, however the medium for volume determination is not water but gas, which is expected to fill even smaller pores (due to the dimension of helium molecules). Volume of studied material is determined by virtue of measurement of gas pressure in chamber and with applying of the Boyle-Marriotte law. In this case the other basic physical properties are derived as follows: Bulk density is determined by gravimetric method: dimensions of dried samples from water vacuum saturation are measured three times and then specimen’s volume is counted as well as the open porosity:

$$\rho = \frac{m_d}{V} = \frac{m_d}{a.b.c} \tag{57}$$

$$\psi_0 = 1 - \frac{\rho}{\rho_{mat}} \tag{58}$$

a, b, c…	dimension of the specimens	[m]

6.2.2 Pore structure

Characterization of a pore structure is determined by mercury intrusion porosimetry. This method is done by measuring the external pressure needed to force the mercury into a pore against the opposing force of the liquid’s surface tension. The pore size is then calculated from the measured pressure using Washburn’s equation [127]. The experiments are carried out using instruments “PASCAL 140 + 440” made by Thermo Fisher Scientific Inc [128]. The range of an applied pressure corresponds to the pore radius from 10 nm to 100 μm.

6.3 Mechanical parameters

6.3.1 Destructive measurements methods

Compressive strength and bending strength, as mechanical properties, were measured according to standards [129]. Bending strength was measured by using a MTS 100 loading device at three samples with dimension of 40 x 40 x 160 mm. The experiment is arranged as a classical three-point bending with 100 mm span length. Loading is continued until the breaking point, and the ultimate force is noted. By evaluating the maximum bending moment and the known section modulus, the bending strength is calculated.

$$W = \frac{a.b^2}{6} \tag{59}$$

$$M_{max} = \frac{F.l}{4} \tag{60}$$

$$f_b = \frac{max\, M}{W} \tag{61}$$

W…	section modulus	[cm^3]
a, b…	dimensions of sample	[cm]
M_{max}…	maximal moment	[N m]
F…	ultimate force	[N]
l…	span length	[m]
f_b…	bending strength	[MPa]

To determine the compressive strength a special loading device (EU40) was employed. Samples taken from the measurement of bending strengths were used; therefore, six for particular temperatures were examined. In the actual experiment samples are put between two steel pressure plates with dimensions of 40 x 40 mm. Since only simple compression should be involved special emphasis has to be given to the centring of the arrangement. The ultimate force is noted, as in the case of bending strength. The compressive strength is calculated by taking into account the active force and the known loading area.

$$f_c = \frac{F}{A_l} \tag{62}$$

f_c…	compressive strength	[MPa]
F…	ultimate force	[N]
A_l…	loading area	[mm^2]

6.3.2 Non-destructive measurements methods

Determination of dynamic modulus of elasticity belonged among non-destructive method which was performed on three samples before destructive experiments were performed. It was done by ultrasound testing [130], specifically The Proceq PunditLab+ ultrasonic velocity test instrument with the 54 kHz pulse transducer was used to determine the ultrasound speed. The one-dimensional adjustment was used. It requires the position of pulse transducer and the receiver on the opposite sides of specimen pointed directly at each other. Dynamic modulus of elasticity [131] was then calculated as follows, when the coefficient was assumed as having value of 1.

$$E_{dyn} = \rho c_L^2 \frac{1}{k^2} \tag{63}$$

E_{dyn}…	dynamic modulus of elasticity	[Pa]
ρ…	bulk density	[kg m^{-3}]
c_L…	pulse velocity	[m s^{-1}]
k…	ambient dimensionality coefficient	[-]

6.4 Hydric properties

6.4.1 Hydric transport

Determination of water liquid transport ability were performed applying the sorption experiment. Three samples with dimensions of 50 x 50 x 50 mm were employed. Specimens are water and vapour proof insulated on four lateral sides. The aim of this insulation is to achieve transport only in one dimension. Then the face side of the specimens are immersed in 1 - 2 mm in the water. A constant water level in the tank is achieved by a Mariotte bottle with two capillary tubes. One of them, with an inside diameter of 2 mm, is submerged under the water level. The second one, with an inside diameter of 5 mm, remains above water level. The automatic balance allows recording of the increase in mass to the specimen. The water absorption coefficient is calculated from the sorptivity plot [132] which is taken from measured data. Apparent moisture diffusivity is calculated from water absorption coefficient by Kumaran's equation [133].

But this is just for an approximation of the real values of apparent moisture diffusivity. This value depends on moisture content, which is disregarded in Kumaran's relation.

$$i = A.\sqrt{t} \tag{64}$$

i…	cumulative mass growth	[kg m^{-2}]
A…	water absorption coefficient	[kg m^{-2} s$^{-1/2}$]
t…	time	[s]

$$\kappa \approx \left(\frac{A}{w_{cap}}\right)^2 \tag{65}$$

κ…	apparent moisture diffusivity	[m s^{-2}]
w_{cap}…	capillary saturated moisture content	[kg m^{-3}]

Measuring water vapour transport parameters was performed by applying the cup methods (dry-cup and wet-cup) [134]. Three cylindrical samples with diameter of 115 mm and 20 mm height were used for the experiment. The aim of this measurement is to create two environments with different water vapour partial pressure. In the dry-cup arrangement, cups contain silica gel, which simulates 5% relative humidity. Specimens are waterproof insulated and vapour proof insulated as in the case of sorption experiment. Then the samples are put on cups containing silica gel and are air-sealed fixed. The cups are then placed into a climatic chamber with a regulated temperature of 25 °C, and a relative humidity of 50 %. For two weeks the cups are periodically weighed. The steady state values of mass gain or mass loss determined by linear regression over the last five readings are used to determine the water vapour diffusion resistance factor. After two weeks of measurement the cups are remade to the wet-cup arrangement. This entails silica gel being exchanged for water, consequently simulating a relative humidity of 95%. Otherwise, conducting an experimental process of wet-cup measurement is the same as in the case of dry-cup experiment.

$$\delta = \frac{\Delta m \cdot d}{A_w \cdot t \cdot \Delta p_p} \tag{66}$$

δ…	water vapour diffusion permeability	[s]
Δm…	mass of transported water vapour	[kg]
d…	thickness of sample	[mm]

A_w…	area of water vapour transport	[mm^2]
t…	time	[s]
$\Delta p_{p...}$	water vapour pressures gradient	[Pa]

$$D = \frac{\delta \cdot R \cdot T}{M} \tag{67}$$

D…	water vapour diffusion coefficient	[m^2 s^{-1}]
R…	universal gas constant	[J mol^{-1} K^{-1}]
T…	thermodynamic temperature	[K]
M…	molar mass of water	[kg mol^{-1}]

$$\mu = \frac{D_a}{D} \tag{68}$$

μ…	water vapour diffusion resistance factor	[-]
D_a…	w. v. diff. coef. of water vapour in the air	[m^2 s^{-1}]

6.4.2 Accumulation of water vapour

The water vapour adsorption isotherms were set to describe moisture storage ability. For the experiments 5 samples with dimension of 30 x 20 x 10 mm were made. The measurements of points at the adsorption curve take place in climatic chamber. After the initial dry state of samples is achieved in a dryer with temperature 105 °C, they are put in the climatic chamber with set relative humidity. The relative humidity is initially set as 20% and it is increased by 20% regularly, when samples reach the steady state. Particular points of sorption isotherms are calculated from measured mass as follows, and then the curve is delineated by them.

$$w = \frac{m_{RH} - m_d}{m_d} \tag{69}$$

w…	mass moisture content	[-]
m_{RH}…	mass at specific relative humidity	[kg]
m_d…	dry mass	[kg]

6.5 Thermal characteristics

Using an ISOMET 2114 device [135], thermal conductivity and specific heat capacity were determined. Measurement was performed at three samples with dimension of 70 x 70 x 70 mm. ISOMET 2114 is portable commercial device which

applies a dynamic measurement method, so that the time it takes to make a measurement is reduced to less than half an hour. The measurement process is based on an analysis of a temperature response of an analysed material to heat flow impulses. The heat flow is induced in a resistor of a probe by a distributed electric power. The temperature is then recorded and evaluated from the polynomial regression. Range of measured properties is as follows: 0.015 – 6.0 W m^{-1} K^{-1} for thermal conductivity and 4.0 x 10^4 – 3.0 x 10^6 J m^{-3} K^{-1} for volumetric heat capacity. Because of the impact of the water presence on the thermal conductivity, as well as on specific heat capacity, both studied characteristics are measured in a dried state as well as in saturated states.

6.6 Physical properties at high temperature

6.6.1 Thermal strain

The measurement of thermal strain depending on temperature was performed by a linear thermal horizontal dilatometer [136, 137, 138]. The device utilizes a comparative method; the real thermal expansion is determined by comparing the analyzed specimen with a standard. For that purpose, corundum having standardized properties is employed in the form of a tube where the measured specimen is placed. One side of the specimen is put against the fixed wall and the second side touch a pull-rod which is connected to the length change indicator. Length changes are recorded by computer program “Dilatometer 1.3” form CLASIC CZ s. r. o. [138] and therefore thermal strain can be calculated as well as the linear thermal expansion coefficient depending on temperature:

$$\varepsilon_t = dl = \frac{l_i - l_0}{l_0} \tag{70}$$

$$\alpha = \frac{1}{l_0}\frac{dl}{dT} = \frac{d\varepsilon}{dT} \tag{71}$$

ε_t …	thermal strain	[-]
l_0 …	initial length	[mm]
l_i …	length at particular temperature	[mm]
α…	linear thermal expansion coefficient	[K^{-1}]
T…	temperature	[K]

The heating rate of the dilatometer was set at 1 °C per min and the maximum temperature of measurement was 1000 °C. For this experiment, three samples with the dimensions of 15 x 15 x 160 mm were used and the average of measured data were presented.

6.7 Statistics

Almost at all cases of the measurements methods, the experiments were carried out on several samples, or the whole experiment were performed multiple times. Presented results are average values, and the standard deviation is also provided. In graphs, it is not possible to delineated all particular standard deviation. In this case, always the maximal standard deviation is used. Statistical calculation is done according to following equations:

$$\bar{X} = \frac{\sum_{i=1}^{n} X_i}{n-1} \tag{71}$$

$\bar{X}$… mean / average value

n … number of results

x_i … particular result

$$\sigma = \sqrt{\frac{\sum_{i=1}^{n} (X_i - \bar{X})^2}{n-1}} \tag{72}$$

σ… standard deviation

7 Studied materials

7.1 Characterization of raw-materials

7.1.1 Cements

Calcium aluminate cement was chosen as the main binder component of studied composites. As it was mentioned hereinabove, this material is applicable for condition with temperatures above 1000 °C. Secar 71 [139] produced by Kerneos Inc. was chosen from commercially available CAC. This material with content of alumina oxide about 70% belongs among medium alumina cement. Detailed chemical composition of CAC can be found in Table 10. In addition, mineralogical analysis was performed, and the results are presented in Table 11 and Figure 8. It is obvious that the main phase of Secar 71 comprises krotite (calcium aluminate CA), highly reactive mineral which give rise higher mechanical strength. The second main phase of calcium alumina cement is grossite (calcium dialuminate CA_2), which is much less reactive but heat-resistant. The other minor phases, which were detected, are corundum (aluminate A), β-Al_2O_3 ($NaAl_{11}O_{17}$) and mayenite ($C_{12}A_7$). Small amount of katoite (C_3AH_6) was observed as well; it indicates partial hydration of CAC already before the samples being produced. Specific surface area of this cement is 381 $m^2\,kg^{-1}$, and it has the maximum of grains with size of 11μm (according to its granulometry in Figure 10). From other technological properties, the initial setting time and final setting time were determined and they are summarized in Table 12.

For the sake of comparison, composites with Portland cements were also prepared, CEM I 52.5R was employed. The higher cement strength class was chosen for the sake of comparability with CAC, or more precisely with the demands of similar compressive strength in 28 days. Portland cement [140] originates from Lafarge, a.s. Čížkovice. Chemical composition is shown in Table 10, while in Table 11 and Figure 9 its mineralogical composition is presented. Both used cements have distinctly different composition; in the case of CAC, the main component is alumina oxide and main phases are calcium aluminate, while in the case of PC, the main component is silica and main phases compose of calcium silicate. The granularity of both cements vary just slightly, CAC is somewhat finer. The maximal amount of grains are in average by about twice time bigger than in the case of CAC; the maximal peak of grains of PC ranges about 22 μm (Figure 10). The specific surface area of PC is 393 $m^2\,kg^{-1}$.

Regarding the technological properties, setting time of CAC is shorter than of PC (Table 12), which is in accordance with general predisposition of both cements.

Table 10 Chemical composition of used cements (XRF)

Cement	CaO	Al_2O_3	Na_2O	SiO_2	MgO	Fe_2O_3	K_2O	SO_3	P_2O_5
CAC	28.2	70.7	0.4	0.4	0.1	0.1	0.06	0.04	-
PC	64.9	6.4	0.3	18.1	1	2.4	1.2	4.9	0.2

Table 11 Mineralogical composition of used cements (XRD)

CAC	**CA**	**CA_2**	**$C_{12}A_7$**	**A**	**β-Al_2O_3**	**C_3AH_6**	**Amorphous**
	54.7	38.1	0.5	0.8	1.4	0.6	3.9
PC	**C_3S**	**C_2S**	**C_4AF**	**Gypsum**	**Anhydride**	**Calcite**	**Quartz**
	71.6	6.5	9.6	1.2	4.2	6.1	0.8

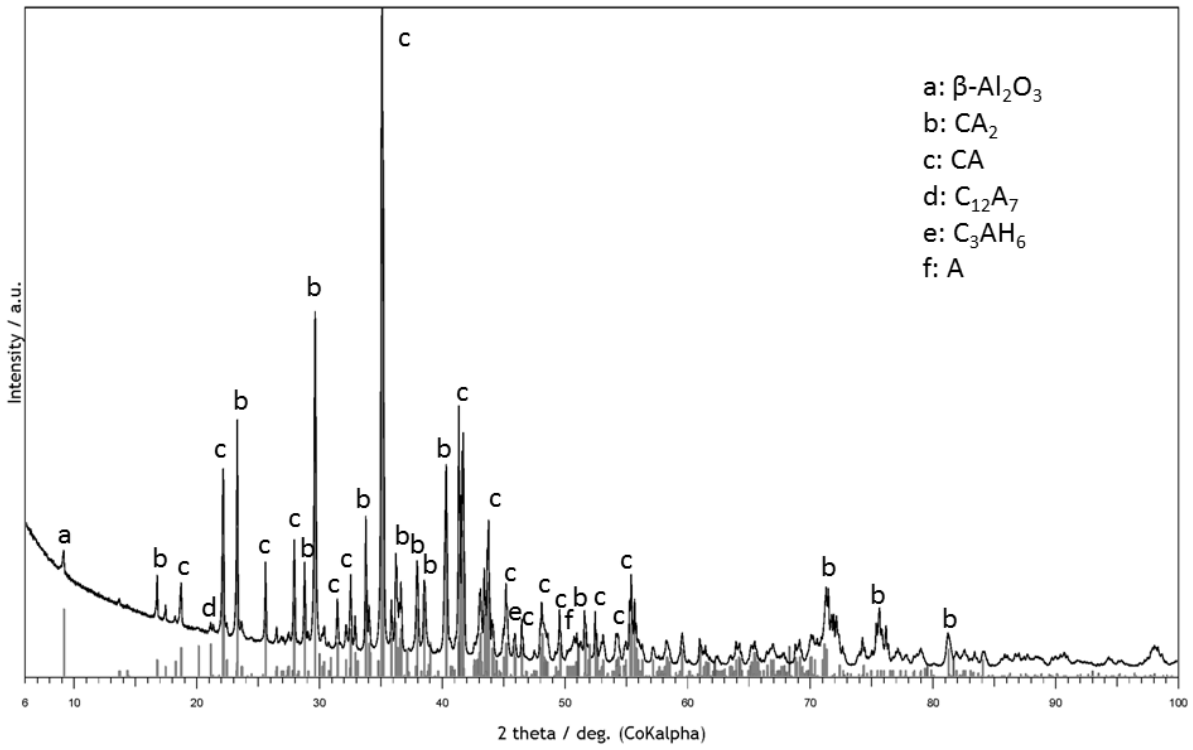

Figure 8 XRD pattern of CAC

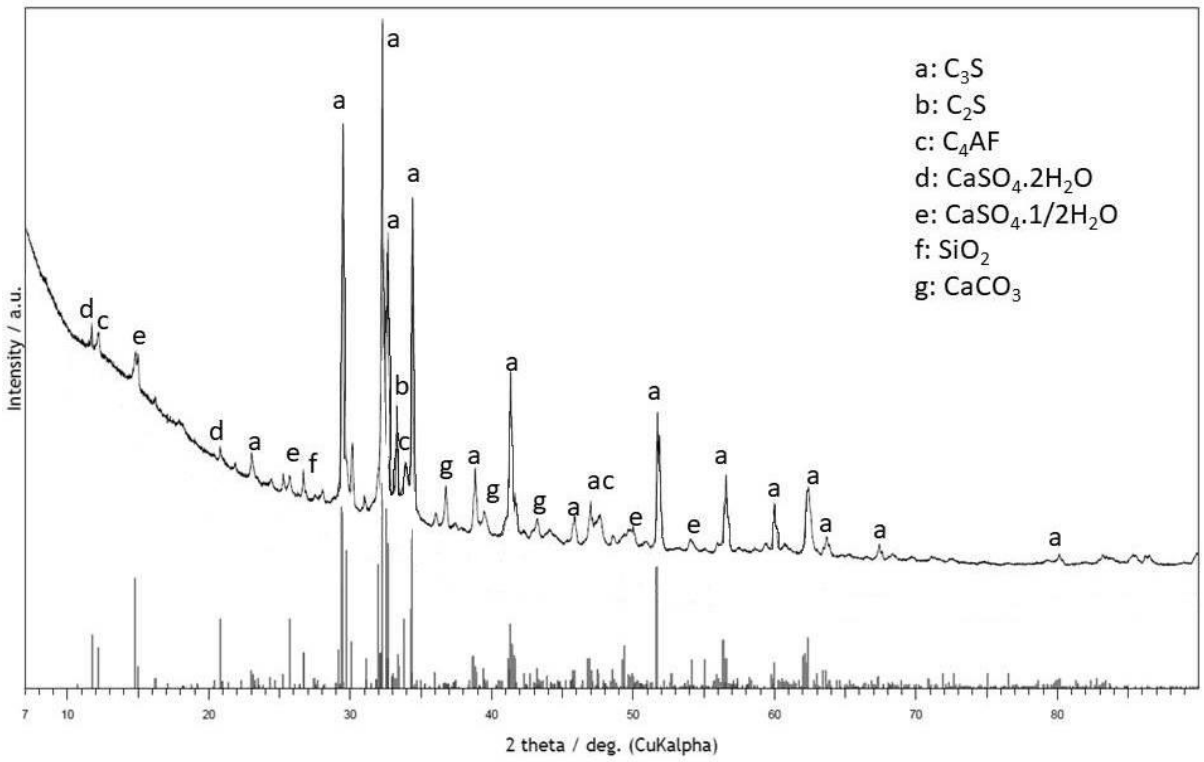

Figure 9 XRD pattern of PC

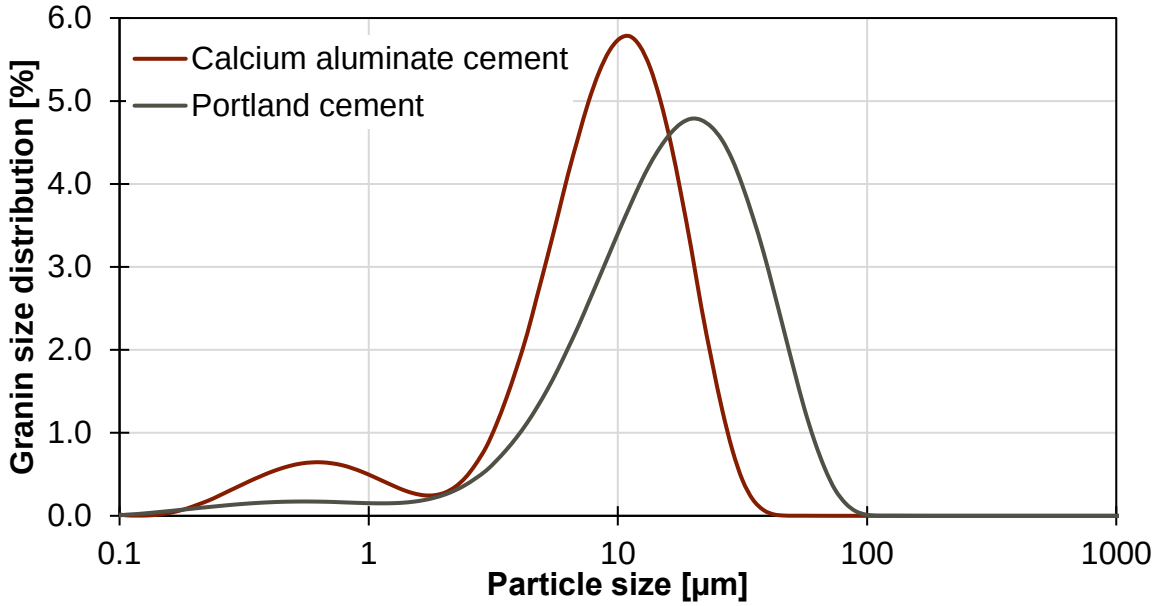

Figure 10 Granulometry of used cement

Table 12 Setting time of used cement

Cement	Initial setting time [min]	Final setting time [min]
CAC	255	285
PC	195	270

7.1.1.1 Hydration of CAC paste

For the sake of more detailed description of CAC behaviour, cement paste (with water/cement ratio 0.3 cured in the air in laboratory conditions at 20 ± 1 °C and relative humidity 25 – 30%) was prepared and its composition was determined in a different time. Achieved results are presented in Figure 11.The CAC pastes´ XRD detected presence of calcium aluminate decahydrate (CAH_{10}), dicalcium aluminate octahydrate (C_2AH_8) and katoite (C_3AH_6) hydrates as well as unreacted calcium aluminate (CA) and calcium dialuminate (CA_2) aluminates. Unfortunately, the quantitative analysis of this system is not possible due to the presence of C_2AH_8 which the structure is not known. However, remarkable growth of intensity of X-ray diffraction in time of CAH_{10} can be seen, while the changes of intensities of other hydrates are not so significant. This leads to the assumption that during hydration the phase of CAH_{10} arose in bigger amount, but other calcium aluminate hydrates were also formed. The presence of all principal hydrates shows, that the commonly accepted temperature depending reaction scheme [55, 141] is just indicative. In the consideration of just minor changes of intensities of CAC in time, it can be assumed that, the major part of hydration happened in the first two days. Another important thing is that the intensity of X-ray diffractions of CA_2 in time did not change at all. That indicates that its rate of hydration was negligible; this observation was in accord with literature [71, 142].

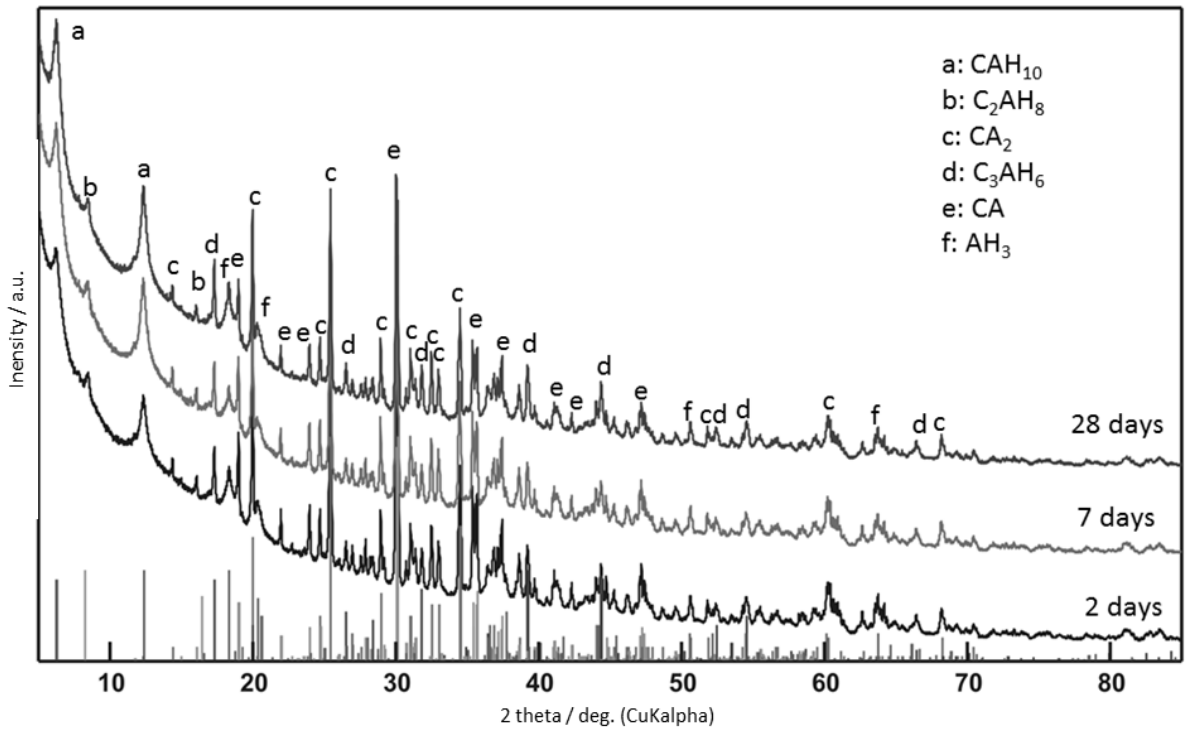

Figure 11 X-ray diffractograms of CAC pastes in time

7.1.1.2 Mechanical properties of cement pastes

Cement pastes (with water/cement ratio 0.3 cured at 20 °C) were also investigated from the point of view of strength development. In this experiment, the influence of varying curing conditions was examined. Samples of CAC pastes were cured in the air in the laboratory condition, as well as submerged in the water. Results of the compressive strength, bending strength and bulk density in varying age are shown in Table 13. CAC generally shows fast hydration and this was confirmed by faster strength increase. In the first two days, CAC paste reached 70% of the 28 days compressive strength when cured in the air, and almost 77% in the case of water curing, while PC cement pastes reached only 68% of the 28 days' compressive strength. Despite the faster strength development, the curing in the water led to lower values of mechanical strengths. Compressive strength in 28 days was by 19% lower than the one of CAC pastes cured in the air. Thus, in contrast with PC, where water curing is generally more beneficial, CAC proposed better properties when air curing.

Table 13 Development of mechanical properties of cement pastes in time

Cement (curing condition)	**Age [day]**	**Bending strength [MPa]**	**Compressive strength [MPa]**	**Bulk density [kg m^{-3}]**
CAC (water)	2	4.21 ± 0.30	60.0 ± 2.7	2085 ± 8
	7	4.68 ± 0.42	63.5 ± 1.3	2084 ± 32
	28	5.47 ± 0.29	78.5 ± 3.1	2077 ± 16
	90	6.14 ± 0.45	87.1 ± 4.5	2138 ± 15
	180	5.69 ± 0.32	88.7 ± 2.9	2172 ± 19
CAC (air)	2	5.09 ± 0.47	68.2 ± 2.5	2161 ± 8
	7	5.37 ± 0.50	76.2 ± 2.5	2190 ± 8
	28	5.53 ± 0.57	97.4 ± 3.1	2249 ± 12
	90	6.37 ± 0.44	107.4 ± 2.5	2244 ± 9
	180	6.36 ± 0.33	106.8 ± 3.0	2222 ± 15
PC (water)	2	12.66 ± 0.88	52.8 ± 1.2	2092 ± 34
	7	12.88 ± 0.81	58.2 ± 2.3	2057 ± 18
	28	13.20 ± 0.64	77.6 ± 3.1	2078 ± 12
	90	13.32 ± 0.33	79.9 ± 4.3	2074 ± 6
	180	13.79 ± 0.85	82.0 ± 3.8	2082 ± 17

At the age of 28 days, the heat treatment of cement pastes were performed, and residual mechanical parameters were determined. Achieved results are summarized in Table 14. It is obvious that dehydration of calcium aluminate hydrate had not so deteriorating effect on the compressive strength, this value decreased due to the exposure to 400 ºC just by about 4%, while PC based pastes showed almost 13% fall. However, the fall of bending strength due to the temperature loading was much more significant; it decreased by more than 60% in the case of CAC and by about 90% in the case of PC. When the loading temperature was 1000 ºC, the differences were much more considerable. Pastes based on CAC showed compressive strength fall by about 40%, while those based on PC reached values lower by more than 82%. These results confirm that PC is almost inapplicable for higher temperature.

Table 14 Residual mechanical properties of cement pastes

Cement (curing condition)	Temperature [°C]	Bending strength [MPa]	Compressive strength [MPa]	Bulk density [kg m^{-3}]
CAC (water)	0	5.47 ± 0.23	78.5 ± 3.2	2077 ± 12
	400	2.14 ± 0.19	76.0 ± 1.8	1760 ± 11
	1000	1.11 ± 0.09	46.9 ± 0.8	1653 ± 25
CAC (air)	0	5.53 ± 0.48	97.4 ± 1.0	2249 ± 9
	400	2.16 ± 0.15	92.1 ± 1.3	1905 ± 7
	1000	1.12 ± 0.07	58.8 ± 2.9	1789 ± 15
PC (water)	0	13.20 ± 1.04	77.6 ± 4.9	2078 ± 12
	400	1.31 ± 0.12	68.0 ± 4.8	1764 ± 2
	1000	0.56 ± 0.07	13.8 ± 0.3	1695 ± 4

7.1.2 Aggregates

Primarily the basalt aggregate was chosen for the preparation of thermal resistant composites. Two grades (0/4 and 2/5) of crushed aggregate [143] were taken from the quarry in Dobkovičky of Kámen Zbraslav, a. s. As it can be seen in Figure 12, used aggregate composed mainly of pyroxenes (specifically of clinopyroxene and augite and in lower amounts diopside), succeeded by analcime, anorthite, musciovite, and in lower amounts by nepheline. However due to the similar and non-defined composition of pyroxenes and plagioclase (specifically anorthite), precise quantitative analysis from XRD measurement cannot be performed. Chemical composition and quantitative

determination of basalt aggregate are presented in Table 15. According to achieved results used aggregate can be identified as basalt.

As in the case of cement, also aggregates were of a two kind and as the reference material ordinary used silica sand was chosen. Specifically four grades (0.1/0.6, 0.3/0.8, 0.6/1.2 and 1/4) of sand [144] originated in Sklopísek Střeleč a.s. were used in mixture design. This material composed entirely of quartz, respectively of silica oxide (Table 15).

Table 15 Chemical composition of used aggregate (XRF)

Component	CaO	Al_2O_3	Na_2O	SiO_2	MgO	Fe_2O_3	K_2O	TiO_2	P_2O_5
Basalt aggregate	12.8	17.2	4.2	41.9	7.2	11	0.9	3.2	1
Silica sand	-	-	-	99.4	-	0.02	-	-	-

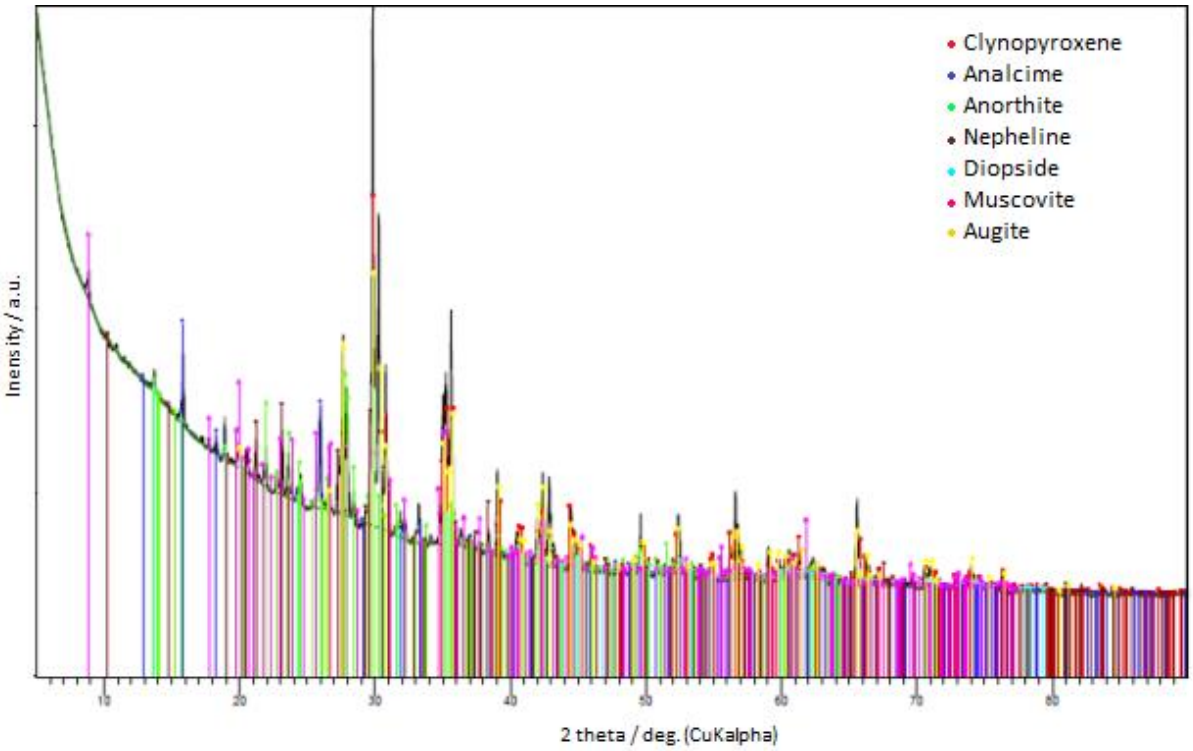

Figure 12 XRD pattern of Basalt aggregate

Particular amounts of used grades of both aggregates were set with respect of reaching an optimal continuous granulometric curves in the area of applicable granularity according standard [145]. Another goal was to reach granulometric curves to be as similar as possible. The designed composition and particular granularity is presented in Table 16 and Figure 13.

Table 16 Designed composition of aggregate gradings

Aggregate	Basalt aggregate		Silicate sand			
Grading	0/4	2/5	0.1/0.6	0.3/0.8	0.6/1.2	1/4
Amount [%]	80	20	25	5	15	55

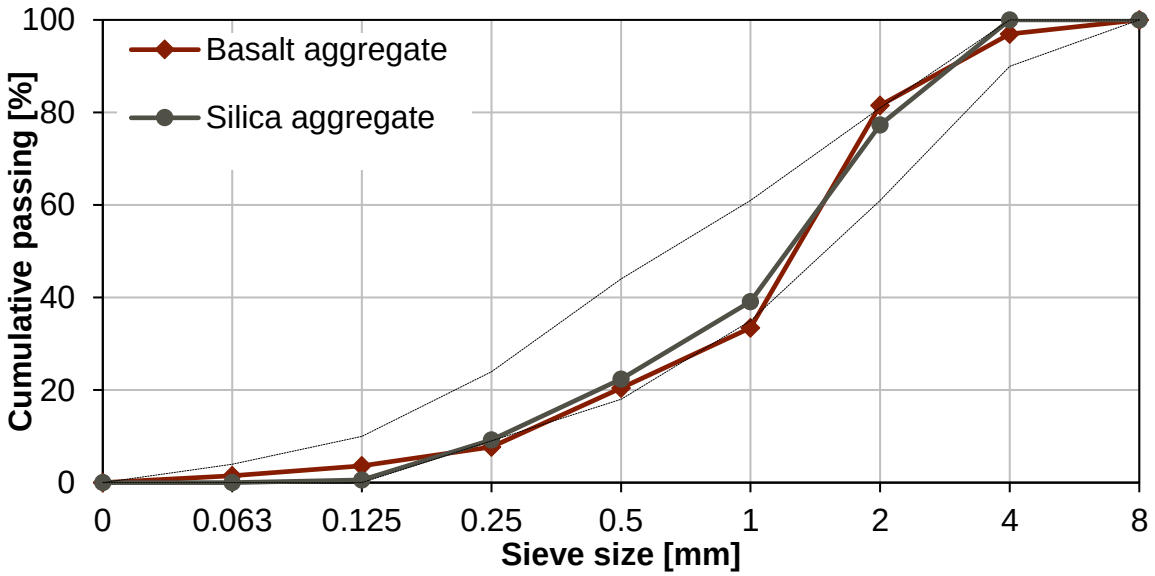

Figure 13 Granulometry of used aggregates

7.1.3 Fibres

Due to their appropriate properties and assumed good compatibility with other raw materials, basalt fibres were chosen for reinforcing designed composites from many possibilities of material kind. Company Basaltex, a.s. produced many kind of basalt fibres varying in their length; they proposed 3.2 mm, 6.35 mm, 9.5 mm and 12.7 mm. For the purpose of this study, 12.7 mm was primarily chosen. In the second part also the combination of different fibres length was examined, specifically the combination of 12.7 mm and 6.35 mm. The diameter of used fibres is 13 μm and their chemical composition is presented in Table 17, while in Table 18 physical properties of the fibres [146] can be found. The fibres were coated with a silanes based sizing, the amount of lubrication was approximately 1 – 1.5%.

Table 17 Chemical composition of used basalt fibres (XRF)

	CaO	**Al_2O_3**	**Na_2O**	**SiO_2**	**MgO**	**Fe_2O_3**	**K_2O**
Basalt fibres	8.92	17.6	2.66	54.39	3.62	9.77	1.66

Table 18 Physical properties of used basalt fibres

Property	**Value**
Bulk density [kg m^{-3}]	2900
Average diameter of fibril [μm]	9 – 12
Content of lubrication [%]	1.0 – 1.5
Moisture content [%]	0.061
Water absorption capacity [%]	0.5
Modulus of elasticity in tension [GPa]	100
Tensile strength [GPa]	1.85 – 2.15
Compressive strength [MPa]	300
Thermal conductivity [W m^{-1} K^{-1}]	0.027 – 0.033
Electric resistance [Ω m]	10^{12}

7.1.4 Others

The remaining components of mixtures were portable water and superplasticizer. The Sika VsicoCrete®-1035CZ [147] based on superplasticizer is based on modified polycarboxylate-ether was used in mixture design.

7.2 Optimization of mixture composition

7.2.1 Cement based composites with combined raw-materials

Optimization of mixture composition was performed experimentally, in several steps. Primarily the appropriate water/cement ratio of calcium aluminate cement was tested. Cement pastes with w/c ratio from 0.2 to 0.45 were prepared, and after 28 days of air curing they were exposed to particular temperature loading (105 °C, 400 °C and 1000 °C) lasted for three hours. Then the measurement of bulk densities, bending strengths and compressive strengths were performed. Achieved results are presented in Table 19. In accordance to the assumption, the lower w/c ratio was used, the higher mechanical strengths of cement pastes were measured. However, due to the deterioration of properties in the case of w/c ratio of 0.2, this one was proved to be insufficient. Cement pastes with w/c ratio of 0.25 achieved the best properties not only in the reference state (105 °C); but this cement paste showed also the lowest deterioration of measured properties due to the temperature exposure.

Table 19 Optimization of water/cement ratio

w/c	Compressive strength [MPa]			Bending strength [MPa]			Bulk density [kg m^{-3}]		
	105° C	400 °C	1000 °C	105 °C	400 °C	1000 °C	105 °C	400 °C	1000 °C
0.20	99.8 ± 2.4	82.7 ± 4.0	40.0 ± 1.5	4.05 ± 0.27	2.12 ± 0.12	0.57 ± 0.04	2116 ± 10	1924 ± 18	1665 ± 10
0.25	**103.9** ± 3.2	**98.0** ± 3.8	**59.8** ± 2.1	**5.36** ± 0.31	**2.34** ± 0.09	**1.68** ± 0.08	**2206** ± 15	**1947** ± 9	**1852** ± 7
0.30	97.4 ± 1.8	92.1 ± 1.7	58.8 ± 3.0	5.53 ± 0.15	2.16 ± 0.15	1.12 ± 0.06	2249 ± 8	1905 ± 6	1789 ± 10
0.35	76.5 ± 4.7	54.6 ± 2.1	28.8 ± 1.8	3.37 ± 0.27	1.87 ± 0.21	0.39 ± 0.02	1848 ± 21	1719 ± 16	1379 ± 9
0.40	54.7 ± 1.9	44.0 ± 3.8	22.7 ± 1.5	2.05 ± 0.18	0.91 ± 0.04	0.16 ± 0.01	1700 ± 13	1632 ± 14	1301 ± 21
0.45	45.8 ± 2.3	27.2 ± 1.9	16.4 ± 1.2	1.77 ± 0.10	0.60 ± 0.02	0.19 ± 0.03	1671 ± 7	1579 ± 19	1219 ± 12

The second optimization was focused on the fibres amount. The basalt fibres with length 12.7 mm were used. The experimental measurement was similar as in the case of w/c ratio, but this time the investigated material was fibre reinforced cement based composites. Specifically, mixtures composed of calcium aluminate cement (900 kg m^{-3}), basalt aggregates (1100 kg m^{-3}), and varying amount of fibres. The quantity of used fibres changed according to the logarithmical sets from a minimum of 0.25 up to 4 % of the volume of the mixture. W/c ratio was 0.25 and it was constant in all studied mixtures. The last component of the mixtures was superplasticizer, which was added in higher amounts (2.5% of cement weight). Such high portion was necessary especially in the case of higher fibre percentage. Due to the superplasticizer, the workability of fresh mixture was improved considerably and thus these mixtures could be prepared. Achieved results are presented in the Table 20. In the lower amount of fibres, they severed as reinforcing agent. However, in the higher percentage (above 0.5%) the agglomerations of fibres were observed. This led to decrease of the compressive strengths.

Table 20 Optimization of fibres amount

Fib. [%]	Compressive strength [MPa]			Bending strength [MPa]			Bulk density [kg m^{-3}]		
	105° C	400 °C	1000 °C	105 °C	400 °C	1000 °C	105 °C	400 °C	1000 °C
0	38.2 ± 1.1	19.9 ± 1.2	15.0 ± 0.7	4.16 ± 0.2	1.68 ± 0.07	1.20 ± 0.05	2330 ± 42	2260 ± 21	2185 ± 29
0.25	51.5 ± 2.4	41.0 ± 2.3	21.7 ± 0.9	10.56 ± 0.51	4.56 ± 0.12	2.72 ± 0.14	2280 ± 10	2175 ± 12	2130 ± 41
0.5	**58.1** ± 3.1	**43.7** ± 1.9	**29.0** ± 1.3	**11.12** ± 0.52	**4.72** ± 0.18	**2.96** ± 0.05	**2440** ± 18	**2320** ± 7	**2270** ± 10
1	50.7 ± 2.8	37.6 ± 1.5	21.1 ± 1.1	10.72 ± 0.53	4.96 ± 0.19	2.96 ± 0.09	2250 ± 6	2180 ± 14	2121 ± 9
2	46.6 ± 2.3	34.5 ± 2.0	23.8 ± 0.8	9.84 ± 0.45	5.28 ± 0.26	3.04 ± .017	2400 ± 19	2225 ± 13	2210 ± 5
4	41.7 ± 1.9	29.7 ± 1.2	16.9 ± 0.5	9.60 ± 0.2	4.64 ± 0.31	3.12 ± 0.19	2186 ± 7	2072 ± 8	1954 ± 21

The last performed optimization was focused on a superplasticizer utilisation. This experiment was performed not only by measurement of basic mechanical properties but also by measurement of the consistency of fresh mixtures with employment of flow table. Studied mixtures were composed of calcium aluminate cement (900 kg m^{-3}), basalt aggregates (1100 kg m^{-3}), basalt fibres (14.5 kg) and superplasticizer Sika ViskoCrete-1035CZ. W/c ratio was constant for all mixtures and it was 0.25. Range of superplasticizer amount was set from 0% up to 2.5% of cement weight. Results of mechanical properties are summarized in Table 21, while in Table 22 different flows can be found. Mixture without plasticizer was not possible to mix, the lowest amount of plasticizer was therefore 0.2%. With growing amount of used plasticizer, the flow grew up. Regarding the mechanical properties, they increased up to 1.5% of w/c ratio. Exceeding this value led to the deterioration of mechanical strengths.

Table 21 Optimization of superplasticizer amount – mechanical properties

SP [%]	Compressive strength [MPa]			Bending strength [MPa]			Bulk density [kg m^{-3}]		
	105° C	400 °C	1000 °C	105 °C	400 °C	1000 °C	105 °C	400 °C	1000 °C
0.2	44.3 ± 3.2	31.5 ± 2.0	12.7 ± 0.7	8.40 ± 0.93	2.38 ± 0.13	1.99 ± 0.08	2266 ± 7	2324 ± 15	2163 ± 38
0.5	64.5 ± 4.7	45.6 ± 1.4	31.6 ± 0.5	9.14 ± 0.68	4.60 ± 0.57	3.62 ± 0.35	2452 ± 20	2452 ± 14	2452 ± 18
1	61.8 ± 3.8	48.8 ± 0.9	26.1 ± 1.1	10.01 ± 0.99	5.15 ± 0.50	2.68 ± 0.19	2465 ± 11	2443 ± 6	2377 ± 19
1.5	**95.9** ± 1.9	**75.4** ± 5.3	**39.5** ± 0.8	**13.40** ± 1.75	**6.60** ± 0.94	**4.30** ± 0.16	**2401** ± 10	**2443** ± 20	**2435** ± 16
2	73.6 ± 7.0	57.7 ± 2.7	33.4 ± 0.4	12.57 ± 1.10	5.61 ± 0.56	3.64 ± 0.16	2441 ± 20	2442 ± 37	2448 ± 11
2.5	58.1 ± 5.4	43.7 ± 3.8	29.0 ± 0.7	11.12 ± 0.15	4.72 ± 0.04	2.96 ± 0.33	2440 ± 7	2320 ± 17	2270 ± 25
3	44.5 ± 2.3	23.0 ± 1.3	15.2 ± 0.7	8.08 ± 0.63	2.74 ± 0.18	1.76 ± 0.08	2400 ± 16	2363 ± 15	2321 ± 10

Table 22 Optimization of superplasticizer - flow

SP [%]	0	0.2	0.5	1	**1.5**	2	2.5	3
Flow [mm]	-	105 /110	125 /130	140 /150	**165 /165**	180 /180	190 /200	210 210

With the respect of the hereinabove presented results, final mixture was designed. The aim of this work was not only to design cement-based composites with better thermal resistivity, but also to analyse the influence of partial raw-materials. Therefore, several mixtures with combined raw-materials were prepared. Their composition is shown in Table 23. The production process was as follows: primarily dry components (aggregate and cement) were properly mixed. Then a portion of water containing plasticizer was added. After a few minutes of additional mixing, fibres were gradually added. Finally, the remaining water was poured in. The resulting fresh mixtures were put into a specific mould. Specimens were made in laboratory condition (temperature 20 ± 1°C and relative humidity 25 – 30%).

Table 23 Mixture composition of composites with combined raw-materials [kg m^{-3}]

Component	PSR	PBR	PSF	PBF	CSR	CBR	CSF	CBF
Calcium aluminate cement	-	-	-	-	900	900	900	900
Portland cement	900	900	900	900	-	-	-	-
Silicate Aggregates 01/06	275	-	275	-	275	-	275	-
Silicate Aggregates 03/08	55	-	55	-	55	-	55	-
Silicate Aggregates 06/12	165	-	165	-	165	-	165	-
Silicate Aggregates 10/40	605	-	605	-	605	-	605	-
Basalt Aggregates 0/4	-	880	-	880	-	880	-	880
Basalt Aggregates 2/5	-	220	-	220	-	220	-	220
Basalt Fibres 12 mm	-	-	14.5	14.5	-	-	14.5	14.5
Plasticizer	13.5	13.5	13.5	13.5	13.5	13.5	13.5	13.5
Water	225	225	225	225	225	225	225	225

7.2.2 Cement based composites with combined fibres length

The part of this investigation was also the assessment of possible advantages of fibres length combination. For this part, designed composite CBF composed of calcium aluminate cement, basalt aggregate, superplasticizer and basalt fibres were chosen. The amount of basalt fibres was set constant, while the ratio of longer and shorter fibres was variable. As it was mentioned hereinabove, the specific lengths were 12.7 mm and 6.4 mm. Primarily, eleven mixtures were prepared and basic mechanical strengths and bulk densities were measured. Achieved results can be found in Table 24. Regarding the compressive strengths, final values varied by about 8% and no specific trend was observed. The influence of fibre combination was more noticeable in the case of the bending strength, where the difference between the smallest and the biggest values was 34%. With the increasing amount of shorter fibres, the bending strength slowly decreased. From that perspective, values of bending strength were the main aspect when choosing the appropriate fibres ratio. For the further research the ratio 100:0, 90:10 and 80:20 were chosen. Specific composition of these mixtures is shown in Table 25, and the production process was same as in the previous cases of cement based composite with different raw materials.

Table 24 Optimization of fibres length ratio

Ratio of fibres 12.7 : 6.4 mm	Compressive strength [MPa]	Bending strength [MPa]	Bulk density [kg m^{-3}]
100:0	**95.9** ± 1.8	**13.40** ± 0.71	**2401** ±12
90:10	**103.6** ± 2.9	**14.45** ± 1.26	**2400** ± 5
80:20	**88.8** ± 1.4	**13.06** ± 0.71	**2397** ± 24
70:30	94.8 ± 1.1	11.91 ± 0.74	2413 ± 10
60:40	88.6 ± 1.9	11.03 ± 0.56	2401 ± 14
50:50	93.4 ± 1.0	11.51 ± 0.79	2398 ± 19
40:60	98.1 ± 1.2	10.77 ± 0.84	2451 ± 17
30:70	92.1 ± 1.7	10.40 ± 1.11	2414 ± 28
20:80	99.1 ± 2.6	10.28 ± 0.49	2398 ± 31
10:90	101.8 ± 2.3	9.47 ± 0.57	2380 ± 6
0:100	94.3 ± 3.3	10.86 ± 1.34	2413 ± 30

Table 25 Mixture composition of composite with different fibres ratio

Component	CBR	CBF0	CBF1	CBF2
Calcium aluminate cement	900	900	900	900
Basalt Aggregates 0/4	880	880	880	880
Basalt Aggregates 2/5	220	220	220	220
Basalt Fibres 12.7 mm	-	14.5	13.05	11.6
Basalt Fibres 6.4 mm	-	-	1.45	2.9
Plasticizer	13.5	13.5	13.5	13.5
Water	225	225	225	225

7.3 Thermal loading of studied materials

7.3.1 Thermal analysis of raw-materials

Thermal analysis of all used raw-materials was performed. Primarily the different cement was of importance but also the aggregate and the fibres were tested. Results of thermogravimetry are presented in Figure 14 and differential scanning calorimetry curves can be found in Figure 15.

The major changes due to the temperature loading were observed in the case of Portland cement paste. Measured curve and particular peaks were in accordance with the already well-known processes [148, 149, 150]. Changes above the 100 °C to

150 °C were connected with the loss of free water. In this range, also the dehydratation of CSH became (this process continued up to 400 °C). In the range of 100 °C to 200 °C, sulfoaluminates (in the order of ettringite, gypsum and monosulphate) dehydrated and physically bounded water disappeared. Second major peak in temperature range of 450 °C to 500 °C correspond with decomposition of portlandit. The last peak of DSC curve (temperature above 700 °C to 800 °C) of Portland cement is decomposition of calcium carbonate (in the form of calcite and vaterite).

The second major changes were measured in the case of CAC paste; however the thermal changes of this material will be described in more detail in the following chapter 7.3.2.

Regarding the other components, their mass changes were so small, compared with both kinds of cement. After 1000 °C the decrease was less than 2%; in the case of basalt fibres even less than 0.6%. This is one of the important factors, which affects the thermal resistance of presented material. The low mass changes of basaltic materials were in accordance with other researchs [39, 40, 151, 152, 153] and they were mostly attributed to the liberating pore water or water-bearing mineral-phases (e.g. analcime or muscovite). However, the DSC curves of basalt varied in all cases of mentioned works. It could be caused by a different composition of studied basalts. In the case of the basalt fibres, the minor endothermal peak (comparing to basalt aggregate) in temperature about 400 °C were observed. This could be attributed to the removal of organic coating of fibres [154]. In higher temperatures (above 700 °C) both basaltic materials showed exothermal peaks. The used basalt aggregate as well as basalt fibres contained high amount of iron (by about 10%, see Table 15 and Table 17) which led to the crystallization of magnesioferrite and hemaitite, and subsequent also recrystallization of pyroxenses and plagioclase [154, 155]. This crystallization process led to the embrittlement of material (especially in the case of the fibres) and thus caused the decrease of tensile strength [151].

When focused on silica sand behaviour the changes are also really minuscule. In the temperature about 573 °C, there is significant discontinuity which present the quartz recrystallization (transformation from β to α-quartz modification). Despite that, this process should not be visible due to its reversibility it was observed also by other research [39, 40]. It was caused probably by a small resolution of performed measurement. The second recrystallization process of quartz in the studied temperature range is transformation of α-quartz to β-tridymite, which take place in

temperatures about 870 °C. Also this transformation should not be visible, but were observed as a small shift of the heat flow curve.

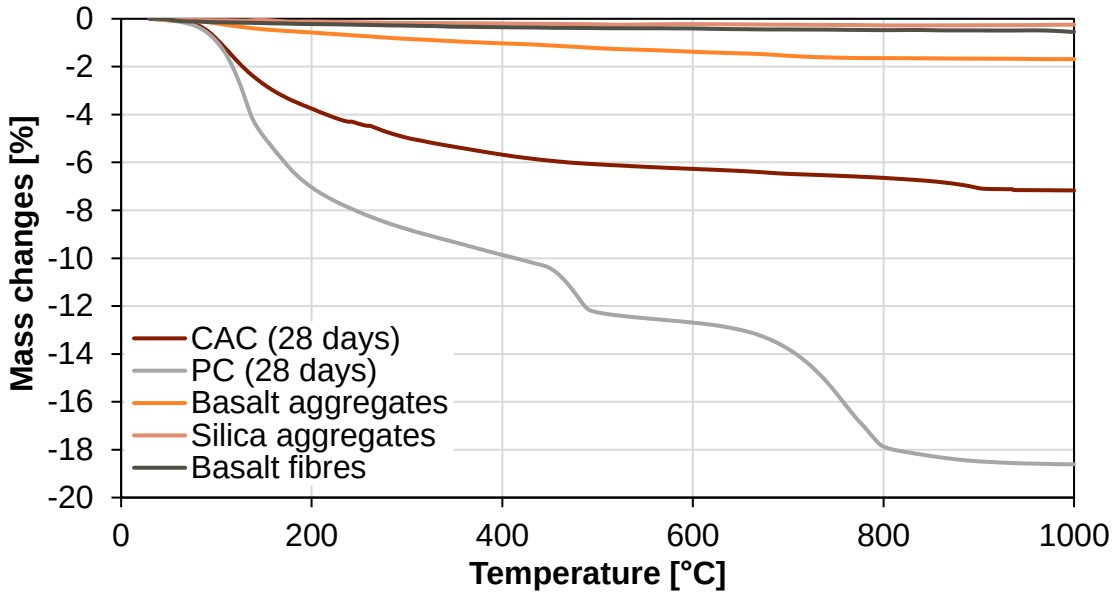

Figure 14 Thermogravimetry of raw-materials

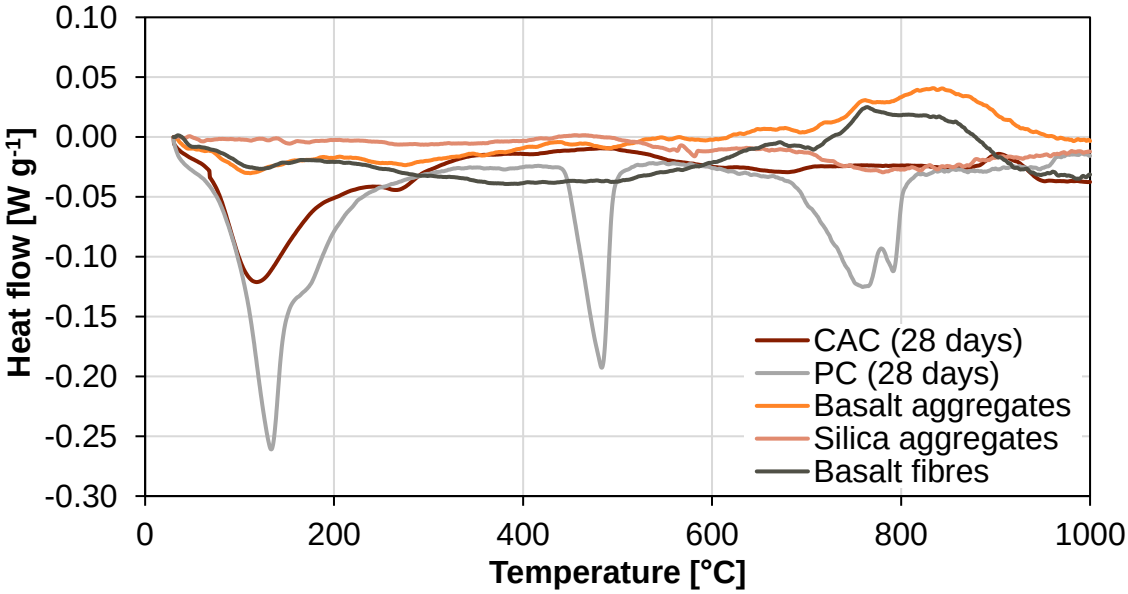

Figure 15 Differential scanning calorimetry curves of raw-materials

7.3.2 Thermal analysis of CAC

Results of thermogravimetry (TG) and differential scanning calorimetry (DSC) are shown in Figure 16 and Figure 17 respectively. This measurement was performed on raw cement and cement pastes in varying age: 2 days, 7 days, 28 days, 90 and 180 days. Calcium aluminate cement showed one visible peak in temperature range from 240 °C to 300 °C. This corresponds to the tricalcium-hexaluminate (C_3AH_6)

temperature decomposition, which raw cement contained 0.6%. However, when focused on TG of raw cement, CAC showed great thermal stability. The change of mass in the mentioned temperature range was less than 0.23%. The second important change was found at temperature over 850 ºC. There were no mass changes during this temperature range, and it could correspond with recrystallization of calcium dialuminate (CA_2).

Regarding the results of cement pastes, similar processes occurred in temperature exposure in all case of varying ages. The main different was found in the amount of reacted material. The older cement paste was the more mass was released during the heat treatment. It signified the higher degree of the hydration process. Generally, processes in temperatures up to 120 °C [71] are connected with the loss of free water in capillary pores and bound water in aluminate hydrate gel (AH_3). The first endothermic peak in temperature about 120 °C do correspond with dehydration of calcium aluminate decahydrate (CAH_{10}). Decomposition temperature of this hydrate ranged from 100 °C to 160 °C [56, 148] and in 28 days cement paste lost 3% of its weight up to the temperature of 160 °C. There were not any significant peaks observed in decomposition temperatures of the other two calcium aluminate hydrates, so it can be conducted that the other calcium aluminate hydrates (C_2AH_8 and C_3AH_6) are presented in minor amounts. Dicalcium aluminate octahydrate (C_2AH_8) dehydrated in temperatures about 140 °C to 240 °C [56, 71, 148] , and its presence could be hidden by major peaks of calcium aluminate decahydrate (CAH_{10}) and the multiple one of gibbsite (AH_3, 210 °C – 320 °C [71, 148]) and tricalcium aluminate hexahydrate (C_3AH_6, 240 °C – 370 °C [56, 71]). Gibbsite (crystalline AH_3) and stable katoite (C_3AH_6) was not form during the hydration process in higher amount, but they rose as a product of the temperature decomposition of thermodynamically unstable hydrates (CAH_{10} and C_2AH_8). Katoite (C_3AH_6) dehydration gave rise to the dodecacalcium heptaaluminate hydrate ($C_{12}A_7H$) that decomposed at temperatures about 750 °C [71]. However according to our results this reaction occurred earlier, at about 690 °C. As a product occurred dehydrated re-new phase of dodecacalcium heptaaluminate ($C_{12}A_7$), which is later in temperatures over 900 °C recrystallized to calcium aluminates (CA and CA_2). The biggest mass changes were caused by the dehydration of common calcium aluminate hydrates; up to the temperature of 370 °C cement paste lost almost 5.5% (at the age of 28 days) of it mass and taking into the account absolute dehydration at 690 °C the mass fall was almost 6.5% (at 28 days).

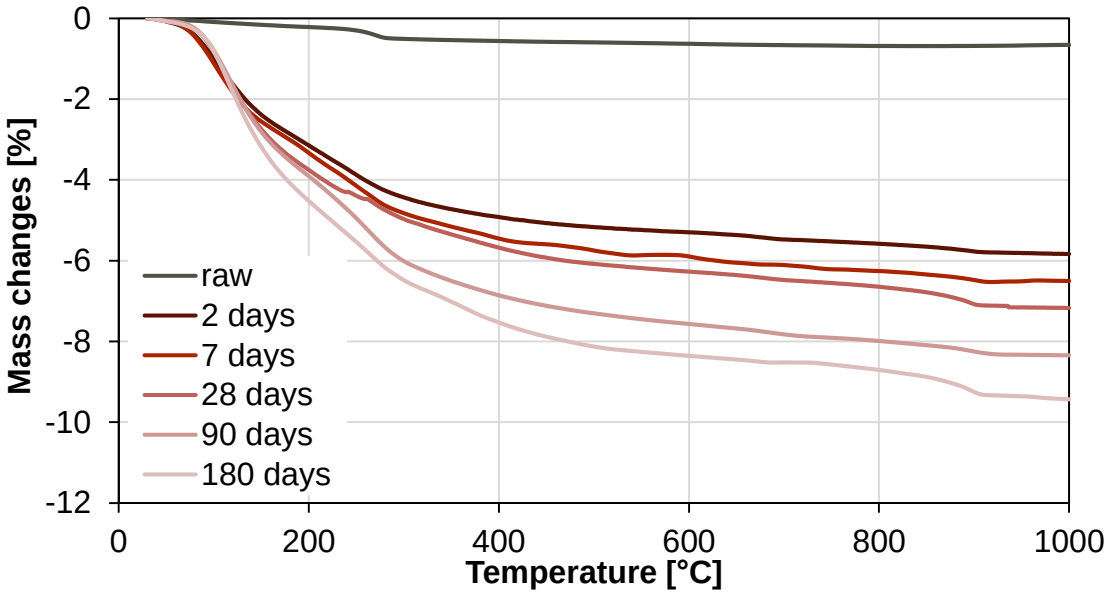

Figure 16 Thermogravimetry of CAC pastes in time

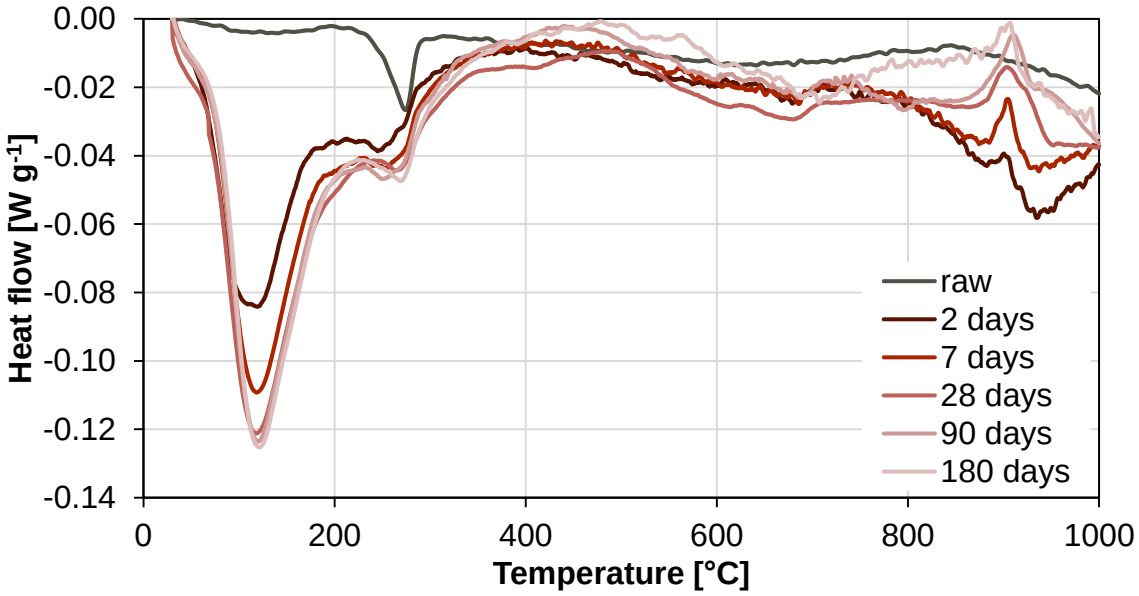

Figure 17 Differential scanning calorimetry curves of CAC pastes in time

For the sake of better comprehension of changes due to the temperature exposure, XRD pattern of cement paste after exposure to 1000 ºC was determined, it can be found in Figure 18. In comparison with material without temperature loading (Figure 11), and with accordance with hereinabove mentioned dehydration processes, CAC paste after temperature exposure composed only of anhydrous phase. Due to dehydration calcium aluminate hydrates, CA and CA_2 and $C_{12}A_7$ re-became the main components. While due to the decomposition of aluminate hydrate AH_3, the β alumina (β-A) occurred. When compared with not hydrated CAC (Figure 8) the patterns were

almost similar. Only significant differences were observed in the case of calcium-aluminate (CA) amount, which the peaks were twice as higher in the case of raw cement. There was no real explanation of this difference. However, this seemed to be caused just by the error of measurement. In the pattern on Figure 18, there were two peaks really close peaks in the position of 35.1 2theta. This double peaks of diffractions were in the case of raw-cement observed in one position and thus proposed twice time higher intensity. Another minor vary was presence of alumina in raw cement, while in the case of unhydrated cement paste there was observed just β-alumina ($NaAl_{11}O_{17}$). The last noticed difference was found in the case of katoite (C_3AH_6), which was naturally observed just in the case of raw cement.

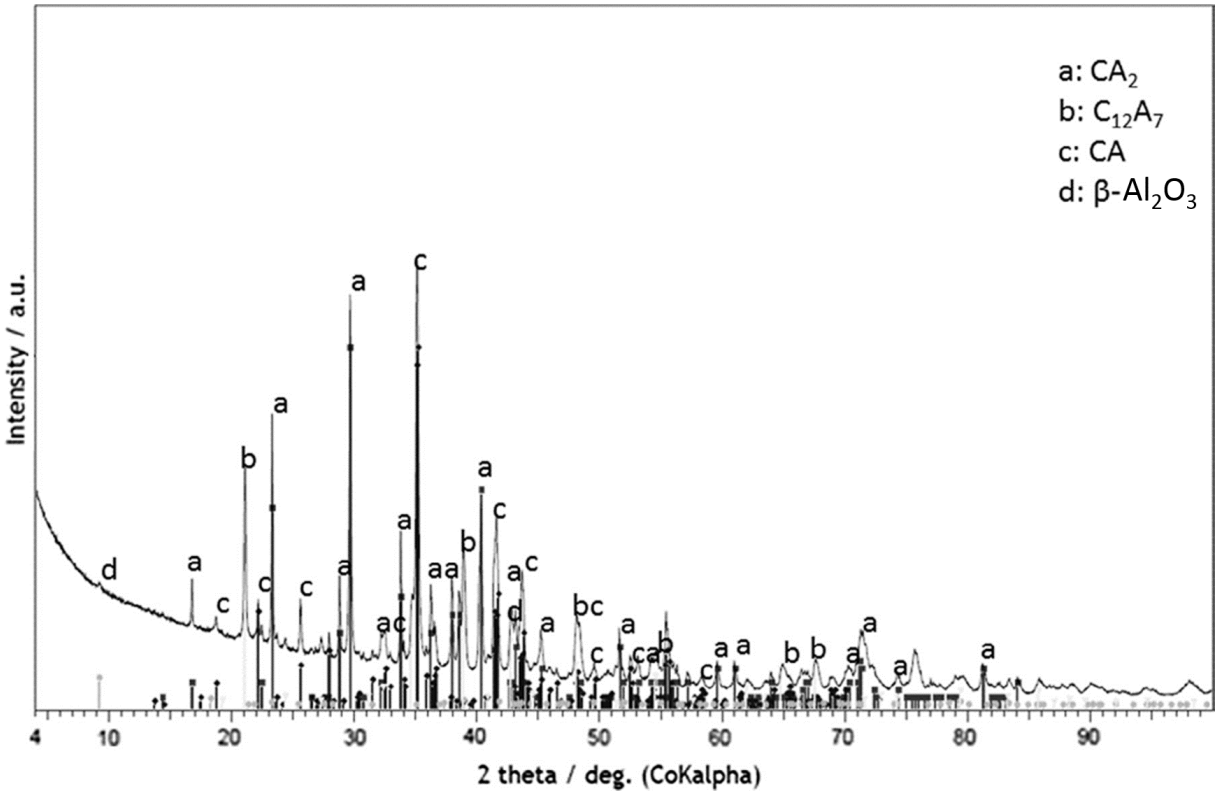

Figure 18 XRD pattern of CAC paste thermally pre-treated at 1000 ºC

7.3.3 Thermal loading of cement based composites

With the respect to results of thermogravimetry and differential scanning calorimetry of raw materials, two temperatures for thermal pre-treatment of cement composites were specified. The most important factor, when choosing appropriate temperatures, was the behaviour of calcium aluminate cement. The first thermal loading temperature was 400 °C, where just dehydration process passed. Processes up to 400 °C comprehended releasing of free and physically bounded water,

dehydration of hydrates (calcium aluminate hydrates or calcium silicate hydrates) and decomposition of sulfoaluminates. The second temperature was 1000°C, when all described recrystallization and decomposition processes were finished, but raw-materials weren't melted.

Temperature pre-treatment was done in a special electric top-cover furnace. Because of evaporating free water from inner pore structure, specimens were dried in an oven at 105 °C for 24 hours before temperature exposure. They were then put in the furnace with heating rate 0.5 °C per min. After reaching a particular temperature (400 °C or 1000 °C), samples were exposed to that temperature for 3 hours. Cooling was spontaneous and also took place in the furnace. Reference series with no temperature loading was also prepared; those specimens were dried in the oven at temperature 105 °C.

8 Achieved results and discussion

8.1 Cement based composites with combined raw-materials

8.1.1 Basic physical characteristics

8.1.1.1 Basic physical properties

Basic physical properties measured by water vacuum saturation method and for the sake of comparison also by helium pycnometry in combination with gravimetric method. Values of bulk density are shown in Figure 19 and Figure 20 respectively for varying measurement methods. Pycnometry generally proposed somewhat smaller values of bulk density, especially after temperature exposure. The difference was caused by the accuracy of used methods. The influence of different cement was not very big in the reference state; bulk densities varied by about 1%. Regarding the influence of varying aggregates, utilisation of basalt leads to the composites, which had in average by about 7% higher bulk densities than in the case of silica aggregates. Less difference could be observed when fibres were employed; the change of bulk densities were by about 3%. When focus on thermal stability, the biggest changes, due to the temperature exposure of 1000 °C, could be observed in the case of utilisation of Portland cement with silica aggregate. In average the deterioration of bulk densities of those composites were about 18%. Because of the strongly weakened materials (both cement and aggregate were seriously deteriorated due to the temperature loading) utilisation of fibres had no advantageous effect. As it should be assumed, the best results were obtained by the composite composed of calcium aluminate cement, basalt aggregate and basalt fibres. In that case, the change of values of bulk density was 1%.

Higher bulk density of concrete based on basalt aggregate in comparison with sandstone was presented also by Hager et al. [39]; the difference was same in reference state and after exposure to 400 °C, in average by about 200 kg m^{-3}.

Bulk density of basalt aggregate based composite designed by Bondárová et al. [112] was slightly higher than at this work. However, when compared the deterioration due to the thermal exposure, their best results was decrease by about 3.3% (in contrast with 1% reached in this work) after 800 °C, reached by composite with CEM III/B 32.5, basalt aggregate and steel fibres. When focused on impact of fibres, they reported residual bulk density after 800 °C by about 0.6% higher due to the steel fibres, while in

this work the improvement at 1000 °C due to the basalt fibres was 1.4% (when PC and basalt aggregate was used).

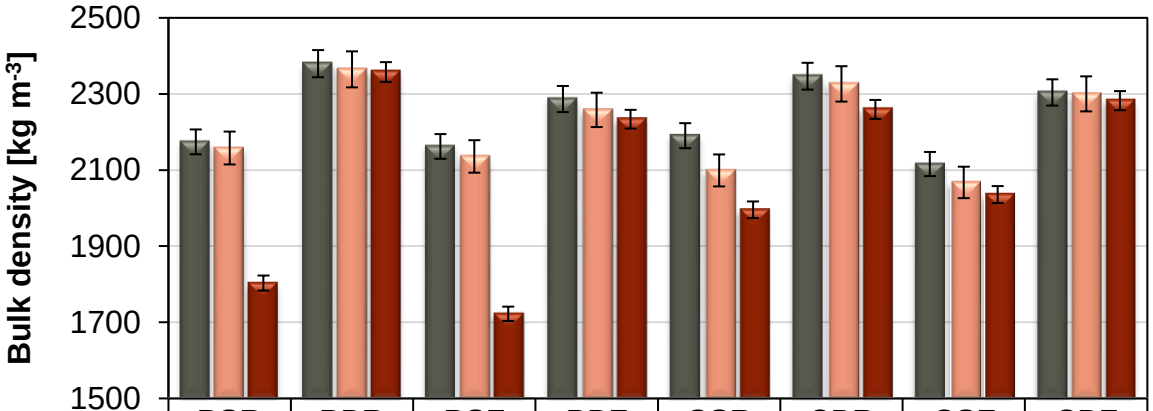

	PSR	PBR	PSF	PBF	CSR	CBR	CSF	CBF
105 °C	2174	2380	2162	2287	2190	2347	2116	2304
400 °C	2158	2365	2136	2258	2099	2326	2068	2300
1000 °C	1803	2358	1722	2234	1996	2259	2036	2282

Figure 19 Bulk densities of composites with combined raw-materials determined by water vacuum saturation

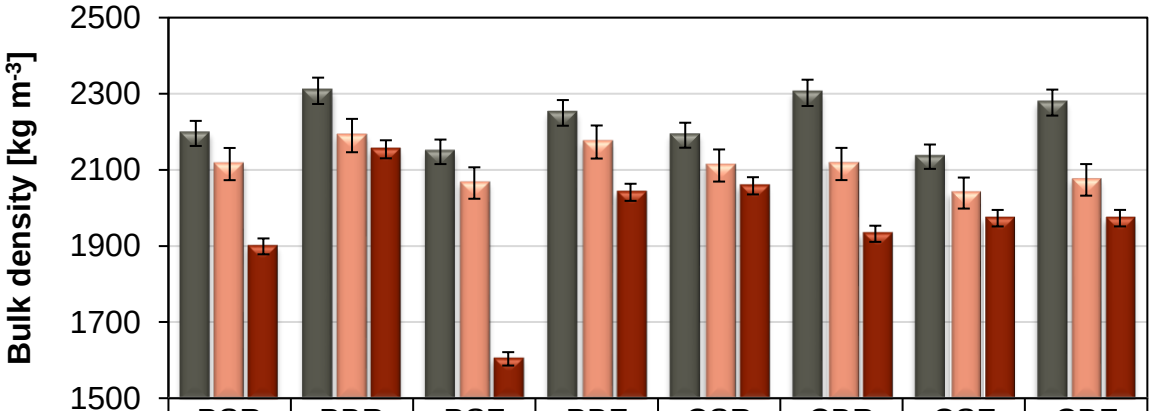

	PSR	PBR	PSF	PBF	CSR	CBR	CSF	CBF
105 °C	2196	2308	2147	2250	2191	2302	2135	2277
400 °C	2115	2190	2065	2173	2111	2115	2039	2074
1000 °C	1899	2154	1603	2041	2058	1932	1973	1973

Figure 20 Bulk densities of composites with combined raw-materials determined by helium pycnometry

Final values of matrix densities are summarized in Figure 21 and Figure 22 respectively. The helium pycnometry proposed higher values of matrix density in reference state in average by 2%. It was caused by the kind of measurement technique, or more precisely by differing diameters of molecules of water and helium which served for volume determinations, and it was assumed that helium pycnometry should provide higher values of matrix densities (especially in the case of materials with higher amounts of smaller pores). However, in the case of thermal pre-treated materials, the matrix densities were lower. Especially when CAC was used the difference was almost 13%. This seemed to be affected by the chemical reaction between renew phases of calcium aluminates with water which led to matrix density increase in the case of water vacuum saturation method. In contrast with hydration of raw-cement, in thermal pre-treated samples to space for hydration product were restricted, which probably to the creation of the denser matrix. In reference state following conclusions can be deduced: Hydration of CAC led to the heavier matrix; values of matrix densities of composites with that cement was by about 8% for water vacuum saturation, respectively 3% for helium pycnometry higher than when ordinary PC was used. In the case of varying aggregate, similar to the bulk densities, composites which composed basalt aggregate reached by about 11%, respectively 3% (higher values than composites with silica aggregate). This result had been assumed because basalt aggregate is heavier than silica aggregate. The influence of basalt fibres on matrix densities of final composites was minimal; values varied by less than 1%. Due to the temperature exposure material transformations occurred; e.g., hydrated phases were decomposed and denser anhydrous minerals were formed. Therefore, the residual matrix densities increased, in average by about 18%, respectively 8% in all cases of the studied composites.

Matrix density of concrete based on PC and CAC was presented in the study from Baradaran-Nasirt and Nematzadeh [108]. They reached slightly higher values in the case of CAC based materials, but the difference was by about 1%. In this thesis the observed growth was 8% or 3% respectively for experimental different methods. Unfortunately, they did not determine basic physical properties after temperature exposure.

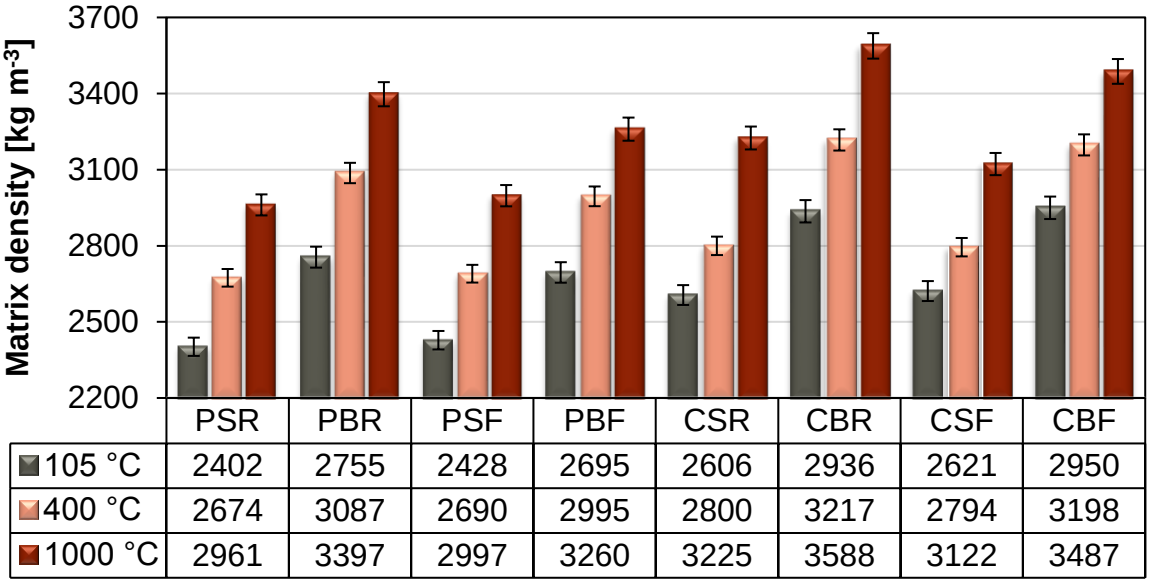

	PSR	PBR	PSF	PBF	CSR	CBR	CSF	CBF
105 °C	2402	2755	2428	2695	2606	2936	2621	2950
400 °C	2674	3087	2690	2995	2800	3217	2794	3198
1000 °C	2961	3397	2997	3260	3225	3588	3122	3487

Figure 21 Matrix densities of composites with combined raw-materials determined by water vacuum saturation

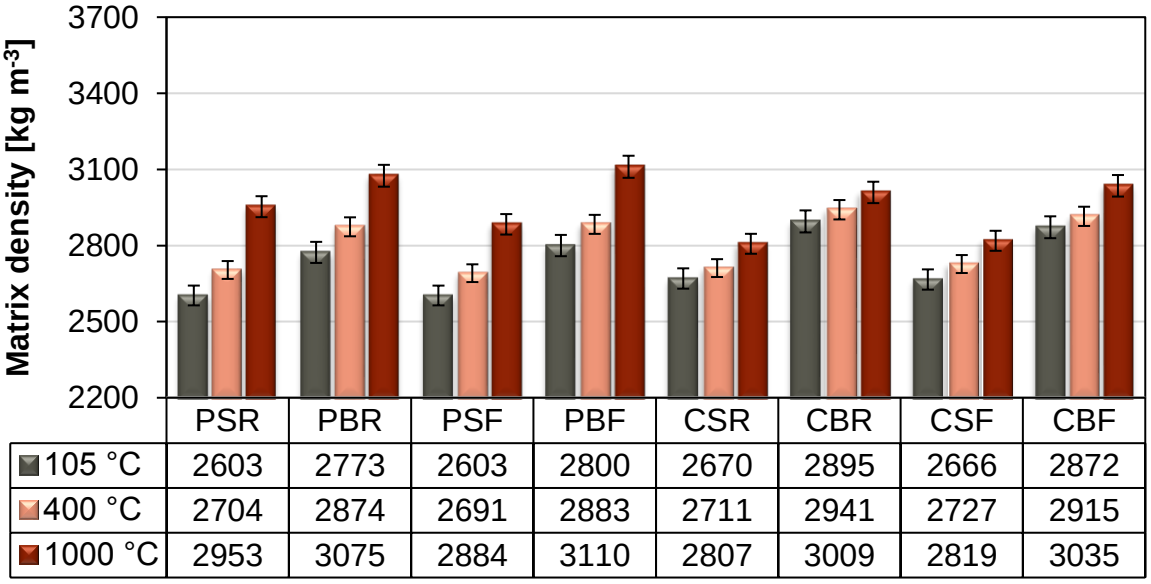

	PSR	PBR	PSF	PBF	CSR	CBR	CSF	CBF
105 °C	2603	2773	2603	2800	2670	2895	2666	2872
400 °C	2704	2874	2691	2883	2711	2941	2727	2915
1000 °C	2953	3075	2884	3110	2807	3009	2819	3035

Figure 22 Matrix densities of composites with combined raw-materials determined by helium pycnometry

The last basic physical characteristic measured by water vacuum saturation method was open porosity. Achieved results are presented in Figure 23 and Figure 24 for water vacuum saturation methods and for helium pycnometry. It is obvious that composites composed of CAC reached in average by 37% (10% respectively in the case of helium pycnometry) higher values of open porosities that the ones with PC. Varying cement had the biggest effect on the final open porosity. Regarding the influence of used aggregates higher values were achieved by composites containing basalt aggregate; the difference was approximately by about 23% and 7% for particular methods. The lowest impact on porosity could be observed in the case of fibre utilisations; open porosity grew up due to reinforcement by about 12% and 11% in average. Anyhow, the influence of temperature exposure was the largest. It is associated with matrix changes (formation of denser hydrates) as well as with aggregate transformations. The biggest increase could be found in the case of PC and silica aggregates; the change, when loading by 1000 °C, the fall was by about 75% respectively 56%. When basalt aggregates were used, the growth was decreased to by about 54% and 44%. Composites with calcium aluminate cement changed the open porosities due to the temperature loading in average by about 46% and 27%. The best results were achieved by composite containing CAC, basalt aggregate, and basalt fibres. The change when exposed to 1000 °C was in that case of raw material combination just 37% measured by water vacuum saturation and 22% by helium pycnometry.

Some results of porosity were found also in Baradaran-Nasirt and Nematzadeh [108] research. They also reached higher values of open porosity in the case of CAC based concrete; but the difference was significantly lower than in this work. They presented in average 3% growth of open porosity due to the CAC utilization, while in this work the difference was about 37% respectively 10%.

Values of open porosity of PC based concrete presented in study by Hager et al [39] was twice time lower in reference state, however in accordance with this work, basalt aggregates showed the lowest growth during heating.

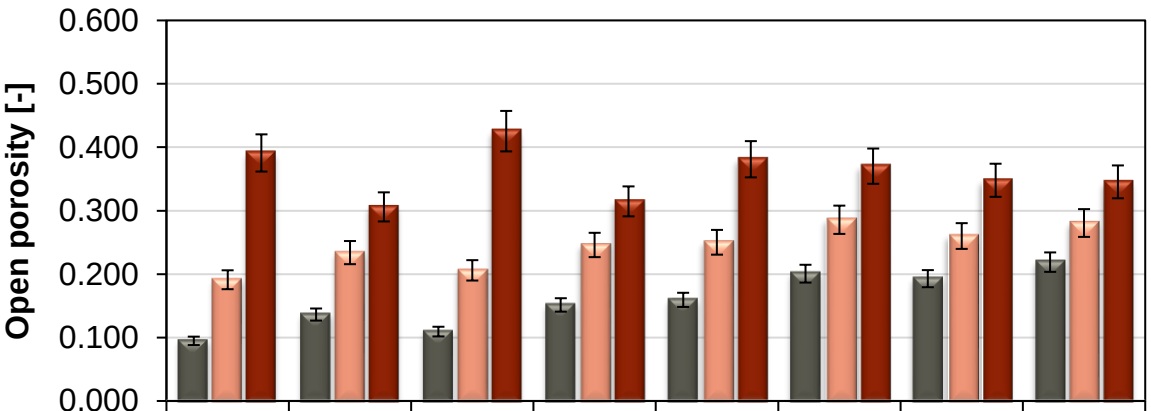

	PSR	PBR	PSF	PBF	CSR	CBR	CSF	CBF
105 °C	0.095	0.136	0.109	0.151	0.159	0.201	0.193	0.219
400 °C	0.191	0.234	0.206	0.246	0.250	0.286	0.260	0.281
1000 °C	0.391	0.306	0.425	0.315	0.381	0.370	0.348	0.345

Figure 23 Open porosities of composites with combined raw-materials determined by water vacuum saturation

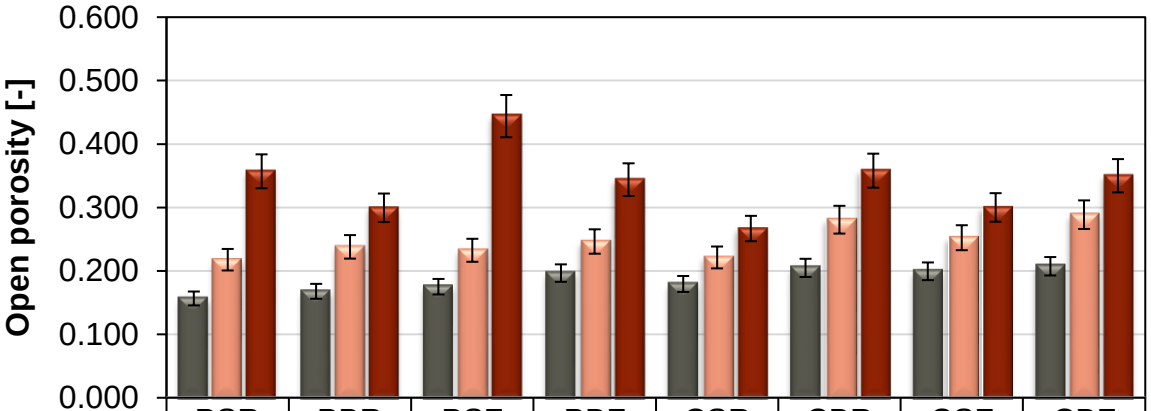

	PSR	PBR	PSF	PBF	CSR	CBR	CSF	CBF
105 °C	0.157	0.168	0.175	0.197	0.179	0.205	0.199	0.207
400 °C	0.218	0.238	0.232	0.246	0.221	0.281	0.252	0.289
1000 °C	0.357	0.300	0.444	0.344	0.267	0.358	0.300	0.350

Figure 24 Open porosities of composites with combined raw-materials determined by helium pycnometry

8.1.1.2 Pore Structure

More detailed description of pore structure changes provided cumulative pore volumes and pore size distribution curves. They are presented in Figure 25 - Figure 27, and Figure 28 - Figure 30 respectively; for the case of better clarity the particular temperature treatments were delineated separately. In the reference state, composites based on the PC confirmed their lower porosity, however they provided higher amount of pores with diameter about 0.1 μm. While in the case of CAC, the distribution of pores is more balanced. Utilisation of basalt aggregate instead of silica sand as well as the fibre reinforcement caused the growth of the pores amount; however it doesn't cause any important changes of pore size distributions. When focused on the influence of temperature loading, the amount of pores increased similarly as in the case of open porosities (Figure 23). In the case of temperature of 400 °C, the cumulative curves got closer, and no specific changes in the pore structure could be seen. By further exposure to 1000 °C the tendencies of pore volumes were reversed; lower results were observed in the case of CAC, basalt aggregate and in general also in the case of fibre reinforcement. Due to the higher temperature loading the pore structures were changed; not only the pores amount went up but also the pore diameters were increased, especially pores in the range of 0.1 μm to 10 μm significantly growth. In the case of PC with silica aggregate the maximal peaks were observed when pores were with the diameter by about 1 μm. The utilisation of basalt instead of silica led to the maximal peaks lowering to diameter by about 0.3 μm. When focused on the CAC the changes were more balanced and no significant modification of pore size distribution were observed.

Despite that, Hager et al. [39] used coarser aggregate, pore size distribution curves of their concretes showed similar tendency; higher amount of pores about 0.1 μm, no matter of aggregates kind. In addition, the lowest growth in the case of basalt aggregate due to the temperature exposure was presented in their work.

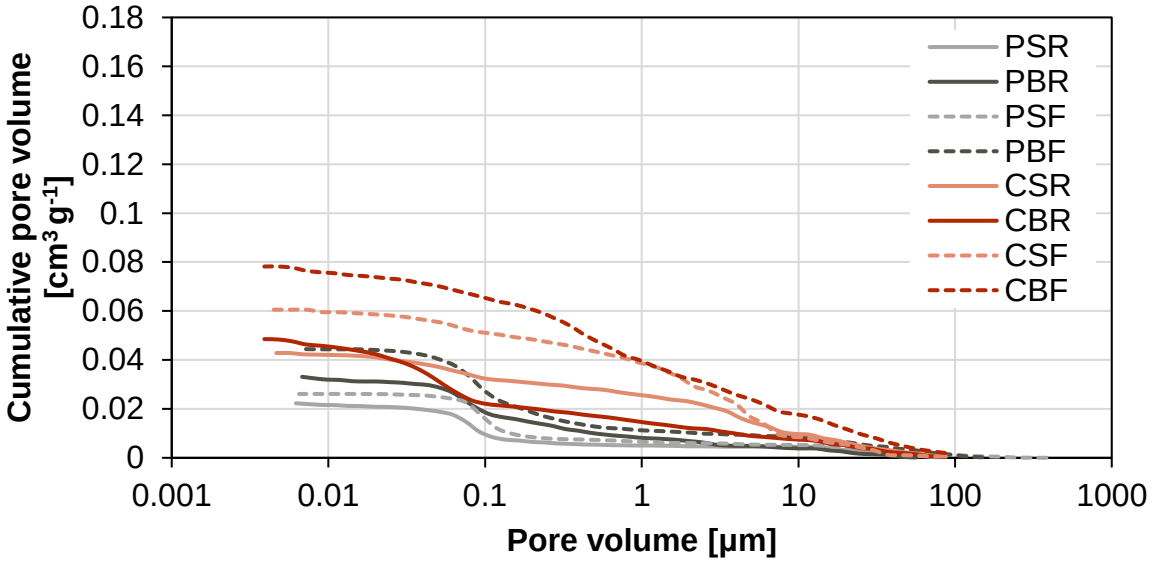

Figure 25 Cumulative pore volumes of composites with combined raw materials in reference state

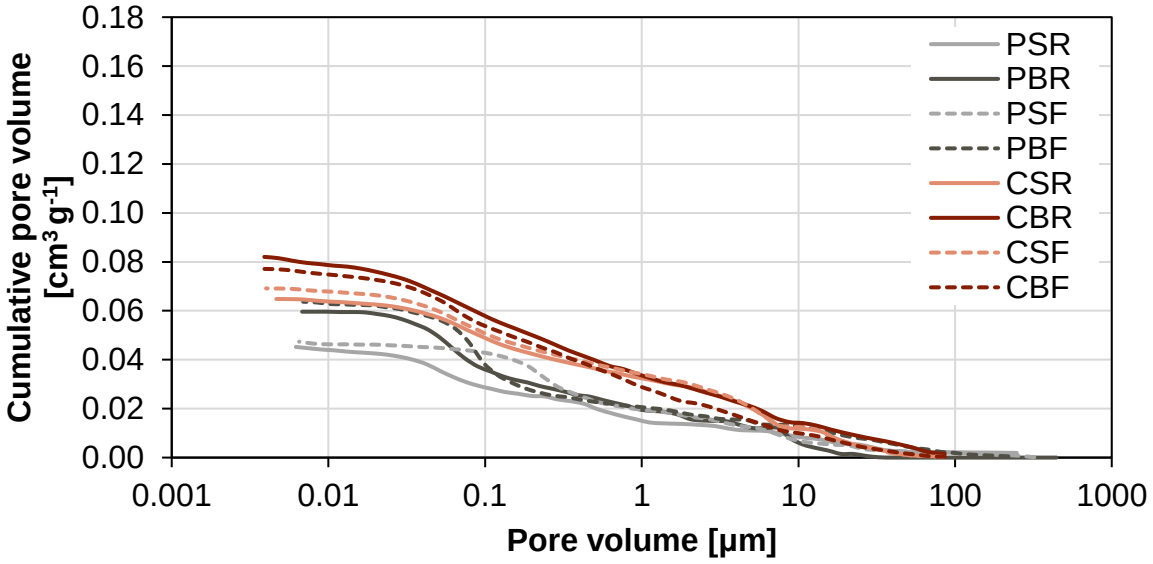

Figure 26 Cumulative pore volumes of composites with combined raw materials after thermal pre-treatment by 400 °C

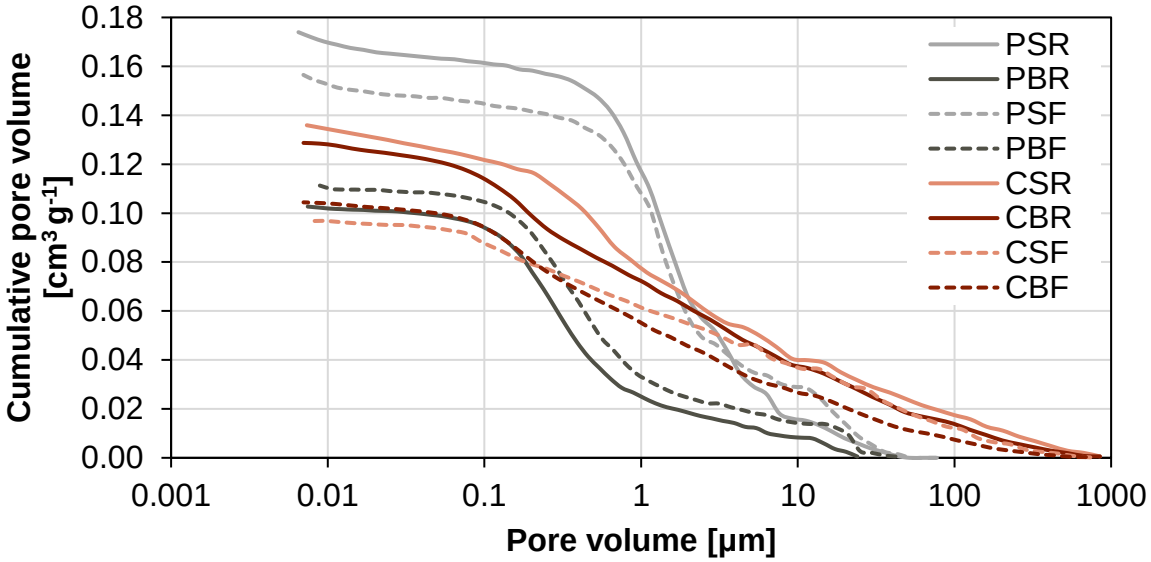

Figure 27 Cumulative pore volumes of composites with combined raw materials after thermal pre-treatment by 1000 °C

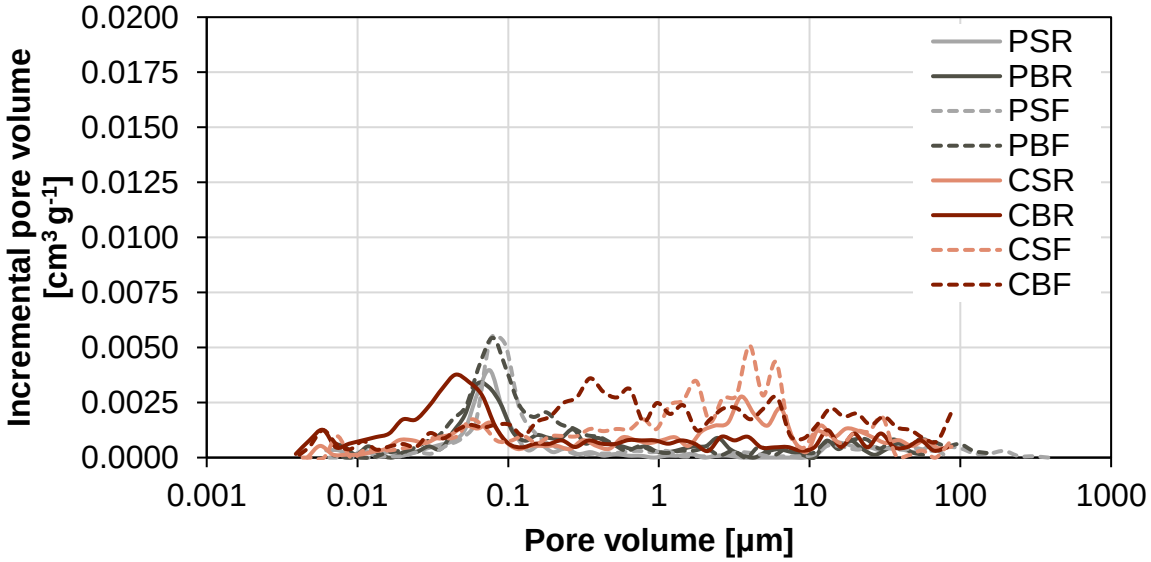

Figure 28 Pore size distribution curves of composites with combined raw materials in reference state

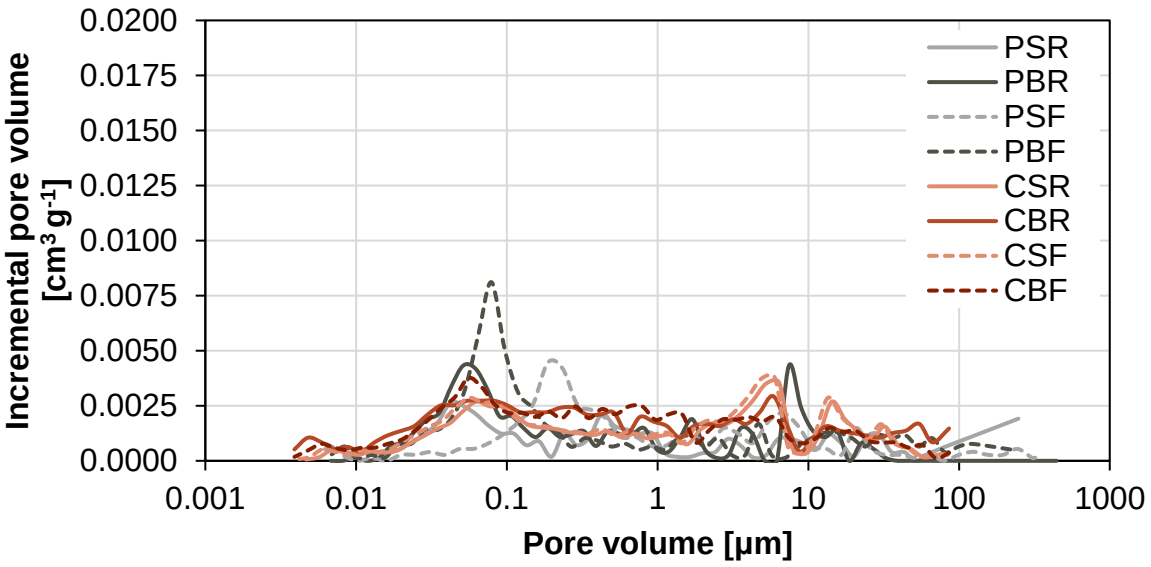

Figure 29 Pore size distribution curves of composites with combined raw materials after thermal pre-treatment by 400 °C

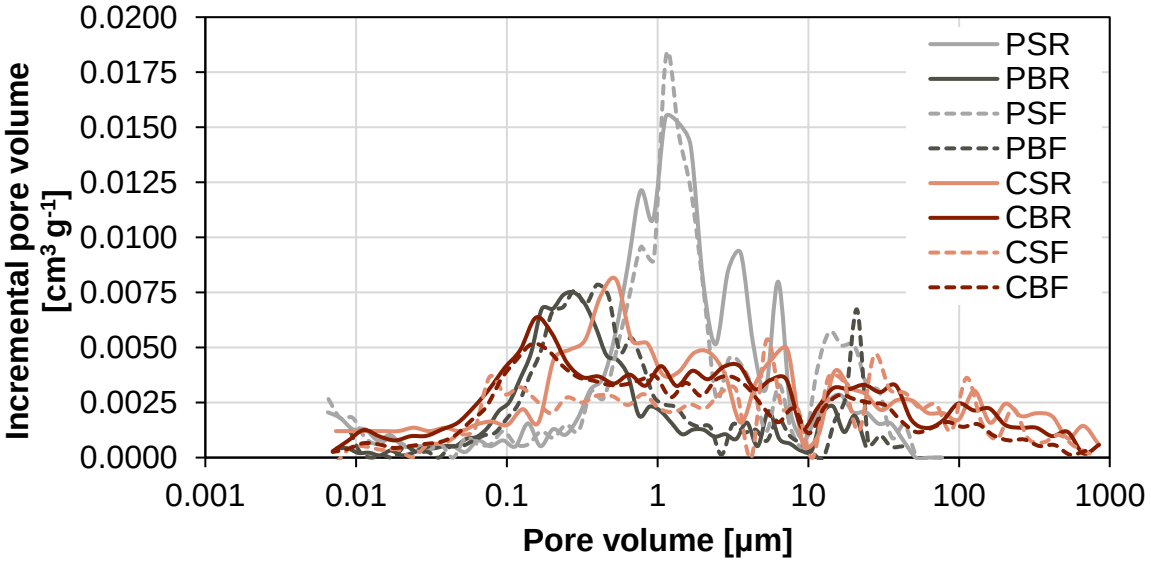

Figure 30 Pore size distribution curves of composites with combined raw materials after thermal pre-treatment by 1000 °C

8.1.2 Mechanical parameters

8.1.2.1 Destructive measurements methods

In Figure 31 the achieved results of compressive strengths depending on temperature exposure are shown. In the reference state without temperature loading, the composites PC reached higher strengths; in comparison CAC by about 12%. Influence of aggregate is lower; compressive strengths of those composites with basalt aggregates were by about 7% higher. Impact of fibres utilisation is indisputably positive; however, it depends on other materials. When PC was used, the improvement was by about 5%, while in the case of CAC the final compressive strength went up by about 10%. In all cases of studied composites, temperature exposure led to the fall of compressive strengths. Temperature loading by 400 °C led to deterioration of compressive strengths in average by about 43% and all studied composites showed residual compressive strength still applicable. However, by temperature exposure to 1000 °C the fall continued up to almost 95% in the worst case of PC and silica aggregates (regardless the fibres were utilised or not). As it was assumed, the degradation of compressive strength was lessen by utilisation of more thermal resistant raw materials. When silica aggregate was replaced by basalt ones the fall of compressive strength was just 83% (it is caused by elimination of quartz transformation). Better results were reached by materials composed of CAC, where the decrease was less than 80%. And in the case of the best results showed by basalt reinforced, CAC based composite with basalt aggregate the change due to the temperature loading was less than 60%. Achieved data are in good agreement with measured results of porosities (Figure 23 - Figure 30). In general, it is assumed that with increasing porosity, the compressive strength decreased and obtained results confirmed this assumption.

Khaliq et al. [37] showed similar behaviour of falling compressive strength due to the temperature loading. In reference state the higher values were obtained by concrete with PC. At 400 °C, the decrease of compressive strength was slightly bigger in the case of CAC; by about 12%. While in this work reversed tendency was observed; CAC proved improvement of the fall by about 10%. At higher temperatures (up to 800 °C), the in accordance with here presented results, their CAC showed higher residual compressive strengths by 10%, when here the difference was by about 20%. The varying impact can be attributed to the different aggregate used in the Khaliq's

study. Limestone aggregate is strongly influenced by temperature over 600 °C and thus concrete despite the better matrix was more deteriorated.

Ogrodnik and Szulej [107] presented higher compressive strengths of concrete based on CAC comparing to the PC in reference state; but it is caused by lower grade of used PC. Regarding the impact of temperature, the decreasing tendency was observed as in the case of this study. However, the CAC based led to the more significant improvement of compressive strength fall, which was by about 36% lower than in the case of PC. In this study the improvement was less than 20%. Similar to previous case the reason for various improvement can be found in the varying aggregate; their sanitary ceramics is more temperature resistant than basalt aggregate used in this work. Moreover, at their studied temperature 1049 °C the sintering and recrystallization processes could take place, which further improved compressive strength of their materials.

Baradaran-Nasirt and Nematzadeh [108] reached in reference state by almost 53% higher compressive strengths in the case of CAC utilization compared to PC based concrete. However, these values decreased due to the drying (at 110 °C) in average by about 54%. This phenomenon was attributed to the rapid conversion of metastable hydrates to stable compounds. Concretes studied in their work were cured in the water, which also may have deteriorating impact on the fall of residual compressive strength.

Hager et al. [39] in their study showed similar fall of compressive strength due to the varying aggregates application. However, their values were somewhat lower, due to used cement. Similar to our results, the basalt shows the best performance in the case of residual strengths.

Contrary results were presented by Masood et al. [109]. They presented compressive strength of basalt concrete lower than the quartzite concrete even at ambient temperature as well as at elevated temperatures. As it was already mentioned, chosen basalt was probably of unappropriated composition. Nevertheless, another more important issue is the general mixture performance. All studied mixture showed same tendency of compressive strength fall. Final values of compressive strength were in average by about 25 MPa, such low strength PC based concrete is strongly deteriorated during heating, and thus the impact of particular aggregate is of less importance. In addition, the heating rate was in their study quite bigger (3 ºC per minute), which increase the deterioration of whole material.

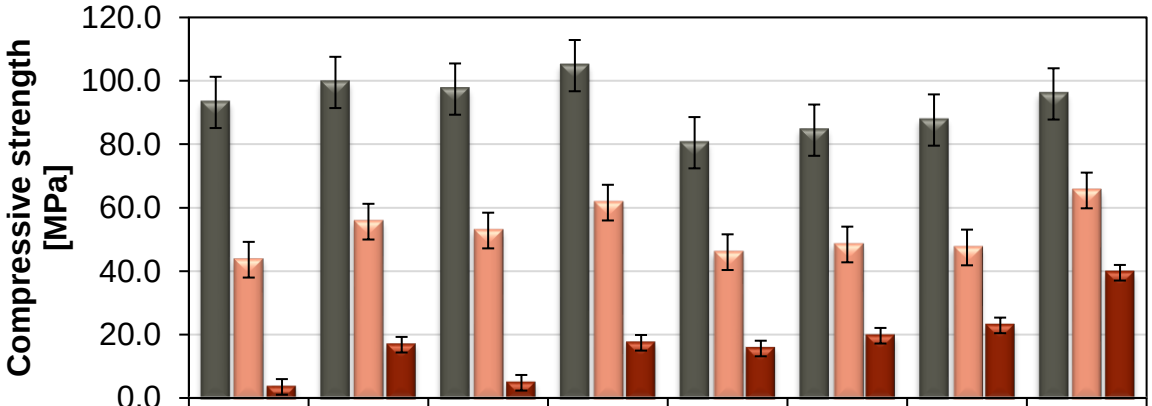

	PSR	PBR	PSF	PBF	CSR	CBR	CSF	CBF
105 °C	93.2	99.5	97.4	104.8	80.5	84.4	87.6	95.9
400 °C	43.6	55.6	52.8	61.6	46.0	48.4	47.5	65.4
1000 °C	3.5	16.8	4.8	17.4	15.6	19.6	22.9	39.5

Figure 31 Compressive strength of composites with combined raw materials

The second determined mechanical properties was the bending strength. The final values are presented in Figure 32. In contrast with compressive strength, the CAC shows higher bending strength in comparison with PC. The difference was by about 22%. The influence of basalt aggregate was similar as in the case of compressive strengths. Its application lead to bending strengths growth by about 10%. Similar positive effect was proved when composites were reinforced. Bending strengths of those with basalt fibres were by about 6% higher. When focused on impact on temperatures, the residual bending strengths were always lower. In the case of 400°C, the deterioration ranged from 65% to 48%, but generally, the decrease of bending strength was higher than the one of the compressive strength. Due to further temperature loading the decrease continued. In the case of PC and silica aggregate, the deterioration was almost 97%. While when CAC were employed the decrease was lowered, the residual bending strengths of composite based on calcium cement decreased to by about 89%. Similar benefit was reached by application of basalt aggregate, which proposed values of residual bending strengths by about 77% lower. In the case of combination of thermal resistant raw materials, the bending strengths reached suitable value and the deterioration was just by about 68%.

At reference state Ogrodnik and Szulej [107] presented same values of flexural strength for both CAC and PC based concrete, while in this study CAC based composite showed higher values. Temperature loading by 1049 °C respectively by 1000 °C led to same 93% bending strength's fall of PC based concrete observed in

their study, respectively in this work. CAC based concrete proposed lower fall, but they obtained better improvement by about 51%, while in this work it was 16%. As in the case of compressive strength, this can be explained by different aggregates of studied mixtures.

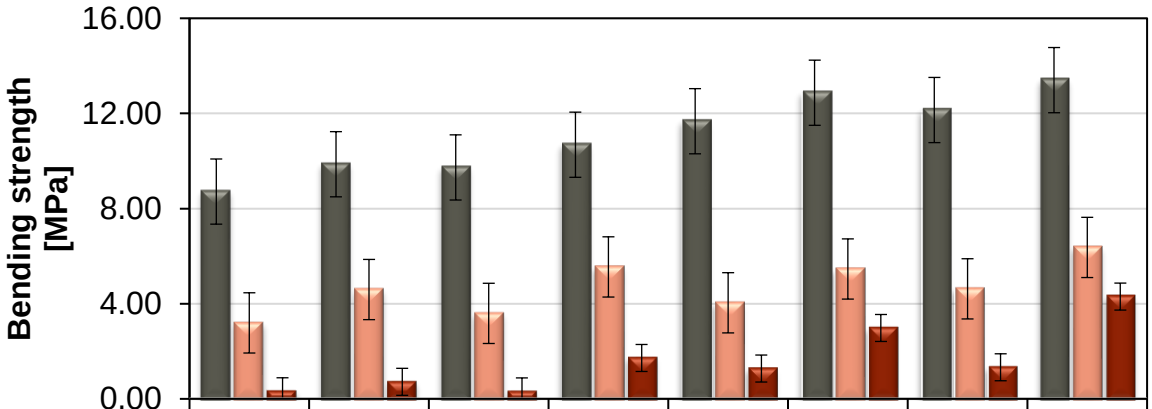

	PSR	PBR	PSF	PBF	CSR	CBR	CSF	CBF
105 °C	8.71	9.86	9.73	10.68	11.67	12.87	12.14	13.40
400 °C	3.19	4.60	3.59	5.55	4.04	5.46	4.63	6.37
1000 °C	0.32	0.72	0.31	1.72	1.27	2.98	1.33	4.30

Figure 32 Bending strength of composites with combined raw materials

8.1.2.2 Non-destructive measurements methods

The last measured mechanical characteristic is dynamic modulus of elasticity, which are summarized in Figure 33. Without temperature loading, the CAC reached higher values of dynamic modulus, the difference was by about 30%. On the other hand, basalt aggregate utilisation led to the decrease of dynamic modulus in average by about 12%. While due to the reinforcement the values were improved by about 2%. Temperature exposure to 400 °C led to the fall, surprisingly the highest decrease was observed when CAC was used (in average by 65%). While in the case of PC the drop was just by about 35%. Regarding the temperature 1000 °C, both cement showed similar fall of dynamic modulus. The worst effect was observed in the case of silica aggregate; the residual modulus of elasticity reached by about 96% lower values, in contrast the basalt aggregate shows the decrease just by about 83%. When focused on the impact of fibres, their positive effect growth due to the temperatures; the improvement was bigger than 7%.

Hager et al. [39] presented statistic modulus of elasticity. In contrast with our results, quite higher values of modulus of elasticity showed concrete with basalt

aggregate; about 45 GPa in reference state. While performance of silica based concrete was same.

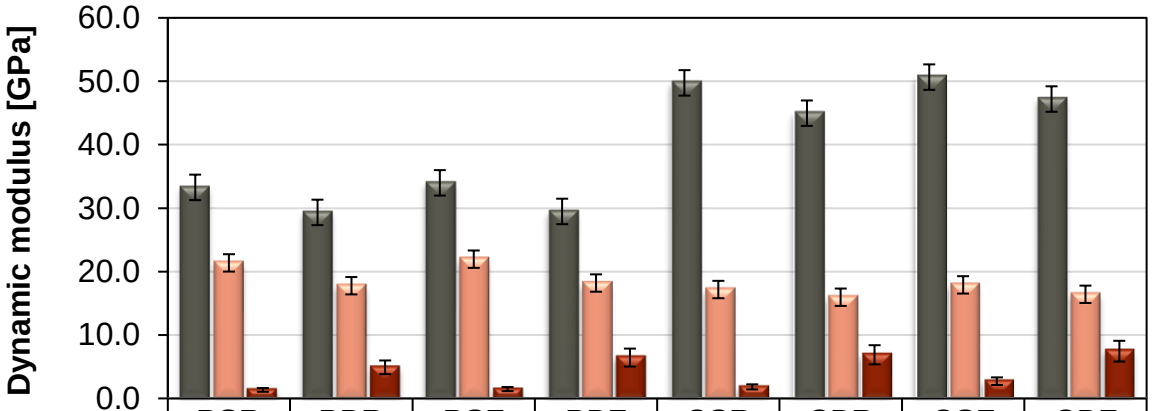

	PSR	PBR	PSF	PBF	CSR	CBR	CSF	CBF
105 °C	33.3	29.3	34.0	29.5	49.7	45.0	50.7	47.2
400 °C	21.4	17.8	22.0	18.2	17.2	16.0	17.9	16.4
1000 °C	1.3	4.9	1.5	6.4	1.8	6.9	2.7	7.4

Figure 33 Dynamic modulus of elasticity of composites with combined raw materials

8.1.3 Hydric properties

8.1.3.1 Hydric transport

Water absorption coefficient, summarized in Figure 34, described water liquid transport ability. In the reference state the main difference was observed in the case of varying cement. Application of PC proposed lower values of water absorption coefficient, the difference is by about 74%. The impact of aggregate could not be classified as simply, but usually composites with basalt aggregate reached higher values of water absorption coefficient. Reinforcement led to the growth of water absorption coefficient also, in average by about 18%. However, this difference was within the range of standard deviation. Regarding the temperature impact, the ability of water transport growth significantly after temperature exposure. The reason is the increase of porosity, specifically of the amount of capillary pores (in the range from 1 μm to 1 mm), which can be found in Figure 25 - Figure 27. After heating to 400 °C the change ranged from 23% to almost 143%. The lowest changes were observed in the case of reinforced composites based on CAC. When the temperature exposure was 1000 °C, the increase was giant. Values of water absorption coefficient went up to almost thirty-three times in the case of PC based material with silica aggregate. Furthermore, the immersed and wet part of samples based on PC and silica aggregate

disintegrated to minor particles after the measurements. When more thermal stable raw materials were used, the growth was much lower. Water absorption coefficient went up just by about 5 times in the case of reinforced CAC based composite with basalt aggregate.

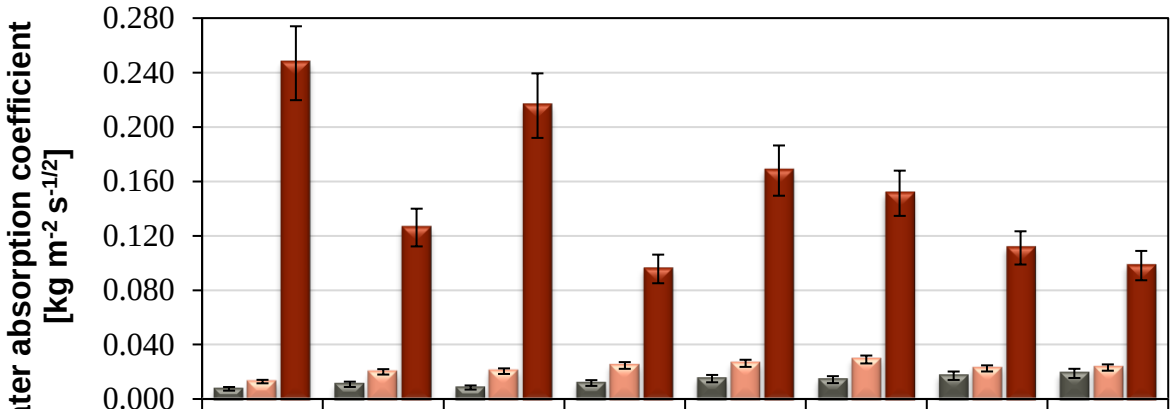

	PSR	PBR	PSF	PBF	CSR	CBR	CSF	CBF
105 °C	0.007	0.011	0.008	0.012	0.015	0.014	0.017	0.019
400 °C	0.013	0.020	0.020	0.025	0.026	0.029	0.022	0.023
1000 °C	0.247	0.126	0.2157	0.096	0.168	0.151	0.111	0.098

Figure 34 Water absorption coefficients of composites with combined raw materials

In contrast, apparent moisture diffusivities, presented in Figure 35, reached similar values in reference state. The differences between particular values were in the scope of the standard deviation. However, after temperature exposure, the differences between particular values of apparent moisture diffusivities went up. Nevertheless, at 400 °C no more specific conclusion could be observed. Basalt aggregate showed lower growth but the particular changes differed in all cases. When focused on residual apparent moisture diffusivity after 1000 °C, similarly to the water absorption coefficients the growth due to thermal pre-treatment was huge. Values growth by two classes. Generally, the biggest increases were observed when silica aggregate was used. This was caused by its crystal transformation at 573 °C, which led to the significant cracking of composites. While the lowest growth, which was in average 10 times, were observed when basalt aggregates and basalt fibres were used regardless which cement were used.

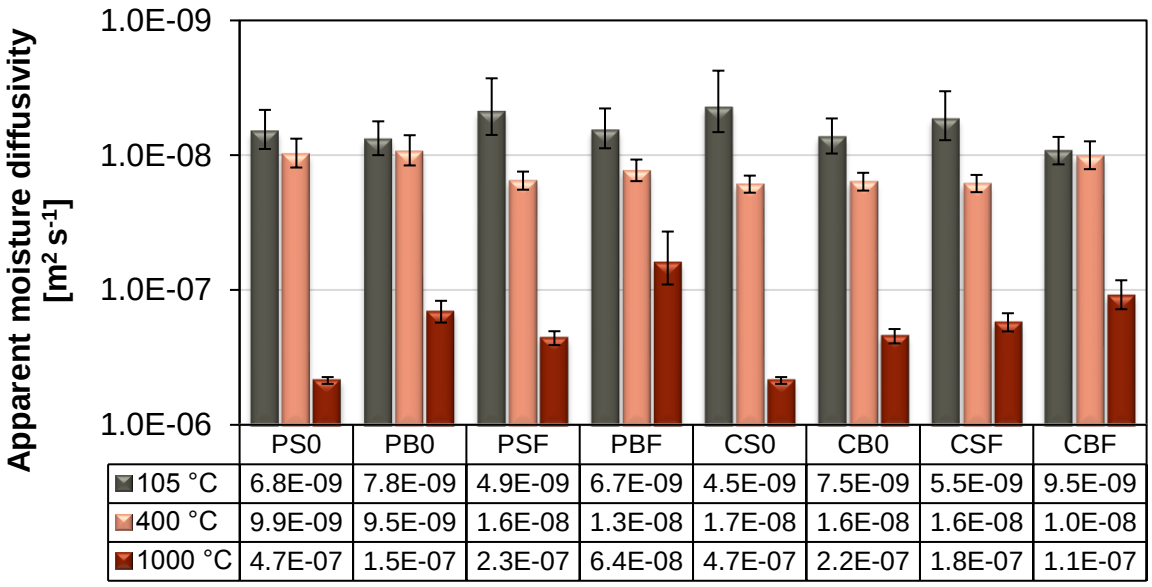

	PS0	PB0	PSF	PBF	CS0	CB0	CSF	CBF
105 °C	6.8E-09	7.8E-09	4.9E-09	6.7E-09	4.5E-09	7.5E-09	5.5E-09	9.5E-09
400 °C	9.9E-09	9.5E-09	1.6E-08	1.3E-08	1.7E-08	1.6E-08	1.6E-08	1.0E-08
1000 °C	4.7E-07	1.5E-07	2.3E-07	6.4E-08	4.7E-07	2.2E-07	1.8E-07	1.1E-07

Figure 35 Apparent moisture diffusivities of composites with combined raw materials

Properties which described water vapour transport in dry cup arrangements are presented in Table 26 and Figure 36, while in Table 27 and Figure 37 achieved results from wet cup arrangement can be found. In reference state, the application of CAC lead to the growth of water vapour transport ability. Water vapour resistance factor went up in average by about 37% and 35% for dry cup and wet cup respectively. Influence of basalt application was opposite; in combination with PC the water vapour resistance factor went down by about 47% in dry cup and by 43% in wet cup, and when CAC was used by 14% and 17%. Similar effect was observed due to the reinforcement. Basalt fibre reinforced composites showed by about 13% or 10% (for dry cup or wet cup) lower values of water vapour resistance factor. When focused on the impact of thermal pre-treatment, due to the temperature exposure water vapour transport ability increased significantly. This was caused by the pores growth; the most important for water vapour transport was amount of open pores and achieved results of water vapour transport characteristics were in accordance with measured open porosities (Figure 23). Exposure to 400 ºC led to the fall of water vapour resistance factor by about 50% in all cases of studied materials. In the case of 1000 ºC, the changes were more various. The biggest growth of water vapour resistance factor was observed in the case of reinforced PC based composite with silica aggregate. Water vapour transport went down by about 94% for both arrangements. While in the case of fibres reinforced CAC based composite with basalt aggregate, the change was just by less than 68% or 70% for dry cup and wet cup. In all cases values of water vapour resistance factor was lower

in the case of wet cup arrangement. This was caused by partial liquid water transport appearing due to high relative humidity [2].

Table 26 Water vapour diffusion characteristics in dry-cup arrangement of composites with combined raw materials

Dry cup	Water vapour diffusion permeability [10^{-12} s]			Water vapour diffusion coefficient [10^{-6} m^2 s^{-1}]		
	105 °C	**400 °C**	**1000 °C**	**105 °C**	**400 °C**	**1000 °C**
PSR	1.23 ± 0.04	2.61 ± 0.01	16.89 ± 0.08	0.17 ± 0.01	0.36 ± 0.01	2.32 ± 0.01
PBR	1.72 ± 0.01	3.39 ± 0.29	7.07 ± 0.01	0.24 ± 0.01	0.47 ± 0.04	0.97 ± 0.01
PSF	1.36 ± 0.06	2.97 ± 0.01	22.21 ± 0.23	0.19 ± 0.01	0.41 ± 0.01	3.05 ± 0.03
PBF	2.09 ± 0.11	3.99 ± 0.23	8.10 ± 0.53	0.29 ± 0.02	0.55 ± 0.03	1.11 ± 0.07
CSR	2.23 ± 0.20	4.17 ± 0.48	13.36 ± 0.20	0.31 ± 0.03	0.57 ± 0.07	1.84 ± 0.03
CBR	2.47 ± 0.07	5.56 ± 0.29	9.92 ± 0.61	0.34 ± 0.03	0.76 ± 0.04	1.36 ± 0.08
CSF	2.44 ± 0.09	4.74 ± 0.46	8.81 ± 0.18	0.34 ± 0.01	0.65 ± 0.06	1.21 ± 0.02
CBF	2.87 ± 0.03	5.52 ± 0.41	8.74 ± 0.35	0.39 ± 0.01	0.76 ± 0.06	1.20 ± 0.05

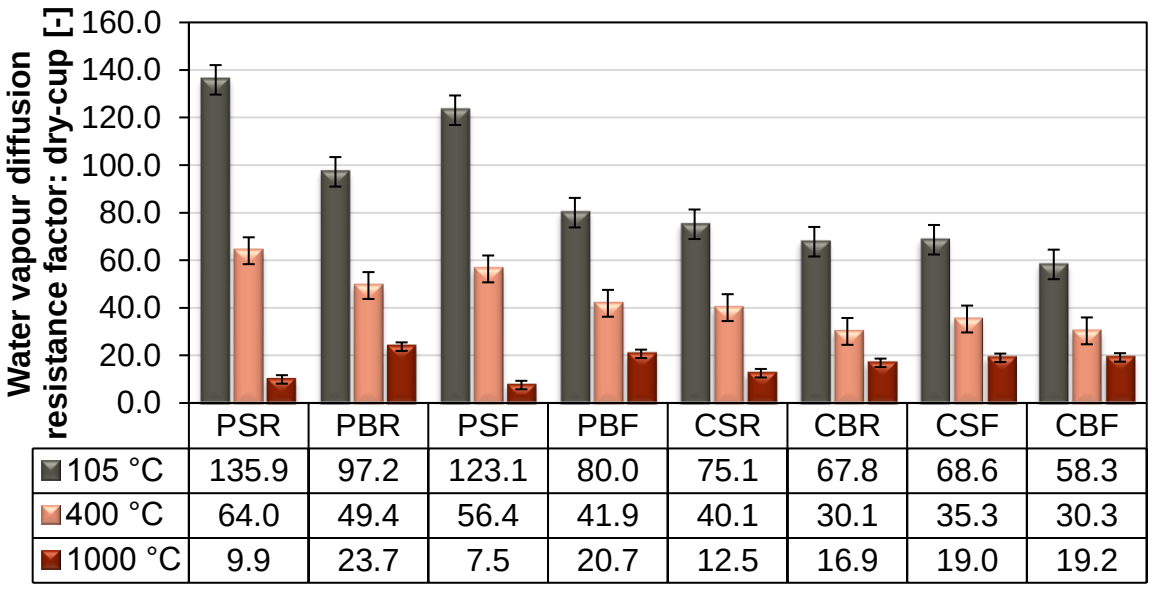

	PSR	PBR	PSF	PBF	CSR	CBR	CSF	CBF
105 °C	135.9	97.2	123.1	80.0	75.1	67.8	68.6	58.3
400 °C	64.0	49.4	56.4	41.9	40.1	30.1	35.3	30.3
1000 °C	9.9	23.7	7.5	20.7	12.5	16.9	19.0	19.2

Figure 36 Water vapour diffusion resistance factors in dry-cup arrangement of composites with raw materials

Table 27 Water vapour diffusion characteristics in wet-cup arrangement of with combined raw materials

Wet cup	**Water vapour diffusion permeability [10^{-12} s]**			**Water vapour diffusion coefficient [10^{-6} m^2 s^{-1}]**		
	105 °C	**400 °C**	**1000 °C**	**105 °C**	**400 °C**	**1000 °C**
PSR	1.47 ± 0.01	2.91 ± 0.08	25.59 ± 0.07	0.20 ± 0.01	0.40 ± 0.01	3.52 ± 0.01
PBR	2.13 ± 0.06	3.69 ± 0.29	9.10 ± 0.16	0.29 ± 0.01	0.51 ± 0.04	1.25 ± 0.02
PSF	1.59 ± 0.01	3.14 ± 0.15	30.48 ± 0.17	0.22 ± 0.01	0.43 ± 0.02	4.19 ± 0.02
PBF	2.22 ± 0.02	4.46 ± 0.28	8.96 ± 0.22	0.31 ± 0.03	0.61 ± 0.04	1.23 ± 0.03
CSR	2.52 ± 0.01	5.21 ± 0.25	18.27 ± 0.20	0.35 ± 0.01	0.72 ± 0.03	2.51 ± 0.03
CBR	2.87 ± 0.01	6.70 ± 0.63	13.87 ± 0.38	0.39 ± 0.02	0.92 ± 0.09	1.91 ± 0.05
CSF	2.69 ± 0.06	5.96 ± 0.45	10.68 ± 0.86	0.37 ± 0.01	0.82 ± 0.06	1.47 ± 0.12
CBF	3.24 ± 0.07	6.88 ± 0.20	10.77 ± 0.63	0.45 ± 0.01	0.94 ± 0.03	1.48 ± 0.09

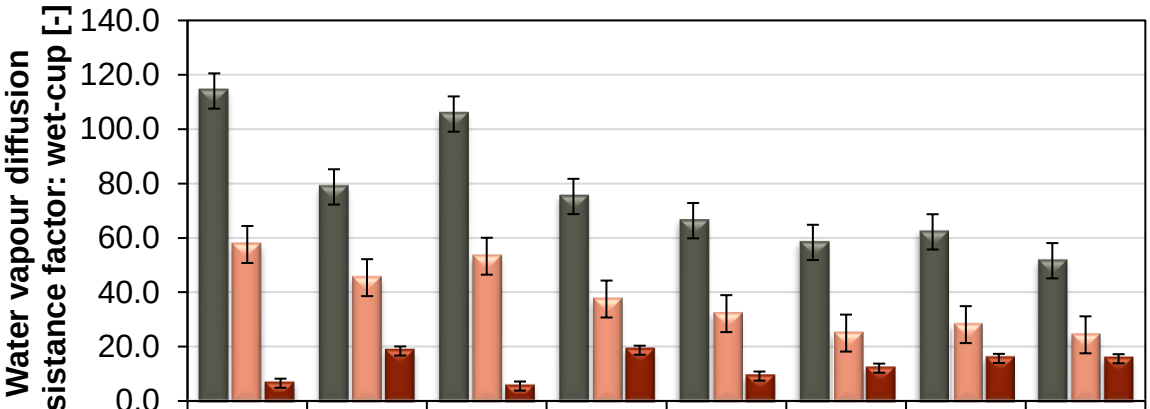

	PSR	PBR	PSF	PBF	CSR	CBR	CSF	CBF
105 °C	114.0	78.7	105.6	75.2	66.3	58.3	62.2	51.6
400 °C	57.6	45.4	53.3	37.5	32.1	25.0	28.1	24.3
1000 °C	6.5	18.4	5.5	18.7	9.2	12.1	15.7	15.5

Figure 37 Water vapour diffusion resistance factors in wet-cup arrangement of composites with combined raw materials

8.1.3.2 Accumulation of water vapour

Measured sorption isotherms of composites with combined raw materials are delineated in Figure 38 - Figure 40. For the sake of clarity, all particular temperature pre-treatments were drawn separately. In reference state, materials with CAC reached somewhat lower ability for water vapour adsorption up to 60%. While at higher moisture content (over 70%) the moisture content of CAC based composites was significantly higher. In contrast, basalt aggregate application led to the water absorption growth in all humidity's stages. Minor increasing impact was observed also in the case of fibres reinforcement. When focused on the effect of temperature loading. All sorption isotherms went up distinctively. The main reasons were presence of unhydrated phases with lower specific volume, which when given rise were accompanied by the volumetric shrinkage and open porosity growth. When focused on temperature 1000 ºC, results of composite based on PC were not evaluable and thus cannot be published. This was due to the higher deterioration of material, which in combination of long term of measurement (almost one year) led to damage of samples and its disintegration. This caused huge inaccuracy of measurements, which in the case of silica aggregate led to negative values of moisture content. However, when compared the impact of temperature loading, after 400 ºC the water vapour adsorption capability was increased by about 53% times when PC was used. While in the case of designed reinforced CAC based composite with basalt aggregate the growth was only by less

than 33%. When temperature loading was 1000 ºC both basalt aggregate and basalt fibres proved their positive effect on capability of water vapour adsorption and the moisture content was in comparison with reference state went up by less than 50%.

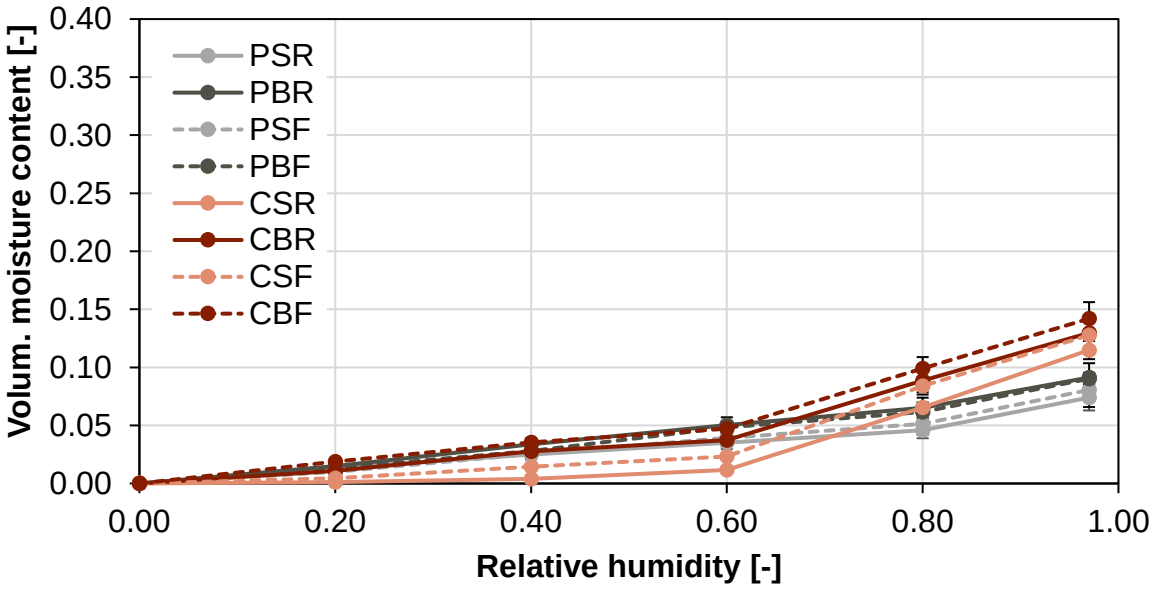

Figure 38 Sorption isotherms of composites with combined raw materials in reference state

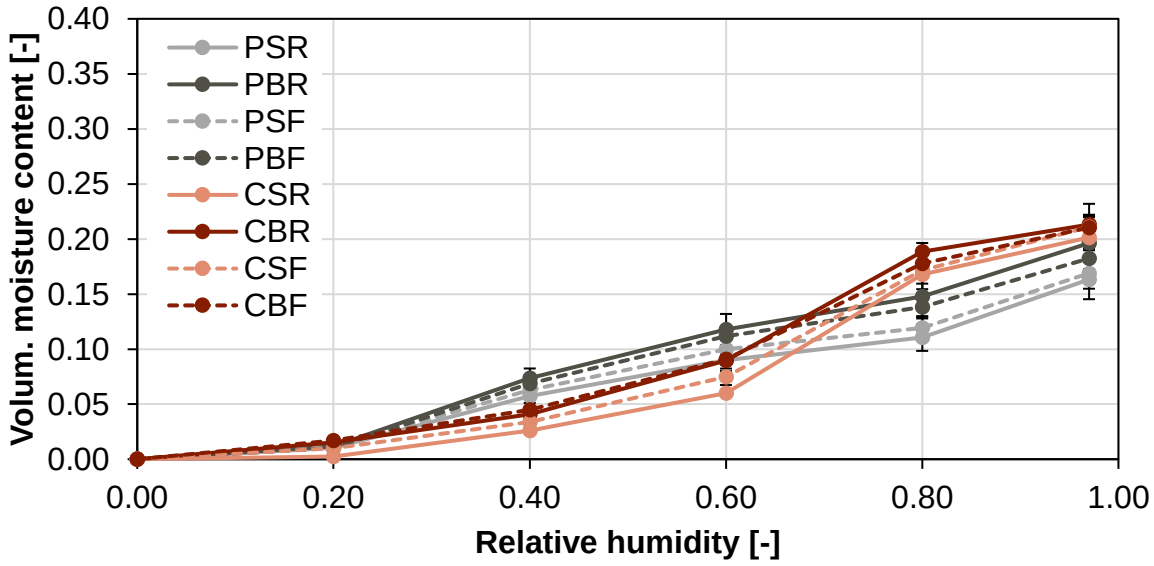

Figure 39 Sorption isotherms of composites with combined raw materials after thermal pre-treatment by 400 °C

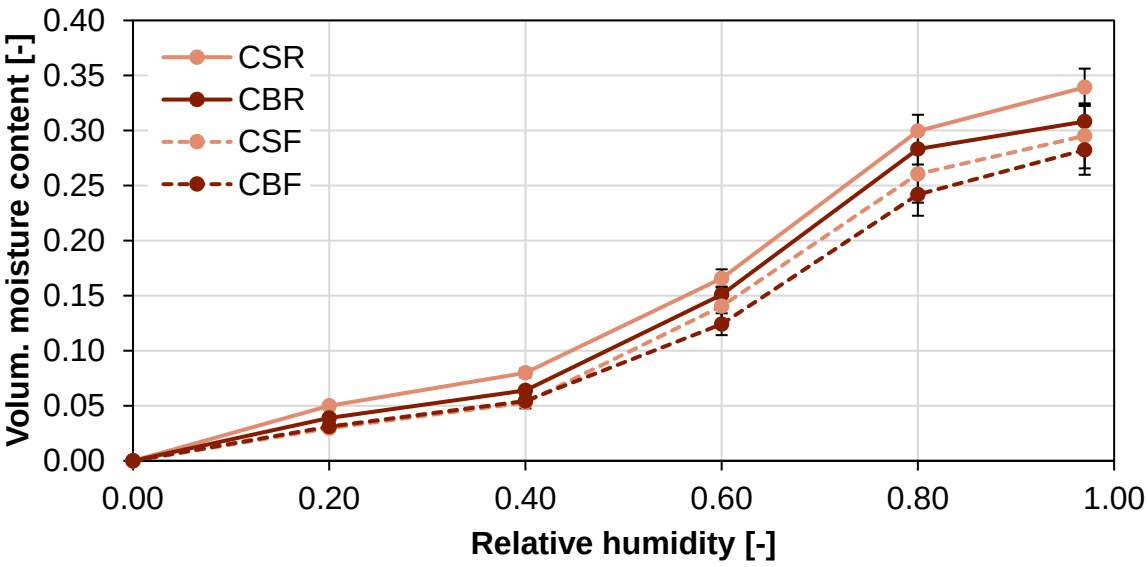

Figure 40 Sorption isotherms of composites with combined raw materials after thermal pre-treatment by 1000 °C

8.1.4 Thermal characteristics

Thermal conductivities depending on moisture content are shown in Figure 41-Figure 43. In reference state, due to different cement thermal conductivities varied by about 32%, when the CAC proposed higher values. This could be explained not only by higher porosity of CAC based composite, but also by different structure of particular matrix. PC composed mainly of amorphous calcium silicate hydrate, while in the case of CAC cement the calcium aluminate hydrates are crystalline, which in general proposed higher thermal conductivities. However, the most important impact was found in the case of aggregates. The composites with silica sand reached by about twice time higher values of thermal conductivity. This was undisputable caused by different thermal conductivities of rocks minerals. Quartz had thermal conductivity in average 7.69 W m^{-1} K^{-1}, while pyroxenes (the main group of basalts minerals) has by about 4.66 W m^{-1} K^{-1}, and the minor components have even lower thermal conductivity (anorthite 2.1 W m^{-1} K^{-1} and muscovite 2.28 W m^{-1} K^{-1}) [156]. Regarding basalt fibres reinforcement, it had decreasing effect on thermal conductivities; in average by about 18%. Similar as in the case of aggregate, this was consequence of pore structure growth as well as small thermal conductivity of basalt fibres (Table 18). When focused on the effect of temperature pre-treatment, in accordance with open porosity growth the porosity (Figure 23) the thermal conductivities went down. At 400 ºC, despite lower porosity growth, composites based on CAC showed higher decrease of thermal

conductivity; by about 28%. Composites based on PC went down just by about 16%. This phenomenon was in accordance with assumption of higher thermal capacity of calcium aluminate hydrate, which were practically decomposed after 400 ºC. Regarding the impact of 1000 ºC, the most considerable change was observed in the case of PC and silica aggregate. Thermal conductivity went down by more than 83%. Other studied composites proved similar changes by about 50% in comparison with reference state, expect for those composed of basalt aggregate and basalt fibres. These composites (regardless the cement type) showed the lowest fall of thermal conductivity, just by about 36%. Last noticeable think dealing with thermal conductivity was its dependency on moisture content. Thermal conductivity always went up with increasing moisture content. This was caused by significantly higher values of thermal conductivity of water in contrast with air (approximately 0.56 W m^{-1} K^{-1} for liquid water in contrast with 0.026 W m^{-1} K^{-1} for air).

Hartileb et al [40] presented values of thermal conductivity of rocks up to 1000 °C. In accordance with our results, basalt rocks showed lower values of thermal conductivity. Moreover, they proved the most constant behaviour of basalt rock during heating. While sandstone and granite showed sharp decrease up to 600 °C.

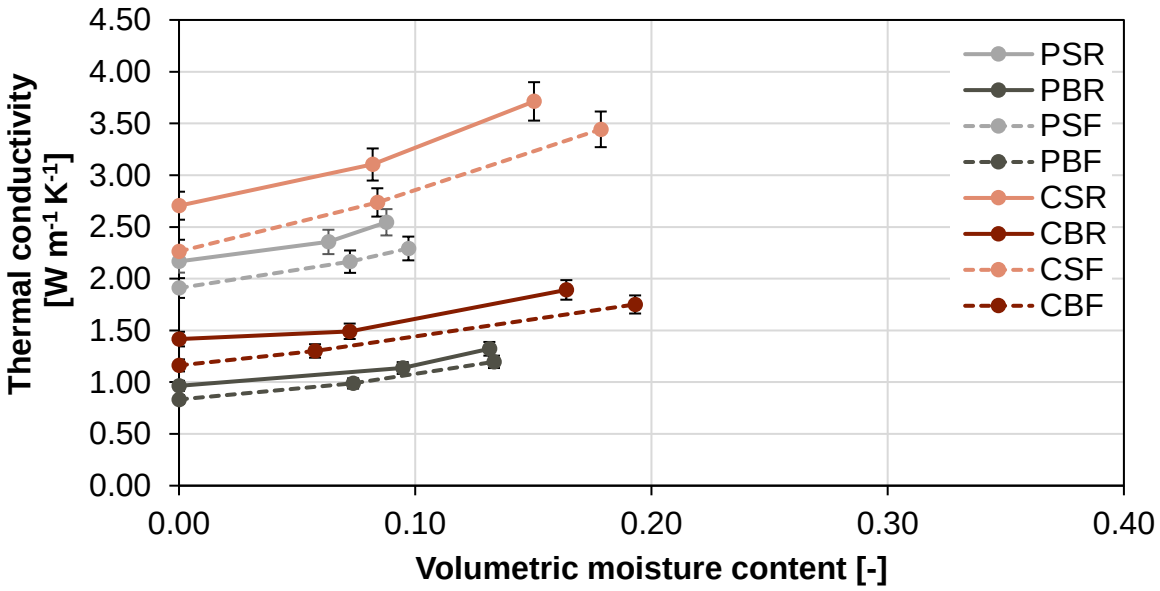

Figure 41 Thermal conductivities of composites with combined raw materials in reference state

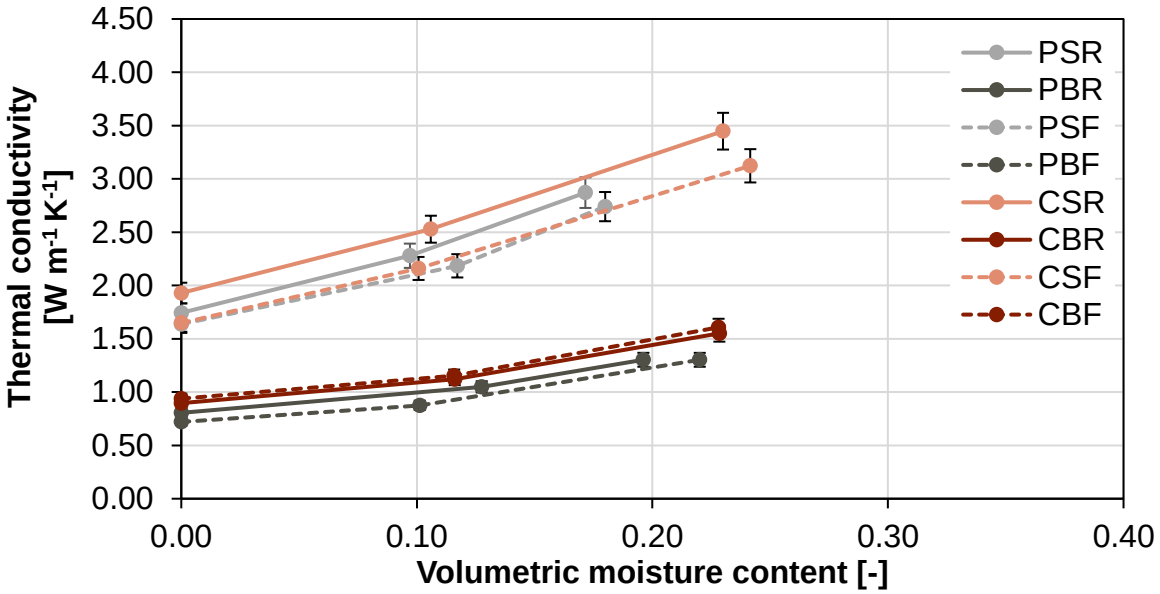

Figure 42 Thermal conductivities of composites with combined raw materials after thermal pre-treatment by 400 °C

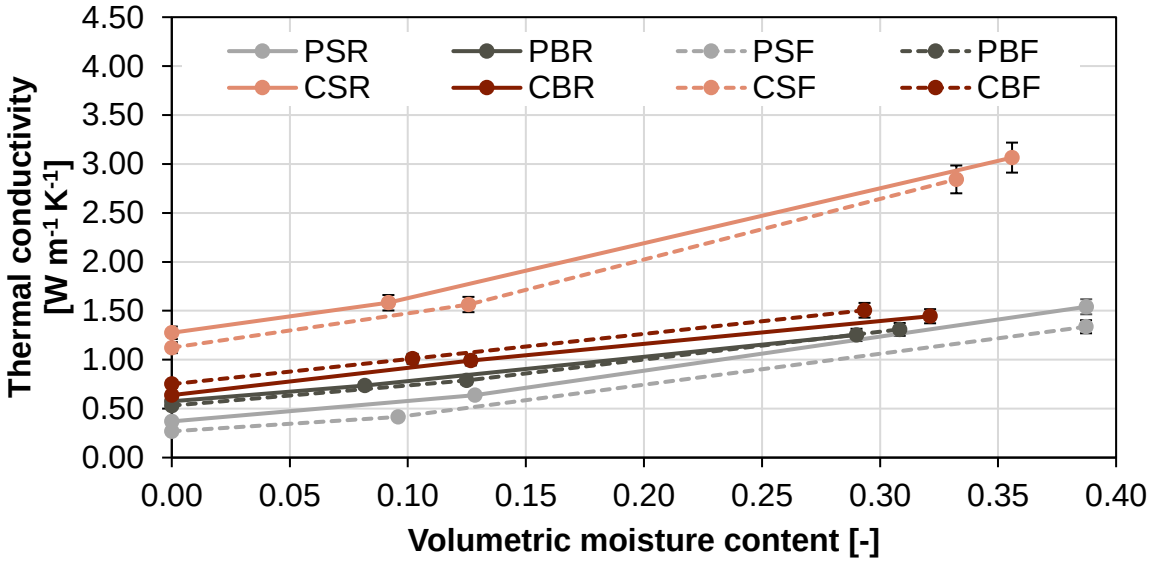

Figure 43 Thermal conductivities of composites with combined raw materials after thermal pre-treatment by 1000 °C

Specific heat capacities are summarized in Figure 44 and Figure 45 for dry and wet state respectively. When focused on dry state values of specific heat capacity of all studied materials varied less than the accuracy of measurements, therefore no reliable conclusion could be done. CAC based composite seemed to had slightly higher specific heat capacity, but the vary was just 7%. In contrast basalt aggregate application led to minor fall of specific heat capacity by about 6%. Reinforcement led

to the little 4% growth. Not even temperature exposure had some noticeable effect; the change was always lower than 10%. Only in the case of saturated state noticeable changes were observed. PC based composite with silica aggregate showed by 38% higher residual specific heat capacity, and in combination with basalt aggregate by 27%. As in the case of thermal conductivity, this is caused by significantly higher value of specific heat capacity for water compared to the air (4180 J kg^{-1} K^{-1} opposite to 1010 J kg^{-1} K^{-1}).

Hartileb et al [40] measured specific heat capacity of stones depending on temperature up to 1000 °C. They reported slightly lower values in the case of sandstone. However, the defences are not significant both in their and this work. The most important is changes due to the temperature loading, which are the lowest in the case of basalt aggregate.

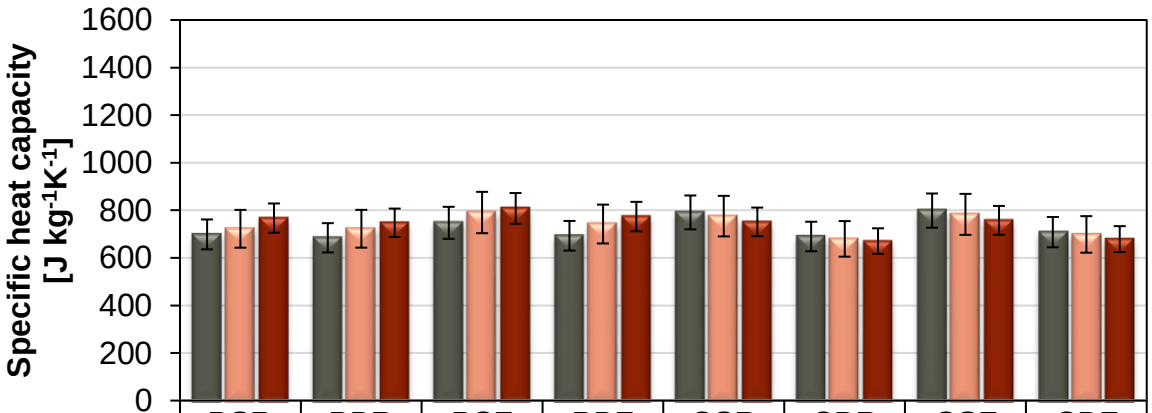

	PSR	PBR	PSF	PBF	CSR	CBR	CSF	CBF
105 °C	699	684	747	693	791	690	799	708
400 °C	722	722	791	742	776	680	783	699
1000 °C	767	748	808	774	751	671	758	679

Figure 44 Specific heat capacities in of composites with combined raw materials in dry state

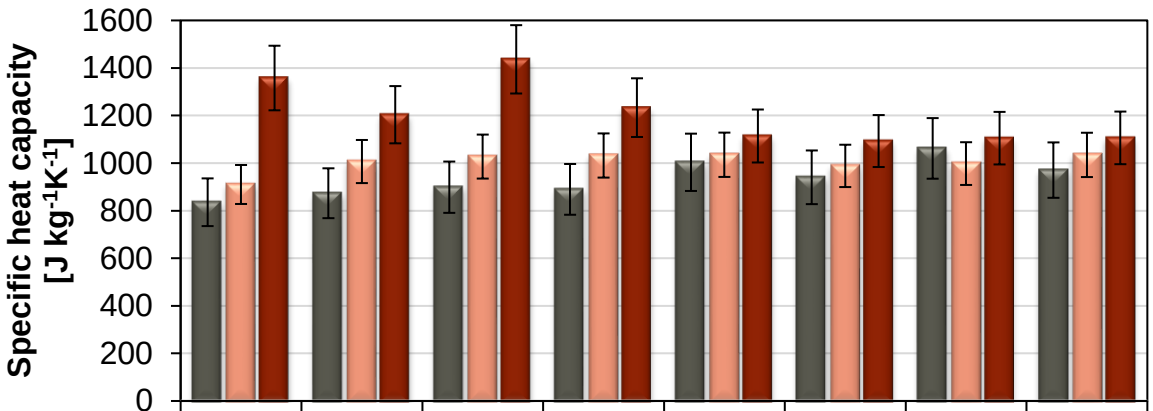

	PSR	PBR	PSF	PBF	CSR	CBR	CSF	CBF
105 °C	836	873	899	890	1003	940	1062	971
400 °C	910	1007	1028	1032	1035	988	998	1035
1000 °C	1358	1204	1436	1233	1114	1093	1105	1106

Figure 45 Specific heat capacities in of composites with combined raw materials in saturated state

8.1.5 Physical properties in high temperatures

8.1.5.1 Thermal strain

In Figure 46 and Figure 47 the measured thermal strains of composites with combined raw materials are delineated. While linear thermal expansion coefficient can be found in Figure 48 and Figure 49 respectively. Regarding the impact of cement, up to 200 ºC the thermal strains was lower in the case of CAC, in average by about 10%. When temperature exceeded 200 ºC, the tendency was reversed and up to 800 ºC CAC showed by about 19% higher thermal strain. Probably due to the vaterite formation and its strain, the curves of PC based composite after 800 ºC became growth more sharply. Much more important was the effect of used aggregate. The difference was already at 40 ºC by about 21% and growth continuously up to 600 ºC to by about 72%. Silica aggregate, specifically α-quartz showed higher thermal strain and when temperature got closer to 573 ºC, where the recrystallization occurred, its increase was extremely steep. In contrast basalt aggregate showed gentle continuous increase of thermal strain without any significant changes. Regarding the impact of basalt fibres, except for combination of basalt aggregate and PC, the effect of reinforcement was positive and thermal strain was decreased. In combination with CAC the fall was by about 7%. However, at high temperature there was observed quite unexpected behaviour of composite with PC, fibres reinforcement and basalt aggregate. It was

drawn more detailed in Figure 47. This steep growth was observed in all cases of performed measurement and thus could not be judged as a random error. Nevertheless, there could be found explanation in combination of specific changes of particular raw materials. As it was mentioned hereinabove, PC showed more sharp increase after 800 ºC due to the presence vaterite. In silica aggregate there was the modification of polymorph, at 870 ºC β-Quartz was changed to β-tridymite. And moreover the softening temperature of basalt fibres was 950 ºC (Table 18). These three facts, which act synergically, caused the steep growth of thermal strain by 6% in temperature range from 800 ºC to 1000 ºC. It is obvious that linear thermal expansion coefficient should be as constant as possible for material application with possible high temperature exposure. This tendency was observed in the case of designed CAC based composite with basalt aggregate. Without reinforcement the value was 1.45 10^{-5} K^{-1}, while when basalt fibres were used it decreased to 7.1 10^{-6} K^{-1}.

Wang et al. [106] presented thermal strain up to temperatures of 1400 °C and reported decrease of linear thermal strain at about 300 °C which was caused by decomposition of tricalcium aluminate hexahydrate (C_3AH_6). In the case of this work, the slight decrease can be observed early, which is caused by the presence of the others metastable calcium aluminate hydrates.

Hartileb et al [40] presented similar tendencies of aggregates thermal strains, quartz transformation is the most significant, while basalt proved continuous tendency. Moreover, they performed cyclic second measurements. Not only the residual thermal expansion was much greater in the case of silica, also the strain at the second measurement was quite bigger.

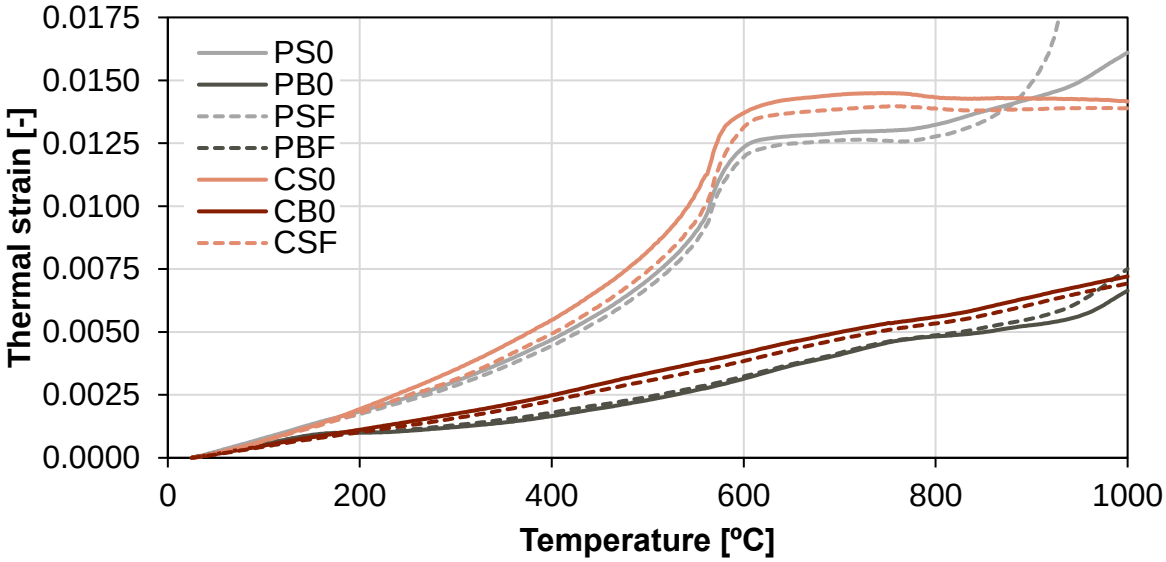

Figure 46 Thermal strains of composites with combined raw materials

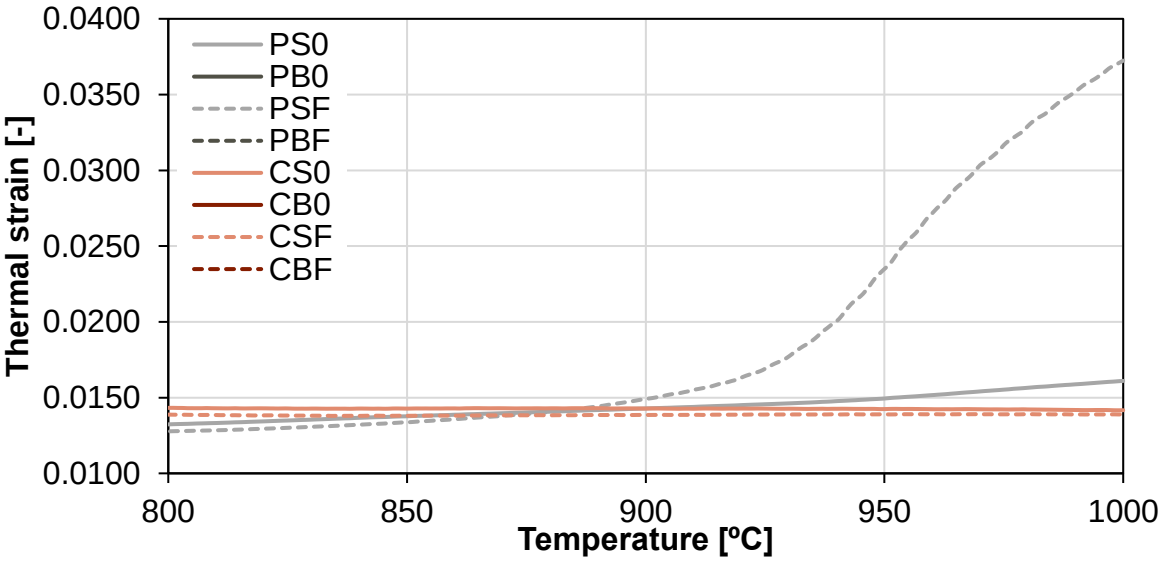

Figure 47 Detail of thermal strains of composites with combined raw materials at high temperature

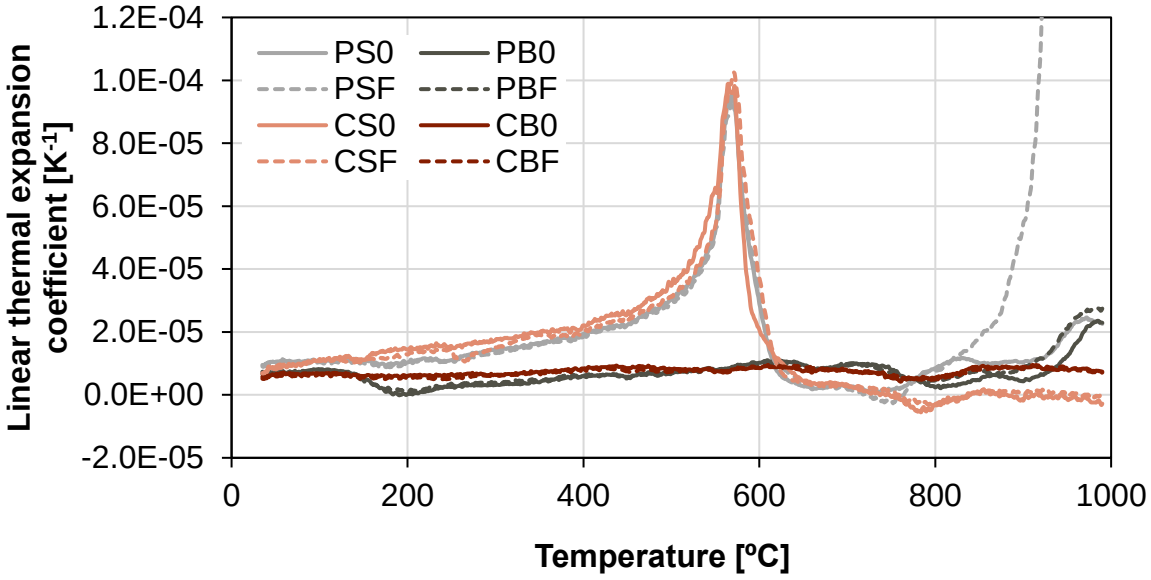

Figure 48 Linear thermal expansion of composites with combined raw materials

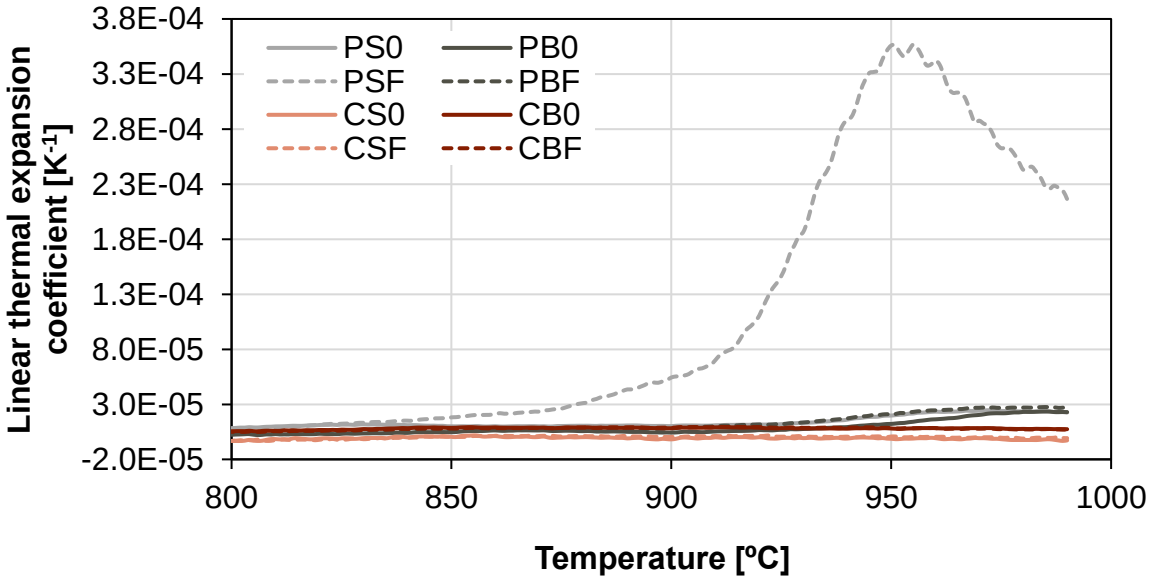

Figure 49 Detail of linear thermal expansion of composites with combined raw materials at high temperature

8.2 Cement based composites with combined fibres

8.2.1 Basic physical characteristics

8.2.1.1 Basic physical properties

The bulk densities of cement based composites with combined fibres length are shown in Figure 50. Equally to the previous part with varying raw materials, the bulk densities showed decreasing tendency with temperature loading. The reference material exhibited the highest bulk density in the reference conditions but also its biggest fall with the increasing temperature; the change was almost 4% in the case of water vacuum saturation method and 16% when used helium pycnometry. The fibre reinforced composites reached similar values from water vacuum saturation in reference state as well as after exposure to 400 °C. As the temperature went up to 1000 °C, the impact of different fibres ratio could be observed. The best behaviour shown composite with the ratio of fibres 90:10, the decrease of bulk density was only 1% after heating to 1000 °C, which was much lesser than the accuracy of this measurement. Deterioration of bulk density due to the temperature loading was significantly higher when helium pycnometry was used. This was caused by markedly higher values of matrix density (as it will be seen in following part of this chapter). Thermal pre-treatment by 400 ºC led to by about 8% of bulk density fall while due to the 1000 ºC, the decrease was in average 14%. Also in this case, the lowest deterioration (7% and 12% for 400 ºC and 1000 ºC respectively) was observed when fibre reinforcement was in the ratio 90:10.

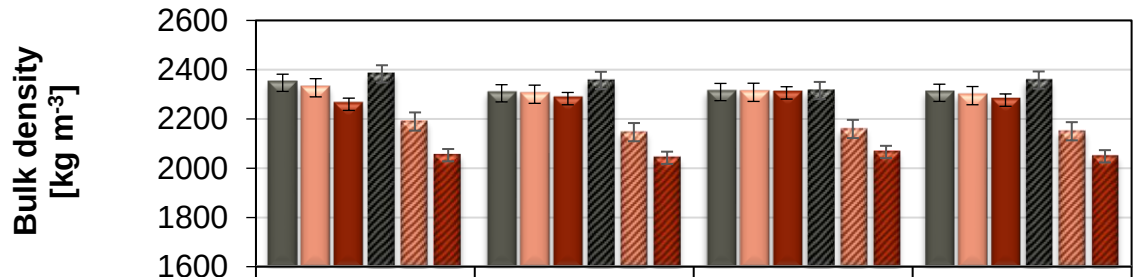

	CBR	CB0	CB1	CB2
105 °C (WVS)	2347	2304	2309	2306
400 °C (WVS)	2326	2300	2308	2295
1000 °C (WVS)	2259	2282	2306	2276
105 °C (HP)	2383	2356	2315	2358
400 °C (HP)	2189	2146	2159	2150
1000 °C (HP)	2053	2042	2066	2048

Figure 50 Bulk densities of composites with combined fibres (WVS –water vacuum saturation, HP – helium pycnometry)

Matrix densities can be found in Figure 51, where values from both used methods are presented. They reached similar values in reference condition, in average 2950 kg m^{-3} and 2976 kg m^{-3} and the difference is less than 1% and 1.6% for water vacuum saturation and helium pycnometry respectively. The changes due to the temperature exposure to 400 ºC were in all cases similar, matrix densities increased by about 9% when measured by water vacuum saturation, while when helium pycnometry was used the growth was less than 2%. However, when the temperature was 1000 ºC, the difference was more apparent when water vacuum saturation was applied. The change of reference composite was more than 22%, while when fibres were used the difference was by about 18%. The measurement by helium pycnometry showed just minor differences: deterioration of reference material was by almost 7%, while when there was reinforcement in the ratio 90:10 the growth was less than 6%.

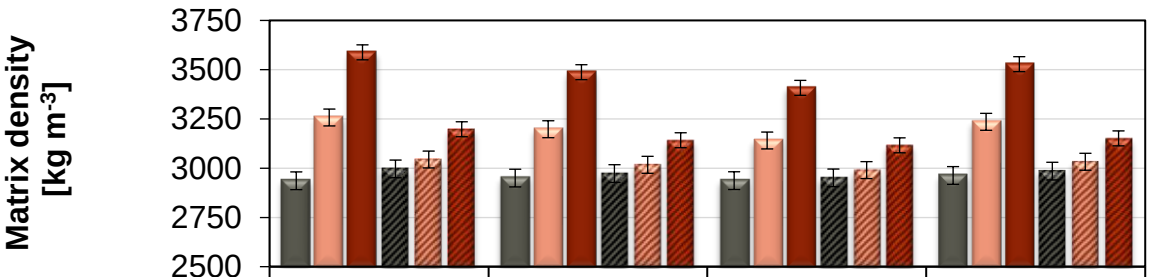

	CBR	CB0	CB1	CB2
105 °C (WVS)	2936	2950	2937	2963
400 °C (WVS)	3257	3198	3140	3235
1000 °C (WVS)	3588	3487	3408	3528
105 °C (HP)	2996	2973	2951	2985
400 °C (HP)	3044	3017	2990	3033
1000 °C (HP)	3197	3142	3116	3151

Figure 51 Matrix densities of composites with combined fibres (WVS –water vacuum saturation, HP – helium pycnometry)

Particular values of open porosities depending on fibres combination are presented in Figure 52. In reference state, no significant differences between the combinations with reinforcement were observed. The impact was not noticeable until the composite were exposed to higher temperatures. Open porosities showed opposite tendency to the bulk densities; they grown due to the temperature loading. Deterioration was the most remarkable in the case of reference material, by about 85% and 75% for water vacuum saturation and helium pycnometry respectively. Due to the reinforcing by basalt fibres, the growth was decreased to by about 50% and 60% (for particular methods) in the case of fibres combined in the ratio of 90:10. The difference between both used methods was much lower than in the previous cases of bulk and matrix densities, particular values after thermal pre-treatment differed maximal by 5%.

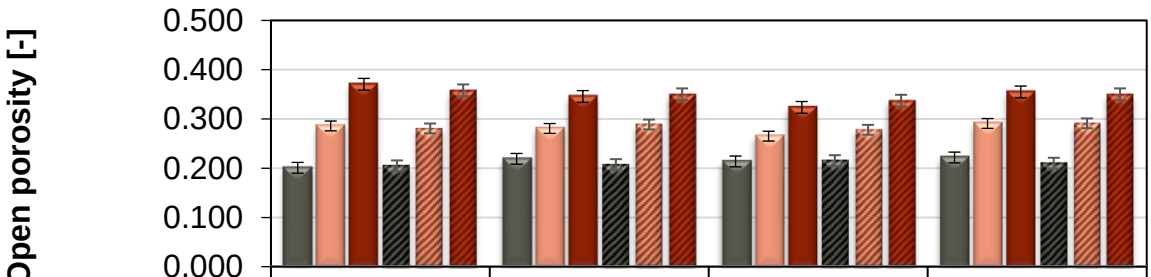

	CBR	CB0	CB1	CB2
105 °C (WVS)	0.201	0.219	0.214	0.222
400 °C (WVS)	0.286	0.281	0.265	0.291
1000 °C (WVS)	0.370	0.345	0.323	0.355
105 °C (HP)	0.205	0.207	0.215	0.210
400 °C (HP)	0.281	0.289	0.278	0.291
1000 °C (HP)	0.358	0.350	0.337	0.350

Figure 52 Open porosities of composites with combined fibres (WVS –water vacuum saturation, HP – helium pycnometry)

8.2.1.2 Pore Structure

For more detailed description of pore structure changes, they are drawn the pore size distributions in Figure 53 and Figure 54. The cumulative pore volume curves shown that in the reference conditions the lowest porosity exhibited the reference composite without fibre reinforcement. The other materials reached somewhat higher porosity but differed only slightly each other. The major difference between the reference material and the fibre reinforced composites was in the range of 100 nm to 10 μm. The tendency observed for the composites not affected by high temperature exposure was though considerably changed after the thermal pre-treatment. Heating to 400 °C resulted in the porosity of the reference material being comparable with the fibre reinforced composites, and in the case of 1000 °C the reference material reached even the highest porosity within the 100 nm to 1 mm range. Regarding the influence of fibres, the best behaviour, the lowest porosity as well as the lowest change, was observed for the composite with the longer-shorter fibres in the ratio of 90:10.

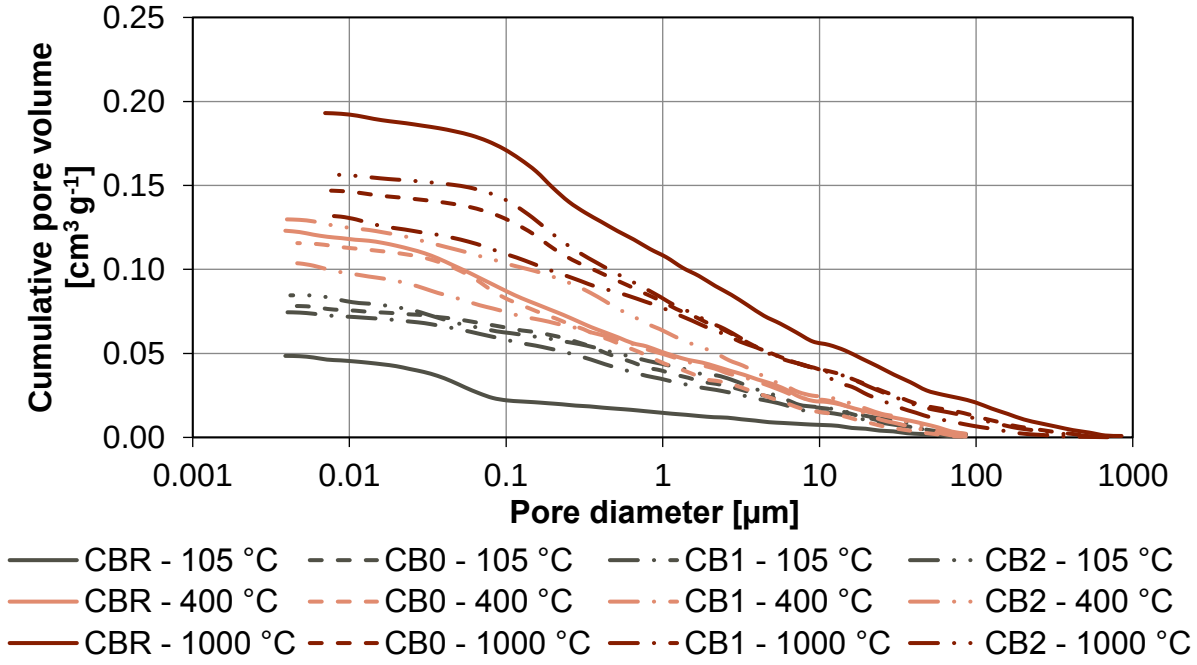

Figure 53 Cumulative pore volumes of composites with combined fibres

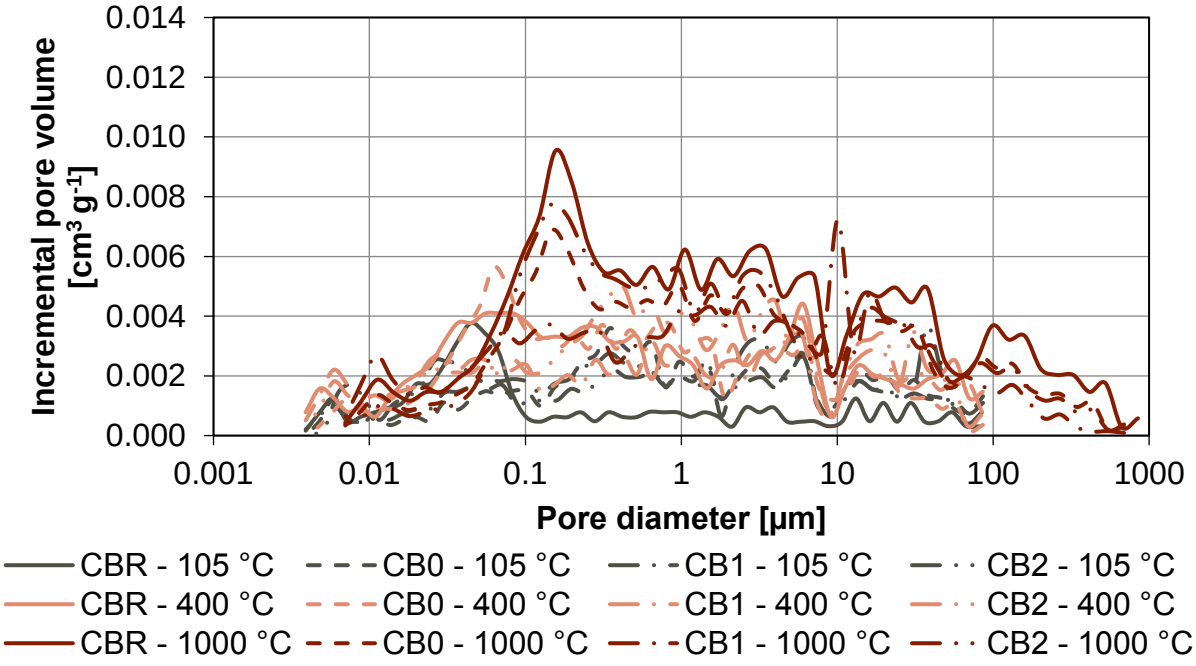

Figure 54 Pore size distribution curves of composites with combined fibres

8.2.2 Mechanical parameters

8.2.2.1 Destructive measurements methods

Compressive strengths of composites with varying fibres combination are presented in Figure 55. The positive effect of fibre reinforcement was indisputable; by application of basalt fibres the compressive strength went up by 5% to 23%. The difference between particular fibres combination was really important, and the best results were obtained in the case of the ratio 90:10. The effect of fibres was magnified due to the temperature exposure. In the case of the best ratio and 400 °C, the improvement of compressive strengths was more than 66%. While when the temperature loading was 1000 °C the compressive strengths of composite with fibres in the ratio 90:10 reached almost 2.6 times higher value than without fibres application. This composite retained about 50% of its original compressive strength, which could be considered as a good result.

Bodnárová et al. [112] presented lower values of compressive strength, which is in accordance with used cement of lower class. Comparison with results presented in this thesis is not so clear, because of unequal temperature loading. However, from their point of view, the best behaviour was shown by application of polypropylene fibres. The decrease of compressive strength was at 800 °C by about 10% lower than in reference state, while their steel fibres led to the 9% of improvement. The best results obtained in the case of combined basalt fibres was the elimination of deterioration by almost 27% at 1000 °C comparing to the reference material.

Because Tanyildzi [114] studied concretes with lightweight aggregate, presented compressive strength are by about twice time lower than in this work. At 400 ºC, the lessening of deterioration due to the temperature loading is by about 12%. Furthermore, carbon fibres at higher temperature burnt out; therefore, the improvement was at higher temperature significantly lower. In comparison, basalt fibres presented in this work proposed improvement by about 20% and seems to be more suitable for composite reinforcement.

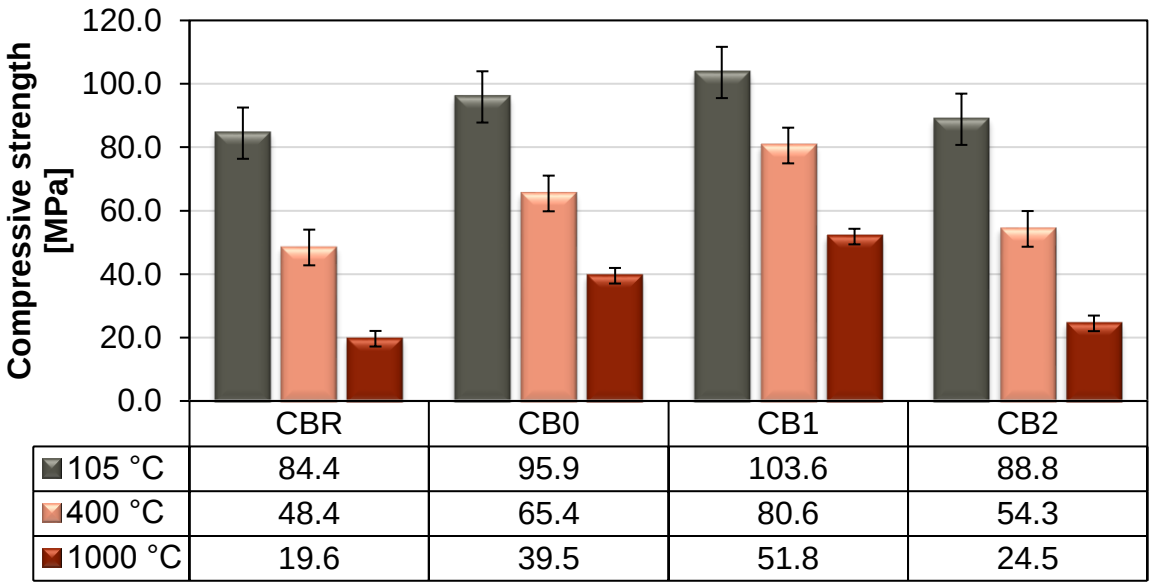

	CBR	CB0	CB1	CB2
105 °C	84.4	95.9	103.6	88.8
400 °C	48.4	65.4	80.6	54.3
1000 °C	19.6	39.5	51.8	24.5

Figure 55 Compressive strengths of composites with combined fibres

Similar tendencies but slightly lower impacts were observed also in the case of bending strengths, which are summarized in Figure 56. In the reference state, the improvement due to the fibres reinforcement range from 1% to 12%. Analogous to the compressive strengths, the best results were reached by utilisation of combination 90:10. In this ratio the improvement due to the temperature loading by 400°C and 1000 °C was 12% and 46% respectively. The residual bending strength showed 34% of the original values.

Similar situation as in the case of compressive strength was reported by Bodnárová et al [112] also in the case of flexural strength. The biggest improvement in the case of polypropylene fibres; the fall was improved by 19% at 800 °C. Steel fibres led to the fall of deterioration by about 19%. While in here the deterioration went down by 11% at 1000 °C due to the basalt fibres reinforcement. The better results obtained by polypropylene fibres seemed to confirmed the important issue of lessening the spalling effect by application of low melting fibres.

Improvement of flexural strength fall due to the carbon fibres utilisation presented by Tanyildzi [114] was even lower than in the case of compressive strength. At 400 °C the decrease of flexural strength fall was by about 3%. While basalt fibres proposed at this temperature improvement by about 12%.

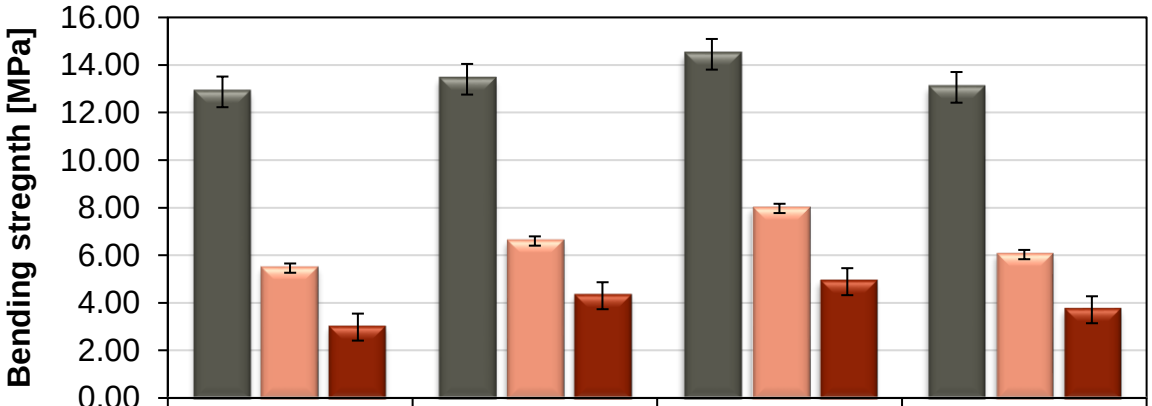

	CBR	CB0	CB1	CB2
105 °C	12.87	13.40	14.45	13.06
400 °C	5.46	6.60	7.97	6.03
1000 °C	2.98	4.30	4.89	3.71

Figure 56 Bending strengths of composites with combined fibres

8.2.2.2 Non-destructive measurements methods

Dynamic modulus of composites with varying reinforcement are shown in Figure 57. The effect of fibres on this property were the lowest from all studied mechanical characteristics. By fibres reinforcement the dynamic modulus went up from 4 to 9%. The difference due to the temperature loading retained similar, in all cases of reinforcement. The positive effect of fibres with higher modulus was probably compensated by increasing of porosimetry, which has negative impact on dynamic modulus. The best results were also observed in the case of the ratio 90:10, which seems to be most appropriate from the point of mechanical behaviour. The difference is however quite low, because the improvement of the elastic modulus fall is below 1%.

Comparison with results presented in Bodnárová et al [112] is, as it was already mention, not really clear. However, they also presented significant fall of dynamic modulus due to the temperature loading. With the lowest deterioration of 59% in the case of polypropylene fibres and 800 °C, which is by 12% lower than without reinforcement. Also steel fibres proposed quite high improvement with the 5% lower deterioration. From that point of view application of those fibres seems to be more effective than basalt fibres which application led to improvement below 1%.

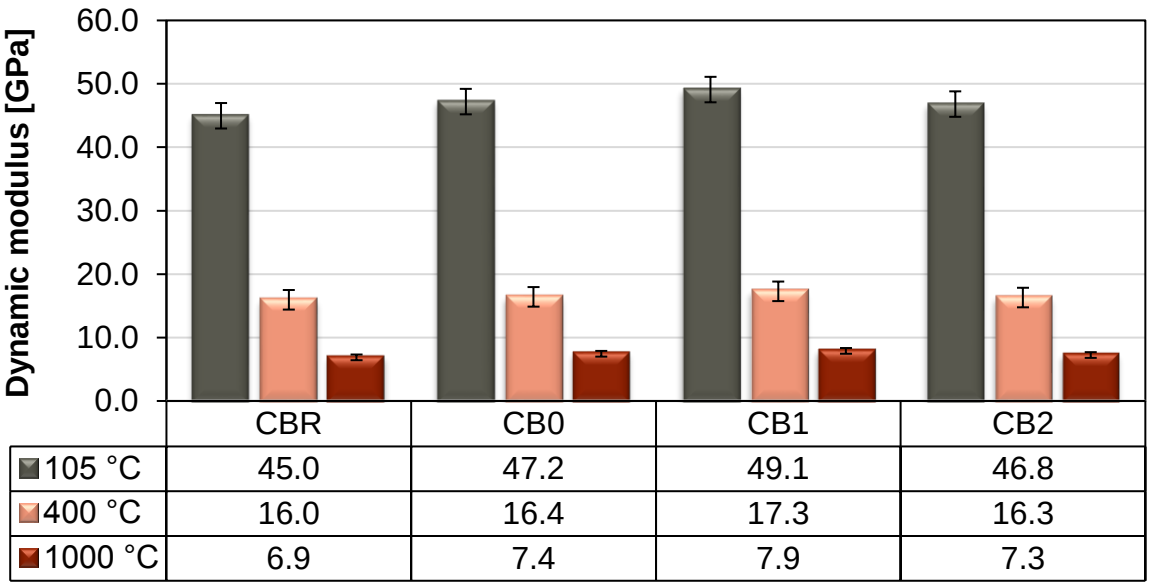

	CBR	CB0	CB1	CB2
105 °C	45.0	47.2	49.1	46.8
400 °C	16.0	16.4	17.3	16.3
1000 °C	6.9	7.4	7.9	7.3

Figure 57 Dynamic modulus of elasticity of composites with combined fibres

8.2.3 Hydric properties

8.2.3.1 Hydric transport

Liquid water transport was primarily characterized by water absorption coefficient (Figure 58). In the reference state, water absorption coefficient went up due to the fibre reinforcement. However, the influence of different combination could not be assessed, because the values varied within the range of standard deviation. When composites were exposed to temperature treatment, the reference material shows the highest value of water absorption coefficient. In comparison with the second worst material with fibres in combination 80:20, the results at 400 °C were almost comparable. Nevertheless, when compared with the one with ratio of 90:10, the water absorption coefficient was decreased by about 31%. The biggest differences between presented composites were observed in the case of 1000°C. The residual water absorption of composite without reinforcement reached by about ten times higher value. This deterioration was decreased due to the reinforcement to less than five times growth in the case of the 90:10 of fibres ratio.

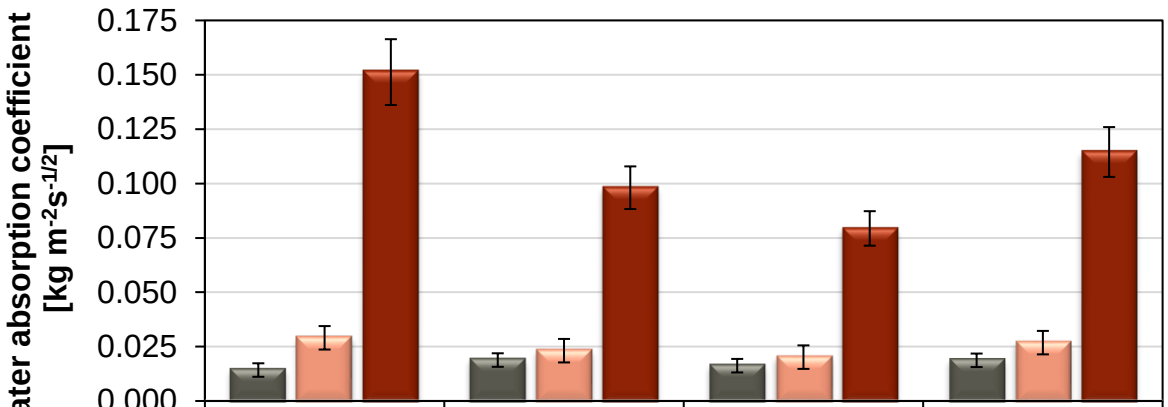

	CBR	CB0	CB1	CB2
105 °C	0.014	0.019	0.016	0.019
400 °C	0.029	0.023	0.020	0.027
1000 °C	0.151	0.098	0.079	0.114

Figure 58 Water absorption coefficients of composites with combined fibres

The second property dealing with liquid water transport were the apparent moisture diffusivity, which can be found in Figure 59. Regarding the apparent moisture diffusivities, they showed similar tendency. However, in this case the difference is less significant. In the reference state, all composites showed similar values. At 400 °C, the growth was noticeable just in the case of the material without reinforcement. Important changes were observed just in the case of the thermal pre-treatment by 1000 °C. The deterioration was worst when no fibres were employed, apparent moisture diffusivity growth almost thirty times. While in the case of fibres reinforcement, the increase was just by about thirteen times. Presented results of water transport characteristics were found to be in accordance with porosity of studied composites; specifically with data of cumulative pores volumes (Figure 53). The most important factor influencing water liquid transport is the amount of capillary pores with diameter approximately from 1 μm to 1 mm and obtained data confirmed this dependency.

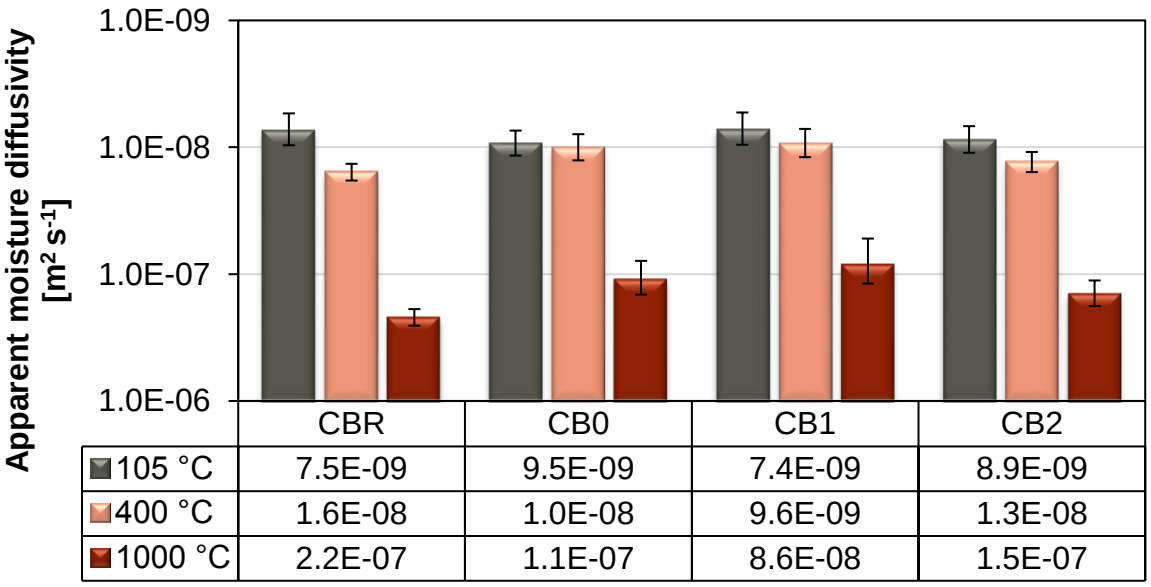

	CBR	CB0	CB1	CB2
105 °C	7.5E-09	9.5E-09	7.4E-09	8.9E-09
400 °C	1.6E-08	1.0E-08	9.6E-09	1.3E-08
1000 °C	2.2E-07	1.1E-07	8.6E-08	1.5E-07

Figure 59 Apparent moisture diffusivities of with combined fibres

Water vapour transport characteristics in dry cup arrangement are summarized in .Table 28 and Figure 60, and in Table 29 and Figure 61 the results from wet cup arrangement are presented. The highest resistance against water vapour transport in the reference conditions showed the reference material without reinforcement, which was in accordance with its lowest open porosity (Figure 52). The composites containing basalt fibres reached by about 14% lower values in the dry-cup arrangement, and by about 11% in the case of wet cup. This tendency was though reversed after high temperature exposure, when composites without fibres reinforcement achieved either comparable (for 400 ºC) or higher (for 1000 ºC) values of the water vapour diffusion resistance factor. After the thermal pre-treatment at 1000 ºC, the difference between reference material and composite with fibres ratio 90:10, which showed the best results, was 27% in the dry-cup and 46% in the wet-cup experiment.

.Table 28 Water vapour diffusion characteristics in dry-cup arrangement of composites with combined fibres

Dry cup	Water vapour diffusion permeability [10^{-12} s]			Water vapour diffusion coefficient [10^{-6} m^2 s^{-1}]		
	105 °C	400 °C	1000 °C	105 °C	400 °C	1000 °C
CBR	2.47 ± 0.07	5.56 ± 0.29	9.92 ± 0.61	0.34 ± 0.03	0.76 ± 0.04	1.36 ± 0.08
CB0	2.87 ± 0.03	5.52 ± 0.41	8.74 ± 0.35	0.39 ± 0.01	0.76 ± 0.06	1.20 ± 0.05
CB1	2.91 ± 0.04	5.16 ± 0.38	7.83 ± 0.27	0.40 ± 0.01	0.71 ± 0.05	1.08 ± 0.04
CB2	2.85 ± 0.07	5.82 ± 0.36	9.22 ± 0.55	0.39 ± 0.01	0.80 ± 0.05	1.27 ± 0.08

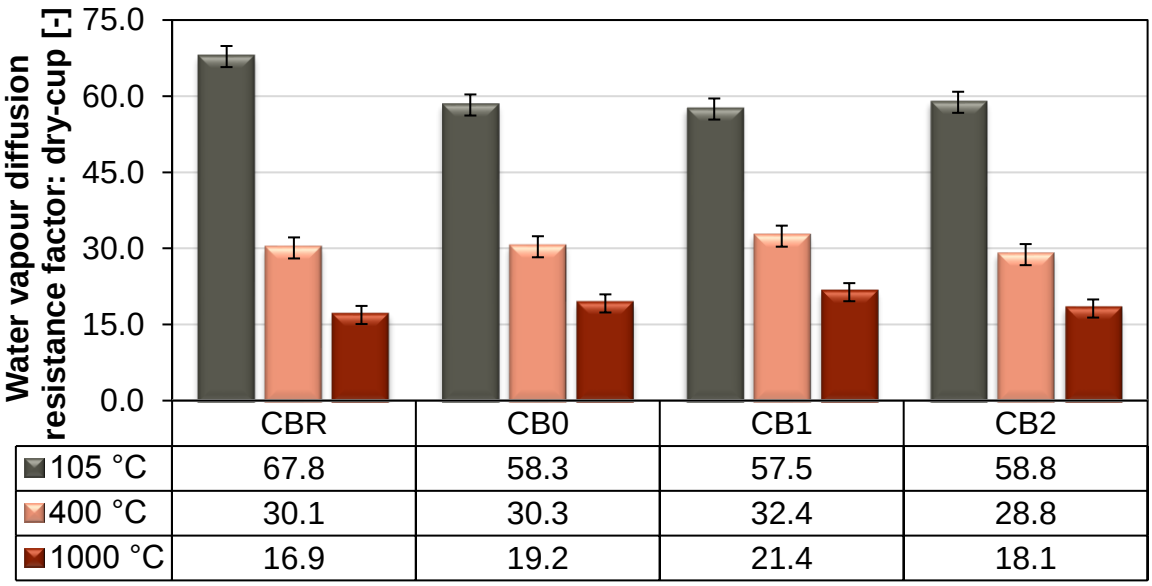

	CBR	CB0	CB1	CB2
105 °C	67.8	58.3	57.5	58.8
400 °C	30.1	30.3	32.4	28.8
1000 °C	16.9	19.2	21.4	18.1

Figure 60 Water vapour diffusion resistance factors in dry-cup arrangement of composites with combined fibres

Table 29 Water vapour diffusion characteristics in wet-cup arrangement of composites with combined fibres

Wet cup	Water vapour diffusion permeability [10^{-12} s]			Water vapour diffusion coefficient [10^{-6} m^2 s^{-1}]		
	105 °C	**400 °C**	**1000 °C**	**105 °C**	**400 °C**	**1000 °C**
CBR	2.87 ± 0.13	6.70 ± 0.63	13.87 ± 0.38	0.39 ± 0.02	0.92 ± 0.09	1.91 ± 0.05
CB0	3.24 ± 0.07	6.88 ± 0.20	10.77 ± 0.63	0.45 ± 0.01	0.94 ± 0.03	1.48 ± 0.09
CB1	3.26 ± 0.16	6.27 ± 0.30	9.47 ± 0.62	0.45 ± 0.02	0.86 ± 0.04	1.30 ± 0.09
CB2	3.13 ± 0.13	6.96 ± 0.10	11.26 ± 0.21	0.43 ± 0.02	0.96 ± 0.01	1.55 ± 0.03

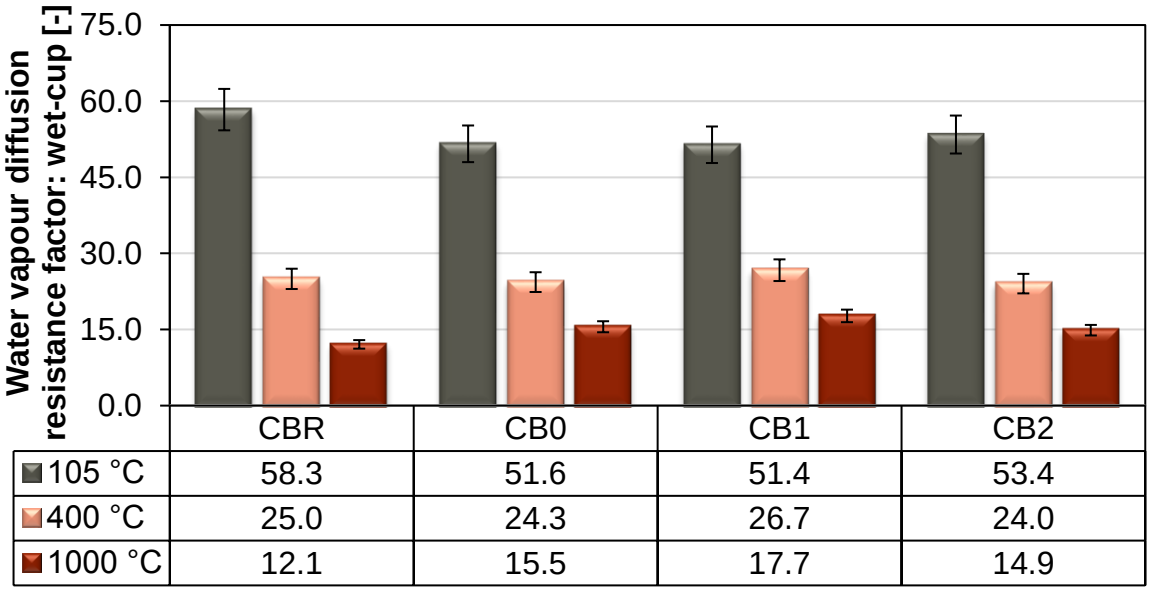

Figure 61 Water vapour diffusion resistance factors in wet-cup arrangement of composites with combined fibres

8.2.3.2 Accumulation of Water Vapour

Sorption isotherms of studied composites with varying fibres are drawn in Figure 62. The water vapour adsorption capability of all composites was relatively high, in particular for the relative humidity over 60%. In the reference conditions the lowest values of moisture content reached reference composite without fibres reinforcement. Its ability to moisture storage was, however, strongly increased as a result of high temperature exposure. This was caused by two main reasons: by significant growth of porosity (Figure 52) due to the temperature exposure, and also by the presence of recrystallized CA and CA_2 (Figure 16 - Figure 18) which were able to react with the surface phase of water adsorbed on the pore walls. After the pre-treatment at 1000 ºC, the lowest water vapour adsorption showed the fibres reinforced composite with ratio 90:10 of longer to shorter fibres.

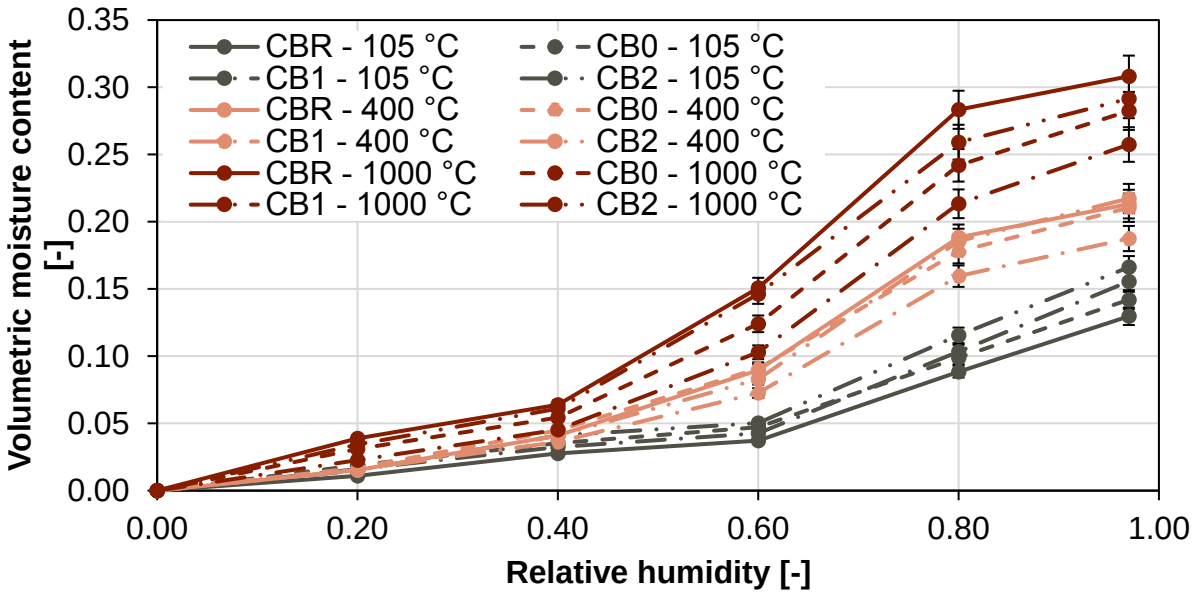

Figure 62 Sorption isotherms of composites with combined fibres

8.2.4 Thermal characteristics

Measured values of thermal conductivity are shown in Figure 63. Material without reinforcement showed in reference condition, without temperature loading, the highest value of thermal conductivity. In dry state the difference was by about 18% in comparison with reinforced materials, whose reached similar values varied just in the range of standard deviation. Due to the deterioration of material when exposed to elevated temperature, the thermal conductivities were significantly decreased. The biggest fall by about 55% was observed in the case of reference material, and the lowest by about 35% in the case of fibre reinforcements. In comparison of reference

composite with fibre reinforced ones, the reference one reached after 1000 °C by about 22% lower value of thermal conductivity. All thermal conductivities of all analysed materials exhibited a significant dependence on moisture content; their values in water saturated state were up to two times higher than in the dry state.

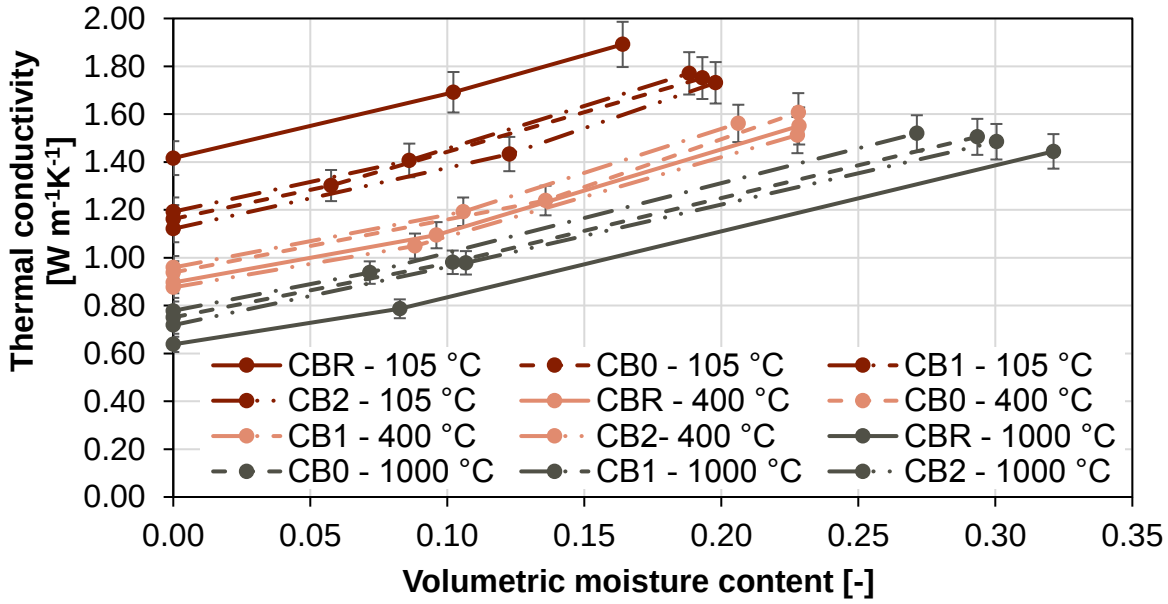

Figure 63 Thermal conductivities of composites with combined fibres

In Figure 64 and Figure 65, there are presented reached values of specific heat capacity in dry and saturated state. It is obvious that in the case of this property, the different between particular measurements was really low, much smaller than the error of used method. More remarkable than the difference between particular materials in varying thermal loading state was the influence of the moisture content. By water saturation the specific heat capacity grew by about 27%, 31% and 38% respectively for reference condition, exposure to 400 °C and 1000 °C respectively.

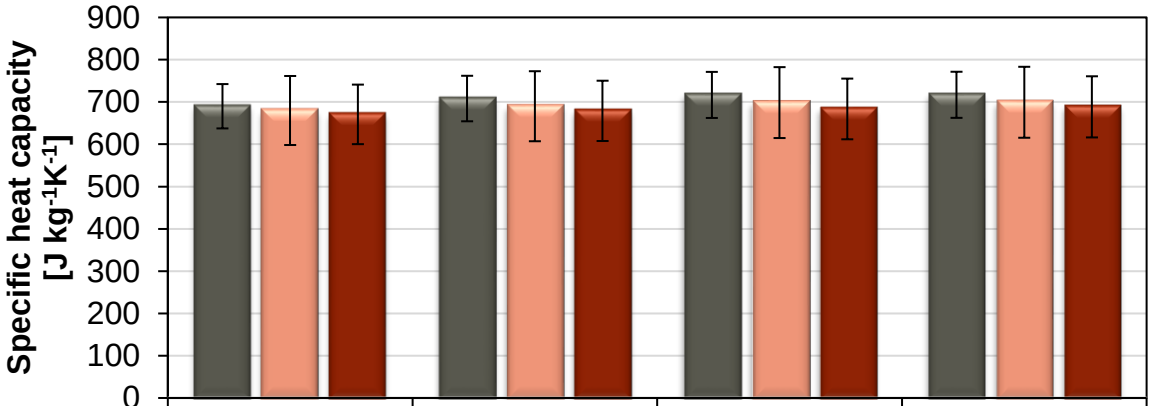

	CBR	CB0	CB1	CB2
105 °C	690	708	717	717
400 °C	680	690	699	699
1000 °C	671	679	684	689

Figure 64 Specific heat capacities of composites with combined fibres in dry state

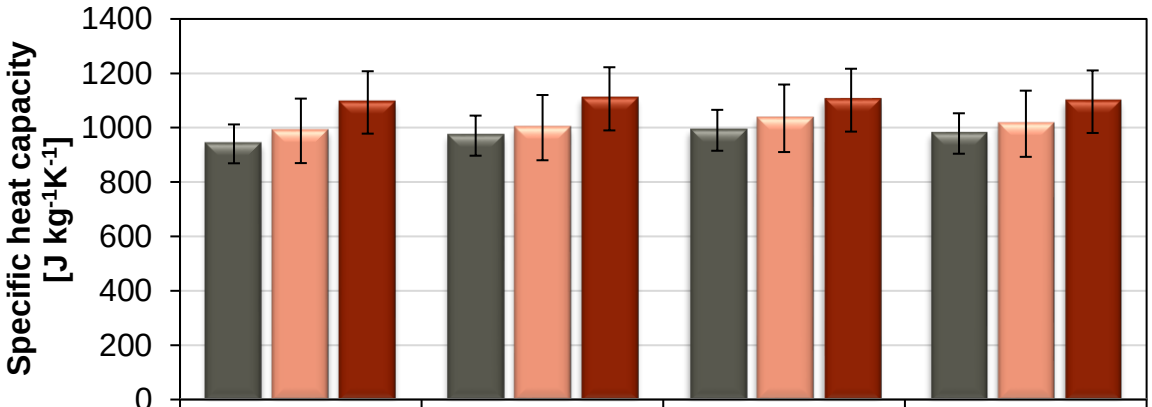

	CBR	CB0	CB1	CB2
105 °C	940	971	990	979
400 °C	988	1000	1035	1015
1000 °C	1093	1106	1101	1096

Figure 65 Specific heat capacities of composites with combined fibres in saturated state

8.2.5 Physical properties at high temperatures

8.2.5.1 Thermal strain

All studied composites exhibited an almost linear dependence of thermal strain on temperature (Figure 66), which was a very positive result. Apparently, the favourable properties of basalt aggregates in high temperature conditions presented the most essential factor in that respect. The differences between particular composites were negligible up to 120 ºC. Then, the effects of decomposition of calcium aluminate hydrates in the cement matrix gained on importance and the positive effect of fibres reinforcement could be observed. The lowest strain over the whole temperature range of 20 – 1000 ºC was found for the material CB1 with the longer-shorter fibres ratio of 90:10; at 1000 ºC it was by 7% lower than for the reference CBR. Linear thermal expansion coefficient was determined also, it can be seen in Figure 67 and Table 30, where particular values are presented. Changes of the coefficient up to by about 500 ºC could be probably connected with the dehydration process of CAC and are mostly influenced by different fibres reinforcement. However, the most important convex peak in temperature about 780 ºC could be assumed to the recrystallization of basalt aggregate; specifically of crystallization of magnesioferrite and hematite, and subsequent also recrystallization of pyroxenes and plagioclase [154, 155].

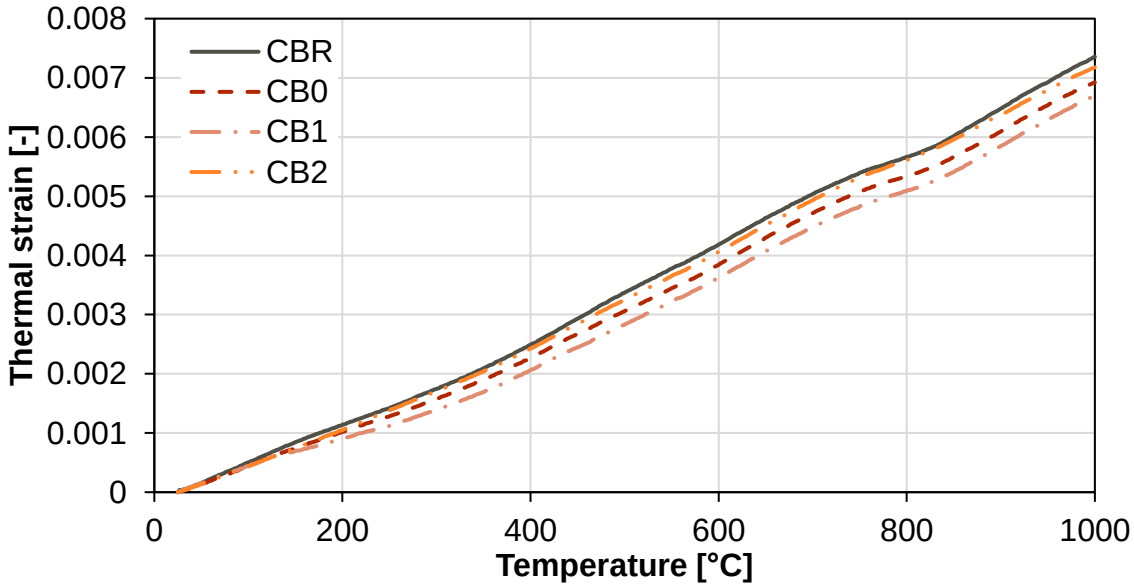

Figure 66 Thermal strains of composites with combined fibres

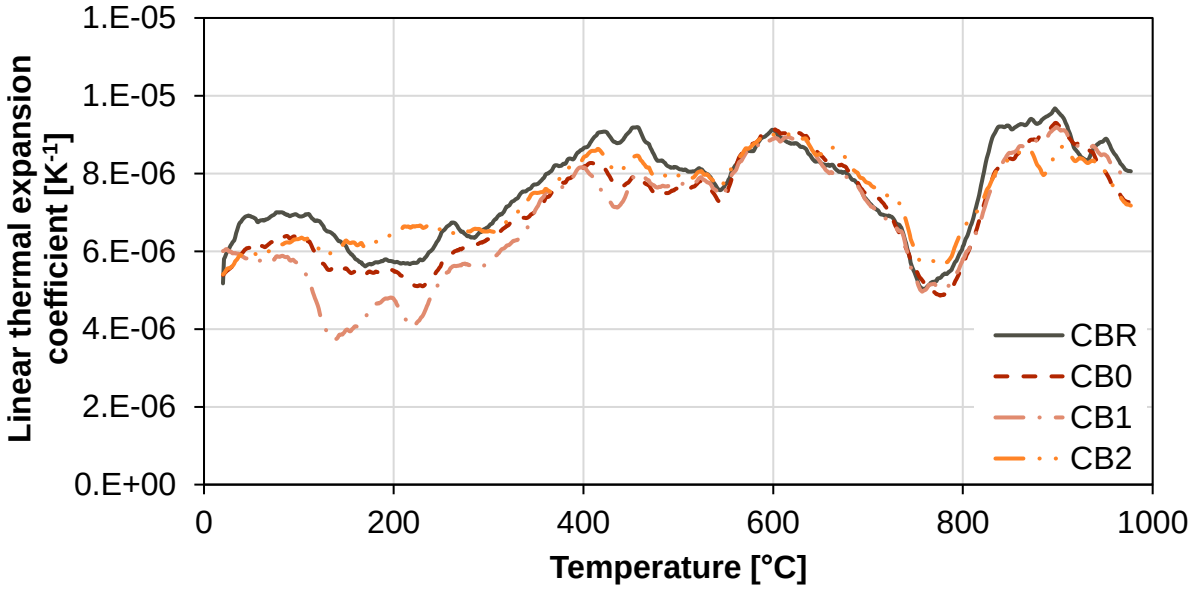

Figure 67 Linear thermal expansion coefficients of composites with combined fibres

Table 30 Linear thermal expansion coefficient of composites with combined fibres

	Linear thermal expansion coefficient [K^{-1}]		
	Average value	**Minimal value**	**Maximal value**
CBR	7,55E-06	4,58E-06	9,89E-06
CB0	7,12E-06	4,57E-06	9,56E-06
CB1	6,87E-06	3,31E-06	9,60E-06
CB2	7,39E-06	5,05E-06	9,42E-06

9 Conclusion

My doctoral thesis is focused on the thermal resistant cement based composites. In this work raw materials were chosen mainly due to their presumed thermal stability. Following materials were employed: calcium aluminate cement was used as a main matrix; as aggregates the basalt ones were chosen; and whole composite was reinforced by basalt fibres. For the sake of comparison also ordinary raw materials as Portland cement and silica aggregates were utilised. After raw-materials had been chosen, their comprehensive characterization was performed. The aim was not only to predict their behaviour in composite's mixtures, but also confirmed thermal resistance of chosen materials. Some important observations can be summarized as follows:

- Faster hydration rate of CAC was confirmed, after two days the most of the phases are hydrated.
- Calcium dialuminate (CA_2) was found to be almost unreactive phase.
- Water curing of CAC paste was found to be inappropriate.

Next step was design of mixture compositions. The setting of raw-material's amounts was performed experimentally by virtue of the measurement of residual compressive strengths, bending strengths and bulk densities. Primarily the impact of varying w/c ratio was investigated. Then the amount of fibres was set, following to superplasticizer optimization. Also appropriate fibres lengths combination was experimentally investigated. As a consequence, 8 mixtures with varying raw-materials and 3 mixtures with different fibres length ratio were chosen. Some interesting points from mixture design are presented herein below:

- Low w/c ratio (0.25) was proved to be most efficient in the case of CAC paste.
- In accordance with other researches, the optimal amount of basalt fibres was found to be 0.5% of volume.
- The necessity of plasticizer application was proved; without the plasticizer the designed mixture was not able to be properly mixed.
- The varying fibres length ratio has the most significant impact of the bending strength.

Thermal stability or resistivity of studied materials was studied by virtue of determination of residual properties after a temperature loading. Particular temperatures were set according to the results of differential scanning calorimetry of used materials, or more precisely according to chemical and physical changes

occurring in used raw-materials. Composites were pre-treated by the exposure to temperature 105 °C, 400 °C or 1000 °C. Again some highlights from this part of the work are summarized as follows:

- The lowest weight and heat changes due to the temperature exposure showed silica aggregate.
- After exposure to 1000 °C, the CAC paste showed to contain the re-new phase, similar as a raw cement. This proposes the idea of rehydrating of the paste during further moisture contact. What should be further investigated.

Experimental program composed of measurement of basic physical properties, mechanical strengths, hydric transport parameters and thermal characteristics. In this work all planed experiments were presented and described in detail. Achieved results were assessed and where it was possible also compared with other researches. According to presented results, several conclusions can be drawn:

- Matrix densities reached higher values in the case of CAC cement as well as basalt aggregate. No specific varying impacts due to different raw-materials were observed at high temperature exposure.
- Utilisation of more resistant raw-materials led to the growth of porosities in reference state, but most importantly to the much lower growth of residual porosities.
- CAC showed somewhat lower compressive strengths in reference state. However, at 400 °C values were comparable of those containing PC. At 1000 °C the CAC cement reached applicable values, while PC application led to the immense deterioration. Basalt aggregate and basalt fibres caused improvement of compressive strengths in all states. Basalt fibres seemed to be more effective than carbon or steel fibres.
- The other mechanical properties (bending strength and dynamic modulus of elasticity) showed same tendencies as the compressive strength. Despite the reference state, where CAC proved to be more beneficial.
- Water transport ability of studied mixtures was in accordance with their varying porosities. However, the impact of high temperature (especially of 1000 °C) was giant. The lowest changes were observed in the case of CAC, basalt aggregate and appropriate ratio of basalt fibres, as their porosity grew the least.
- Water vapour adsorption capabilities of studied composites were after temperature exposure really high, which was significantly increased. One of the

possible reasons is rehydration of cement's renewed phases, which in the case of 1000 °C and PC utilisation led to the total degradation of specimens.

- The biggest impact on thermal properties was observed in the case of different aggregate, when basalt proposed lower thermal conductivities.
- Thermal strain showed surprisingly slightly higher values in the case of CAC utilisation. It was proved that the thermal strain could be decreased by fibre reinforcement. However, the biggest impact on high values of thermal strain could be attributed to crystalline transformation of aggregates. Thus, silica aggregate confirmed its unsuitability for high temperature applications.

From presented results can be deduced that designed composite based on CAC, basalt aggregate and appropriate fibre reinforcement as well as all particular thermal resistant raw-materials proved its better applicability for high temperature applications.

Possibility of further investigation:

During the preformed research, several issues worth for the future investigation were noticed. Some points of a possible research can be outlined as follows:

- As it was already mentioned, a further investigation of cyclic temperature loadings of CAC paste should be performed, including the possibility of the rehydration of thermal treated composites.
- Another issue is a determination of the properties at high temperatures, not only after the temperature exposures. Measurements of the thermal properties have already been started. Moreover, a designing of an experimental measurement for a determination of mechanical properties at high temperatures would be of a great importance.
- Regarding the cement based composite, its composition can be further improved. One possibility is the application of some pozzolanic materials with an adequate chemical composition (e.g. metakaoline, metashale, brick waste ash). This could bring lower consumption of expensive CAC and probably also conversion elimination or reduction.
- When focus on a reinforcement, adding of low melting fibres could proposed another improvement of thermal resistant. However, this would increase the porosity, also in the reference state, which could be eliminated by further addition of some fine fractions.

References

[1] PHILLPOT, S. R. and McGAUGHEY, A. J. H. Introduction to Thermal Transport. *Materials Today.* 2005, **8**(6), 18-20.

[2] ČERNÝ, R. and ROVNANÍKOVÁ, P., 2002. *Transport Processes in Concrete.* London: Spon Press.

[3] ČERNÝ, R., 1993. *FYZIKA Transportní Jevy*, Prague: Publishing House CTU in Prague.

[4] KAPIČKOVÁ, O. and VODÁK, F., 2006. *FYZIKA 20 Termodynamika*, Prague: Publishing House CTU in Prague.

[5] PHILIP, J. R. and De VRIES, D. A. Moisture Movement in Porous Materials under Temperature Gradients. *Transactions American Geophysical Union.* 1957, **38**(2), 222-232.

[6] De VRIES, D. A. The Theory of Heat and Moisture Transfer in Porous Media Revisited. *International Journal of Heat and Mass Transfer.* 1987, **30,** 1343-1350.

[7] MILLY, P. C. D. Moisture and Heat Transport in Hysteretic, Inhomogeneous Porous Media: a Matrix Head-based Formulation and a Numerical Model. *Water Resources Research.* 1982, **18**, 489-498.

[8] KRISCHER, O., 1963. *Die Wissenschaftlichen Grundlagen der Trocknungstechnik*, Berlin: Springer Berlin Heidelberg.

[9] LYKOV, A. V., 1956. *Teplo i Massoobmen v Processach Sushki*, Moskva: Gostechizdat.

[10] KIESSL, K. *Kapillarer und Dampfförmiger Feuchtetransport in Mehrschichtigen Bauteilen*, Essen, 1983. Doctoral Thesis. Universität Essen.

[11] HÄUPL, P. and STOPP, H. Ein Beitrag zum Feuchtigkeitstransport in Bauwerksteilen. In: *Proceedings of 3. Bauklimatisches Symposium*. Dresden: TU Dresden, 1980, 93-102.

[12] KÜNZEL, H. M. *Simultaneous Heat and Moisture Transport in Building Components*, Stuttgart, 1995. Doctoral Thesis. IRB Verlag.

[13] BALAJI, C., 2014. *Essentials of Radiation Heat Transfer*. Chennai (India): John Wiley & Sons.

[14] KOTHANDARAMAN, C. P., 2006. *Fundamentals of Heat and Mass Transfer*, Daryaganj: New Age International.

[15] ČERNÝ, R. and VENZMER, H. Ein Modifiziertes Lykow-Modell zum Warmeund Feuchtetransports in Kapillarporosen Stoffen. *Gesundheitsingenieur.* 1991, **112**, 41-44.

[16] ČERNÝ, R. Heat and Moisture Transport during a Fire. A Model with Moving Boundary. *Stavebnícky časopis.* 1989, **37**, 89-99.

[17] BAŽANT, Z. P. and THONGUTHAI, W. Pore Pressure in Heated Concrete Walls. *Magazine of Concrete Research,* 1979, **31**, 67-76.

[18] FEDEROV, A. G. and PILON, L. Glass Foams: Formation, Transport Properties, and Heat, Mass, and Radiation Transfer. *Journal of Non-Crystalline Solids.* 2002, **311**, 154-173.

[19] CHENG, X. and FAN, J. Simulation of Heat and Moisture Transfer with Phase Change and Mobile Condensates in Fibrous Insulation. *International Journal of Thermal Sciences.* 2004, **43**, 665-676.

[20] Regulation (EU) 305/201. *Construction Products Regulation*. Brussels: European Council, 2011.

[21] Council Directive 89/106/EEC*. Construction Products Directive.* Brussels: European Council, 1988.

[22] ČSN 73 0810*. Fire Protection of Buildings - General Requirements.* Prague: Czech Standardization Agency, 2016.

[23] ČSN 73 0802. *Fire Protection of Buildings – Non-industrial Buildings.* Prague: Czech Standardization Agency, 2009.

[24] ČSN 73 0804*. Fire Protection of Buildings – Industrial Buildings.* Prague: Czech Standardization Agency, 2010.

[25] Act no. 225/2017. *The Building Act.* Prague: Parliament of the Czech Republic, 2018.

[26] Act no. 133/1985. *The Fire Protection Act.* Prague: Parliament of the Czech Republic, 1985.

[27] ČSN EN 13501-1+A1. *Fire Classification of Construction Products and Building Elements – Part 1: Classification Using Test Data from Reaction to Fire Tests.* Prague: Czech Standardization Agency, 2010.

[28] ČSN EN ISO 1182*. Reaction to Fire Tests for Products – Non-combustibility Test.* Prague: Czech Standardization Agency, 2010.

[29] ČSN EN ISO 1716. *Reaction to Fire Tests for Products – Determination of the Cross Heat of Combustion (Calorific Value).* Prague: Czech Standardization Agency, 2010.

[30] ČSN EN ISO 11925-2. *Reaction to Fire Tests – Ignitability of Building Products Subjected to Direct Impingement of Flame – Part 2: Single-flame Source Test.* Prague: Czech Standardization Agency, 2011.

[31] ČSN EN 13823*. General Principles on the Design of Structures for Durability.* Prague: Czech Standardization Agency, 2014.

[32] KUPILÍK, V., NOORI, M., POKORNÝ M. and ŠIMMER, D., 2007. S*tavební Konstrukce z Požárního Hlediska dle Evropských Norem*, Prague: Tisk Powerprint.

[33] GAIGL, C. and MENSINGER, M., February 2017. Vývoj Teplot Žárově Zinkovaných Ocelových Prvků Během Požáru. *KONSTRUKCE Odborný Časopis pro Stavebnictví a Strojírenství* [online]. Ostrava: KONSTRUKCE Media, s.r.o., [Accessed August 2018]. Available: http://www.konstrukce.cz/clanek/vyvoj-teplot-zarove-zinkovanych-ocelovych-prvku-behem-pozaru/

[34] SVOBODA, L., 2007. *Stavební Hmoty*. Bratislava: JAGA Group, s.r.o.

[35] SARKAR, R., 2017. *Refractory Technology - Fundamentals and Applications*, Boca Raton: Taylor & Francis Group.

[36] ČSN ISO 10080 (726011). *Refractory Products - Classification of Dense, Shaped Acid-resisting Products.* Prague: Czech Standardization Agency, 1993.

[37] *MatWeb - Material property Data*, 2018 [online]. Blacksburg, VA: MatWeb, LLC. [Accessed September 2018]. Available: http://www.matweb.com/index.aspx

[38] MIKULINEC, D. *The Concrete with a Higher Resistance to High Temperatures.* Brno, 2012. Diploma Thesis. Brno University of Technology.

[39] HAGER, I., TRACZ, T., ŚLIWIŃSKI, J. and KRZEMIEŃ, K. The Influence of Aggregate Type on the Physical and Mechanical Properties of High-performance Concrete Subjected to High Temperature. *Fire and Materials.* 2015, **40**(5), 668-682.

[40] HARTLIEB, P., TOIFL, M., KUCHAR, F., MEISELS, R. and ANTRETTER, T. Thermo-physical Properties of Selected Hard Rocks and Their Relation to Microwave-assisted Comminution. *Materials Engineering.* 2016, **91**, 34-41.

[41] KUTZENDORFER, J. and MÁŠA, Z., 1991. *Žárovzdorné Tepelně Izolační Materiály*, Prague: Informatorium.

[42] ANANDAMURTHY, A., GUN, V., ILANGOVAN, M. and REDDY, N. A Review of Fibrous Reinforcements of Concrete. *Journal of Reinforced Plastics & Composites.* 2017, **36**(7), 519-552.

[43] MAZHARUL I. K. *Textile Learner* [Online]. 2018. [Accessed September 2018]. Available: http://textilelearner.blogspot.com/p/about-me.html

[44] EZEKIEL, N., NDAZI, B., NYAHUMWA, C. and KARLSSON, S. Effect of Temperature and Durations of Heating on Coir Fibres. *Industrial Crops and Products.* 2011, **33**(3), 638-643.

[45] ČSN EN 993-12*. Methods of Test for Dense Shaped Refractory Products - Part 12: Determination of Pyrometric Cone Equivalent (Refractoriness).* Prague: Czech Standardization Agency, 1998.

[46] ČSN EN 993-13*. Methods of Test for Dense Shaped Refractory Products - Part 13: Specification for Pyrometric Reference Cones for Laboratory Use.* Prague: Czech Standardization Agency, 1996.

[47] ČSN EN 993-8. *Methods of Testing Dense Shaped Refractory Products – Part 8: Determination of Refractoriness-under-load.* Prague: Czech Standardization Agency, 1998.

[48] ČSN EN 993-11*. Methods of Test for Dense Shaped Refractory Products - Part 11: Determination of Resistance to Thermal Shock.* Prague: Czech Standardization Agency, 2008.

[49] ČSN EN 993-10*. Methods of Test for Dense Shaped Refractory Products - Part 10: Determination of Permanent Change in Dimensions on Heating.* Prague: Czech Standardization Agency, 1999.

[50] KOPANDA, J. E. and MacZURA, G. Processes, Properties and Applications for Calcium Aluminate Cements. In: *Alumina Chemicals Science and Technology Handbook*. Westerville: American Ceramic Society, 1990, 171-181.

[51] MATOUŠEK, M. and DROCHYTKA, R., 1998. *Atmosférická Koroze Betonu*. Prague: IKAS.

[52] SCRIVENER, K. L. and CAPMAS, A. 13 Calcium Aluminate Cements. In: *Lea's Chemistry of Cement and Concrete.* Oxford: Elsevier Butterworth-Heinemann, 2003, 713-782.

[53] SMITH, A., CHOTARD, T., GIMET-BREART, N., and FARGEOT, D. Correlation between Hydration Mechanism and Ultrasonic Measurements in an Aluminous Cement: Effect of Setting Time and Temperature on the Early Hydration. *Journal of the European Ceramic Society.* 2002, **22**, 1947-1958.

[54] TEGEL, M. *Foundry Mould Sand with Cement Binder*. Brno, 2001. Doctoral thesis. Brno Technical University.

[55] UKRAINCZYK, N. and MATUSINOVIĆ, T. Thermal Properties of Hydrating Calcium Aluminate Cement Pastes. *Cement and Concrete Research*. 2010, **40**(1), 128-136.

[56] ANTONOVIČ, V., KERIENE, J., BORIS, R. and ALEKNEVIČIUS, M. The Effect of Temperature on the Formation of the Hydrated Calcium Aluminate Cement Structure. *Procedia Engineering.* 2013, **57**, 99-106.

[57] BARTHELMY, D., 2014. Mineralogy Database [Online]. Spring, Texas. [Accessed September 2018]. Available: http://webmineral.com/.

[58] ADAMS, M. P. and IDEKER, J. H. Influence of Aggregate Type on Conversion and Strength in Calcium Aluminate Cement Concrete. *Cement and Concrete Research.* 2017, **100**, 284-296.

[59] *Technology of Monolithic Refractories*, 1999. Tokyo: Plibrico Japan Company Limited.

[60] MIDGLEY, H. G. and MIDGLEY, A. The Conversion of High Alumina Cement. *Magazine of Concrete Research.* 1975, **27**(91), 59-77.

[61] PACEWSKA, B. and NOWACKA, M. Studies of Conversion Progress of Calcium Aluminate Cement Hydrates by Thermal Analysis Method. *Journal of Thermal Analysis and Calorimetry*. 2014, **117**(2), 653-660.

[62] KHALIQ, W. and KHAN, H. A. High temperature material properties of Calcium Aluminate Cement Concrete. *Construction and Building Materials.* 2015, **94**, 475-487.

[63] COLLEPARDI, M., MONOSI, S. and PICCIOLI, P. The Influence of Pozzolanic Materials on the Mechanical Stability of Aluminous Cement. *Cement and Concrete Research.* 1995, **25**(5), 961-968.

[64] HEIKAL, M., RADWAN, M. M. and Al-DUAIJ, O. K. Physico-mechanical Characteristics and Durability of Calcium Aluminate Blended Cement Subject to Different Aggressive Media. *Construction and Building Materials.* 2015, **78**, 379-385.

[65] FERNÁNDEZ-JIMÉNEZ, A., VÁZQUEZ, T. and PALOMO, Á. Effect of Sodium Silicate on Calcium Aluminate Cement Hydration in Highly Alkaline Media: a Microstructural Characterization. *Journal of the American Ceramic Society.* 2011, **94**(4), 1297-1303.

[66] SUGAMA, T. and CARCIELLO, N. R. Sodium Phosphate-derived Calcium Phosphate Cements. *Cement and Concrete Research.* 1995, **25**(1), 91-101.

[67] FERNÁNDEZ-CARRASCO, L., PUERTAS, F., BLANCO-VARELA, M. T. and VÁZQUEZ, T. Carbonatacion de Pastas de Cemento de Aluminato de Calcio. *Materiales de Construcción.* 2001, **51**(263-264), 127-136.

[68] FERNÁNDEZ-CARRASCO, L., RIUS, J. and MIRAVITLLES, C. Supercritical Carbonation of Calcium Aluminate Cement. *Cement and Concrete Research.* 2008, **38**(8-9), 1033-1037.

[69] GRACÍA-ALCOCEL, E., GARCÉS, P. and CHINCHÓN, S. General Study of Alkaline Hydrolysis in Calcium Aluminate Cement Mortars under a Broad Range of Experimental Conditions. *Cement and Concrete Research.* 2000, **30**(11), 1689-1699.

[70] PARK, S. M., JANG, J. G., SON, H. M. and LEE, H. K. Stable Conversion of Metastable Hydrates in Calcium Aluminate Cement by Early Carbonation Curing. *Journal of CO2 Utilization.* 2017, **21**, 224-226.

[71] MAAROUFI, M.-A., LECOMTE, A., DILIBERTO, C., FRANCY, O. and Le BRUN, P. Thermo-hydrous behaviour of hardened cement paste based on calcium aluminate cement. *Journal of the European Ceramic Society.* 2015, **35**, 1637-1646.

[72] ZHU, B., FANG, B. and LI, X. Dehydration reactions and kinetic parameters of gibbsite. *Ceramics International.* 2010, **36**, 2493-2498.

[73] J. PETRÁNEK. *Geologic Encyclopaedia – Basalt* [online]. Brno: State Geological Survey, 2007. [Accessed November 2015]. Available: http://www.geology.cz/aplikace/encyklopedie/term.pl?bazalt.

[74] FIORE, V., SCALICI, T., Di BELLA, G. and VALENZA, A. A Review on Basalt Fibre and its Composites. *Composite Part B: Engineering.* 2015, **74**, 74-94.

[75] BEST, M. G., 2003. *Igneous and Metamorphic Petrology*. Malden: Blackwell Publishing Company.

[76] PRODESCU, I. Comparative Study of Physical and Mechanical Properties of Basalts Exploited in Romania. *Romanian Journal of Mineral Deposits*. 2010, **84**, 131-136.

[77] GOODMAN, R. E., 1993. *Engineering Geology: Rock in Engineering Construction*. New York: John Wiley & Sons Inc.

[78] ASU, I. M. Evaluating of Different Asphalt Concrete Mixes. *Building and Environment.* 2007, **42**, 325-329.

[79] TASONG, W. A., LYNSDALE, C. J. and CRIPPS, J. C. Aggregate-cement Paste Interface. ii: Influence of Aggregate Physical Properties. *Cement and Concrete Research.* 1997, **27**(2), 165-170.

[80] ÖZTURAN, T. and CECEN, C. Effect of Coarse Aggregate Type on Mechanical Properties of Concretes with Different Strengths. *Cement and Concrete Research.* 1997, **27**(2), 165-170.

[81] REITERMAN, P., HOLČAPEK, O., JOGL M. and KONVALINKA, P. Physical and Mechanical Properties of Composites Made with Aluminous Cement and Basalt Fibres Developed for High Temperature Application. *Advances in Materials Science and Engineering.* 2015, **2015**, 1-10.

[82] HOLČAPEK, O., REITERMAN, P. and KONVALINKA, P. Influence of Ceramic Fibres on Mechanical Characteristics of Refractory Composites. *Advanced Material Research.* 2014, **1054**, 22-26.

[83] LEHNER, J. and SURÝ, L., 1975. *Silikátová Vlákna v Průmyslu a Stavebnictví.* Praha: Státní Nakladatelství Technické Literatury.

[84] DHAND, V., MITTAL, G., RHEE, K. Y., PARK, S.-J. and HUI, D. A Short Review on Basalt Fibre Reinforced Polymer Composites. *Composites Part B: Engineering.* 2015, **73**, 166-180.

[85] KOGAN, F. M. and NIKITINA, O. V. Solubility of chrysotile asbestos and Basalt Fibres in Relation to their Fibrogenic and Carcinogenic Action. *Environ Health Prospect,* 1944, **102**, 205-206.

[86] Mc CONNELL, E. E., KAMSTRUP, O., MUSSELMAN, R., HESTERBERT, T. W., CHEVALIER, J. and MILLER, W. C. Chronic Inhalation Study of Size-separated Rock and Slag Wool Insulation Fibres in Fischer 344/N rats. *Inhalation Toxicology.* 1994, **6**, 571-614.

[87] MONNI, F., QUAGLIARINI, E., LENCI, S. and BONDIOLI, F. Tensile Characterization of Basalt Fibre Rods and Ropes: a First Contribution. *Construction and Building Materials.* 2012, **34**, 327-380.

[88] MILITKY, J., KOVAČIČ V., and RUBNEROVÁ, J. Influence of Thermal Treatment on Tensile Failure of Basalt Fibres. *Engineering Fracture Mechanics.* 2002, **69**(9), 1025-1033.

[89] FIORE, V., SCALICI, T. and Di BELLA, G. Glass-basalt/epoxy Hybrid Composites for Marine Applications. *Materials and Design.* 2011, **32**, 2091-2099.

[90] SIM, J., PARK, C. and MOON, D. Y. Characteristics of Basalt Fibre as a Strengthening Material for Concrete Structures. *Composites Part B: Engineering.* 2005, **6-7**(36), 504-512.

[91] NOVITSKII, A. G. High Temperature Heat Insulating Materials Based on Fibres from Basalt Type Rock Materials. *Refractories and Industrial Ceramics.* 2004, **45**(2), 144-146.

[92] HAO, L. C. and YU, W. D. Evaluation of thermal protective performance of Basalt Fibre Nonwoven Fabrics. *Journal of Thermal Analysis and Calorimetry.* 2010, **100**(2), 551-555.

[93] JIANG, C., FAN, K., WU, F. and CHEN, D. Experimental study on the Mechanical Properties and Microstructure of Chopped Basalt Fibre Reinforced Concrete. *Materials and Design.* 2014, **58**, 187-193.

[94] KABAY, N. Abrasion Resistance and Fracture Energy of Concretes with Basalt Fibre. *Construction and Building Materials.* 2014, **50**, 95-101.

[95] JOGL, M., REITERMAN, P., HOLČAPEK, O. and KOŤÁTKOVÁ, J. Effect of High Temperature Treatment on the Mechanical Properties of Basalt Fibre Reinforced Aluminous Composites. *Applied Mechanics and Materials.* 2015, **732**, 111-114.

[96] RYBIN, V. A., UTKIN, A. V. and BALKANOVA, N. I. Alkali Resistance, Microstructural and Mechanical Performance of Zirconia-coated Basalt Fibres. *Cement Concrete Research.* 2013, **53**, 1-8.

[97] SCHEFFLER, C., FÖRSTER, T., MÄDER, E., HEINRICH, G., HEMPEL, S. and MECHTCHERINE, V. Aging of Alkali-resistant Glass and Basalt Fibres in Alkaline Solutions: Evaluation of the Failure Stress by Weibull Distribution Function. *Journal of Non-Crystalline Solids.* 2009, **355**, 2588-2595.

[98] IVASHCHENKO, E. A. Sizing and Finishing Agents for Basalt and Glass Fibres. *Technology of Polymeric and Composite Materials*. 2008, **9**(1), 16-21.

[99] SADASISNI, F., TIRILLÒ, J., SERGI, C., SEGHINI, M. C. and COZZARINI, L. Effect of Basalt Fibre Hybridisation and Sizing Removal on Mechanical and Thermal Properties of Hemp Fibre Reinforced HDPE Composites. *Composite Structure.* 2018, **188**, 394-406.

[100] IORIO, M., SANTARELLI, M. L., GONZÁLEZ-GAITANO, G. and GONZÁLEZ-BENITO, J. Surface Modification and Characterization of Basalt Fibres as Potential Reinforcement of Concretes. *Applied Surface Science.* 2018, **427**, 1248-1256.

[101] CAGRIALP, A. and DOGAN, M. The Effects of Silane Coupling Agents on the Mechanical Properties of Basalt Fibre Reinforced Poly(Butylene Terephthalate) Composites. *Composites Part B.* 2018, **146**, 145-154.

[102] AFROZ, M., PATNAIKUNI, I. and VENKATESAN, S. Chemical Durability and Performance of Modified Basalt Fibre in Concrete Medium. *Construction and Building Materials.* 2017, **154**, 191-203.

[103] WEI, F., FANG, C. and WU, B. Fire Resistance of Concrete-filled Steel Plate Composite (CFSPC) Walls. *Fire Safety Journal.* 2017, **88**, 26-39.

[104] SHEKASTEHBANDA, B., TAROMI, A. and ABEDI, K. Fire Performance of Stiffened Concrete Filled Double Skin Steel Tubular Columns. *Fire Safety Journal.* 2017, **88**, 13-25.

[105] SONG, T. Y., TAO, Z., RAZZAZZADEH, A., HAN, L. H. and ZHOU, K. Fire Performance of Blind Bottled Composite Beam to Column Joints. *Journal of Constructional Steel Research.* 2017, **132**, 29-42.

[106] WANG, Y., LI, Y., ZHU, B. and CHEN, P. Microstructure Evolution during the Heating Process and its Effect on the Elastic Properties of CAC-bonded Alumina Castables. *Ceramics International.* 2016, **42**, 11355-11362.

[107] OGRODNIK, P. and SZULEJ, J. The Impact of Aeration of Concrete Based on Ceramic Aggregate Exposed to High Temperatures, on its Strength Parameters. *Construction and Building Materials.* 2017, **157**, 909-916.

[108] BARADARAN-NASIRI, A. and NEMATZADEH, M. The Effect of Elevated Temperatures on the Mechanical Properties of Concrete with Fine Recycled Refractory Brick Aggregate and Aluminate Cement. *Construction and Building Materials.* 2017, **147**, 865-875.

[109] MASOOD, A., SHARIQ, M., MASROOR ALAM, M., AHMAD, T. and BEG, A. Effect of Elevated Temperature on the Residual Properties of Quartzite, Granite and Basalt Aggregate Concrete. *Journal of The Institution of Engineers (India): Series A.* 2018, **99**(3), 485-494.

[110] FRANTZIS, P. and BAGGOTT, R. Bond between Reinforcing Steel Fibres and Magnesium Phosphate/Calcium Aluminate Binders. *Cement & Concrete Composites.* 2000, **22**, 187-192.

[111] BORIS, R., ANTONOVIČ, V., KERIENE, J. and STONYS, R. The Effect of Carbon Fiber Additive on Early Hydration Of Calcium Aluminate Cement. *Journal of Thermal Analysis and Calorimetry.* 2016, **125**(3), 1061-1070.

[112] BODNÁROVÁ, L., HROUDOVÁ, J., BROZOVSKY, J., ZACH, J. and VALEK, J. Behaviour of Cement Composites with Lightweight and Heavyweight Aggregates at High Temperatures. *Periodica Polytechnica Civil Engineering.* 2017, **61**(2), 272-281.

[113] LIU, J.-C. and TAN, K. H. Fire Resistance of Strain Hardening Cementitious Composite with Hybrid PVA and Steel Fibres. *Construction and Building Materials.* 2017, **135**, 600-611.

[114] TANYILDIZI, H. Prediction of the Strength Properties of Carbon Fiber-Reinforced Lightweight Concrete Exposed to the High Temperature Using Artificial Neural Network and Support Vector Machine. *Advances in Civil Engineering,* 2018, **2018**, ID5140610, 10.

[115] JALASUTRAM, S., SAHOO, D. R. and MATSAGAR, V. Experimental Investigation of the Mechanical Properties of Basalt Fibre-reinforced Concrete. *Structural Concrete.* 2017, **36**(7), 519-552.

[116] REN, W., XU, J. and SU, H. Dynamic compressive behaviour of Basalt Fibre Reinforced Concrete after Exposure to Elevated Temperatures. *Fire and Materials.* 2016, **40**, 738-755.

[117] *ANALYSETTE 22 NanoTec - Laser Particle Sizer* [online]. Idar-Oberstein: Fritsch GmbH, 2018. [Accessed September 2018]. Available: https://www.fritsch-international.com/particle-sizing/static-light-scattering/details/product/laser-particle-sizer-analysette-22-nanotec-measuring-unit/downloads/

[118] ČSN EN 196-6 (722100). *Methods of Testing Cement – Part 6: Determination of Fineness.* Prague: Czech Standardization Agency, 2010.

[119] *Automatic Vicat Needle Device - Leaftleat L108.01E* [online]. Riedlingen: FORM+TEST Seidner & Co. GmbH, May 2006 [Accessed September 2018]. Available: https://www.formtest.de/de-wAssets/docs/Catalogue/L108.01E---Vicatnadelgeraet-B26600---NQ.pdf

[120] ČSN EN 196-3 (722100). *Methods of Testing Cement - Part 3: Determination of Setting Times and Soundness.* Prague: Czech Standardization Agency, 2017.

[121] ČSN EN 72 2400. *Methods of Test of Mortar for Masonry - Part 3: Determination of Consistence of Fresh Mortar (by Flow Table).* Prague: Czech Standardization Agency, 2000.

[122] ČSN EN 933-1 (721193). *Tests for Geometrical Properties of Aggregates – Part 1: Determination of Particle Size Distribution – Sieving Method.* Prague: Czech Standardization Agency, 2012.

[123] *X-ray Diffraction (XRD)* [online]. Royston, United Kingdom: Malvern Panalytical Ltd., 2018 [Accessed September 2018]. Available: https://www.malvernpanalytical.com/en/products/technology/x-ray-diffraction/

[124] *Brochure - LABSYS evo* [online]. Cranbury Township, New Jersy: SETARAM Instrumentation, September 2017 [Accessed September 2018]. Available: https://us.setaram.com/wp-content/uploads/2018/04/LABSYSevo-8PAGES_SEPT2017_BAT1.pdf.

[125] ROELS, S., CARMELIET, J., HENS, H., ADAN, O., BROCKEN, H., ČERNÝ, R., PAVLÍK, Z., HALL, C., KUMARAN, K., PEL, L. and PLAGGE, R. Interlaboratory Comparison of Hygric Properties of Porous Building Materials. *Journal of Thermal Envelope and Building Science.* 2004, **27**(4), 307-325.

[126] *Pybinatuc ATC – Brochure* [online]. Milan, Italy: Thermo Fisher Scientific Inc., 2007 [Accessed September 2018]. Available: https://www.pragolab.cz/documents/2_Pycnomatic%20Brochure.pdf

[127] WASHBURN, E. W. The Dynamics of Capillary Flow. *Physical Review.* 1921, **17**, 273-284.

[128] *Pascal Series – Brochure* [online]. Milan, Italy: Thermo Fisher Scientific Inc., 2007 [Accessed September 2018]. Available: https://assets.thermofisher.com/TFS-Assets/CMD/brochures/Pascal-Series-Mercury-Intrusion-Porosimeter-D01631.pdf

[129] ČSN EN 1015*. Methods of Test for Mortar for Masonry - Part 11: Determination of Flexural and Compressive Strength of Hardened Mortar.* Czech Standardization Institute, 2000.

[130] ČSN EN 12504-4. *Testing Concrete - Part 4: Determination of Ultrasonic Pulse Velocity.* Prague: Czech Standardization Agency, 2005.

[131] ČSN 73 1371*. Non-destructive Testing of Concrete – Method of Ultrasonic Pulse Testing of Concrete.* Prague: Czech Standardization Agency, 2011.

[132] VEJMELKOVÁ, E., PAVLÍKOVÁ, M., JERMAN, M. and ČERNÝ, R. Free Water Intake as Means of Material Characterization. *Journal of Building Physics.* 2009, **33**, 29-44.

[133] KUMARAN, M. K. Moisture Diffusivity of Building Materials from Water Absorption Measurements. *Journal of Thermal Envelope and Building Science*. 1999, **22**, 349-355.

[134] ČSN 72 7031*. Determination of water vapour diffusion coefficient of Building Materials by Method without Temperature Gradient.* Czech Standards Institution, 2001.

[135] *ISOMET 2114 – Catalogue* [online]. Bratislava, Slovakia: Applied Precision Ltd., 2018 [Accessed September 2018]. Available: https://www.appliedp.com/download/catalog/isomet_pc_en.pdf.

[136] TOMAN, J., TRNÍK, A. and KRIČKA, A. *Apparatus to Measure Linear Changes in Material at High Temperatures.* Utility model 21752, The Industrial Property Office (IPO CZ), 2011.

[137] TRNÍK, A., MEDVEĎ, I. and ČERNÝ, R. Measurement of linear Thermal Expansion Coefficient of Concrete at High Temperatures: A Comparison of Isothermal and Non-isothermal Method. *Cement Wapno Beton.* 2012, **79**, 363-372.

[138] *Dilatometry* [online], Řevnice: CLASIC CZ s.r.o., 2017 [Accessed September 2018]. Available:https://www.clasic.cz/index.php/cz/?option=com_sppagebuilder&view=page&id=21

[139] *Product Data Sheet: Secar 71* [online]. Chesapeake, Virginie: Kerneos Inc., 2006 [Accessed March 2017]. Available: www.kerneosinc.com/pdfs/new/Secar71.pdf.

[140] *Product Data Sheet: CEM I 52.5R* [online]. Čížkovice: Lafarge Cement, a.s., 2017 [Accessed March 2017]. Available: www.lafarge.cz/Technicky_list_CEM_I_52_5_R.pdf.

[141] CHOTARD, T. J., SMITH, A., BONCOEUR, M. P., FARGEOT, D. and GAULT, C. Characterisation of Early Stage Calcium Aluminate Cement Hydration by Combination of Non-destructive Techniques: Acoustic Emission and X-ray Tomography. *Journal of the European Ceramic Society.* 2003, **23**(13), 2211-2223.

[142] BENSTED, J., SMITH, J. R. High alumina cements – some important aspects. *Cement Wapno Beton.* 2015, **82**, 215-223.

[143] *Pricelist: Crushed Aggregates from Quarry Dobkovičky* [online]. Zbraslav: Kámen Zbraslav, a.s., 2017 [Accessed March 2017]. Available: http://kamenzbraslav.cz/files/kz-12-cenik-kamen-dobkovicky-03.pdf

[144] *Product Data Sheet: Technical Sands* [online]. Hrdoňovice: Sklopísek Střeleč, a.s., 2010 [Accessed March 2017]. Available: http://www.glassand.eu/pisky/techpisky.pdf.

[145] ČSN EN 206 (73 2403)*. Concrete – Specification, Performance, Production and Conformity.* Czech Standardization Agency, 2014.

[146] *Characterisation of Basalt Fibres* [online]. Šumperk: Basaltex, a.s, 2017. [Accessed March 2017] Available: http://www.basaltex.cz/cedic/cedic_charakteristika_cz.htm

[147] *Product Data Sheet: Sika ViscoCrete-1035 CZ* [online]. Brno: Sika CZ, s.r.o., 2018 [Accessed March 2017]. Available: https://cze.sika.com/dms/getdocument.get/.../Sika%20ViscoCrete-1035_CZ.pdf

[148] COLLIER, C. N. Transition and Decomposition Temperatures of Cement Phases - A Collection of Thermal Analysis Data. *Ceramics – Silikaty.* 2016, **60**(4), 338-343.

[149] SABEUR, H., PLATRET, G. and VINCENT, J. Composition and Microstructural Changes in an Aged Cement Pastes upon Two Heating–cooling Regimes, as Studied by Thermal Analysis and X-ray Diffraction. *Journal of Thermal Analysis and Calorimetry.* 2016, **126**(3), 1023-1043.

[150] ZHANG, Q. and YE, G. Dehydration Kinetics of Portland Cement Paste at High Temperature. *Journal of Thermal Analysis and Calorimetry.* 2012, **110**(1), 153-158.

[151] KESSLER, E., GADOW, R. and STRAUB, J. Basalt, Glass and Carbon Fibres and their Fibre Reinforced Polymer Composites under Thermal and Mechanical Load. *AIMS Materials Science.* 2016, **3**(4), 1561-1576.

[152] HAGER, I. Behaviour of Cement Concrete at High Temperature. *Bulletin of the Polish Academy of Sciences: Technical Sciences.* 2013, **61**(1), 145-154.

[153] SARAYA, M. E. S. I. Study Physico-Chemical Properties of Blended Cements Containing Fixed Amount of Silica Fume, Blast Furnace Slag, Basalt and Limestone, a Comparative Study. *Construction and Building Materials.* 2014, **72**, 104-112.

[154] SARASINI, F., TIRILLÓ, J. and SEGHINI, M. C. Influence of Thermal Conditioning on Tensile Behaviour of Single Basalt Fibres. *Composites Part B.* 2018, **132**, 77-86.

[155] MANYLOV, M. S., GUTNIKOV, S. I., POKHOLOK, K. V., LAZORYAK, B. I. and LIPATOV, Y. V. Crystallization Mechanism of Basalt Glass Fibres in Air. *Mendeleev Communications.* 2016, **23**(6), 361-363.

[156] CLAUSER C. and HUENGES, E. Thermal Conductivity of Rocks and Minerals. *Rock physics & phase relations.* 1995, **3**, 105-126.

List of figures

List of tables

List of abbreviations

a, b…	dimensions of sample	[cm]
A…	water absorption coefficient	[kg m^{-2} $s^{-1/2}$]
A_l…	loading area	[mm^2]
A_w…	area of water vapour transport	[mm^2]
c …	concentration of transported medium	[-]
C_1…	first radiation constant	[W m^{-2}]
C_2…	second radiation constant	[m K]
CAC…	calcium alumina cement	
CAH…	calcium aluminate hydrates	
c_L…	pulse velocity	[m s^{-1}]
c_p…	specific heat capacity at specific process	[J kg^{-1} K^{-1}]
CSH…	calcium silicate hydrates	
D…	water vapour diffusion coefficient	[m^2 s^{-1}]
d…	thickness of sample	[mm]
D_a…	w. v. diff. coef. of water vapour in the air	[m^2 s^{-1}]
E_b…	emissivity power	[W m^{-2}]
E_{dyn}…	dynamic modulus of elasticity	[Pa]
F…	ultimate force	[N]
F_{12}…	apparent shape factor	[-]
f_b…	bending strength	[MPa]
f_c…	compressive strength	[MPa]
i…	cumulative mass growth	[kg m^{-2}]
j_c…	mass flux	[kg m^{-2} s^{-1}]
j_q …	heat flow	[W m^{-2}]
j_{qr} …	heat flow caused by radiation	[W m^{-2}]
j_{qt} …	total heat flow	[W m^{-2}]
k…	ambient dimensionality coefficient	[-]
k_c…	diffusion-thermo coefficient (Dufour coef.)	[kg m^{-1} s^{-1}]
k_p…	diffusion-baro coefficient	[s]
l…	span length	[m]
l_0 …	initial length	[mm]
l_i …	length at particular temperature	[mm]
M…	molar mass of water	[kg mol^{-1}]
m…	mass	[kg]

m_a …	Archimedes mass	[kg]
m_d…	dry mass	[kg]
M_{max}…	maximal moment	[N m]
m_{RH}…	mass at specific relative humidity	[kg]
m_s …	saturated mass	[kg]
n …	number of results	
p …	pressure	[Pa]
P …	work	[J]
PC…	Portland cement	
Q …	heat	[J]
R…	universal gas constant	[J mol^{-1} K^{-1}]
S…	entropy	[J kg^{-1}]
t …	time	[s]
T…	temperature	[K]
U …	internal energy	[kg m-^{2}]
V …	volume	[m^3]
w…	mass moisture content	[-]
W…	section modulus	[cm^3]
w_{cap}…	capillary saturated moisture content	[kg m^{-3}]
$\overline{X}$…	mean / average value	
x_i …	particular result	
XRD…	X-ray diffraction	
XRF…	X-ray fluorescence spectrometry	
α…	linear thermal expansion coefficient	[K^{-1}]
δ…	water vapour diffusion permeability	[s]
Δm…	mass of transported water vapour	[kg]
$\Delta p_{p...}$	water vapour pressures gradient	[Pa]
δs…	thermodiffusion coefficient (Soret coef.)	[m^2 s^{-1} K^{-1}]
ε…	spectral emissivity at particular temperature	[-]
ε_t …	thermal strain	[-]
κ…	apparent moisture diffusivity	[m s^{-2}]
$\lambda(T)$ …	thermal conductivity	[W m^{-1} K^{-1}]
λ^*…	generalized thermal conductivity	[kg K^{-1} m^{-1} s^{-1}]
Λ…	wavelength	[m]
μ…	water vapour diffusion resistance factor	[-]

μ…	chemical potential	[J kg^{-1}]
ρ…	bulk density	[kg m^{-3}]
ρ_c …	bulk density of transported medium	[kg m^{-3}]
ρ_{H2O} …	density of water	[kg m^{-3}]
ρ_{mat} …	matrix density	[kg m^{-3}]
σ…	standard deviation	
σ_0…	Stefan-Boltzman constant	[W m^{-2} K^{-4}]
φ…	barodiffusion coefficient	[m^3 s kg^{-1}]
Ψ_0 …	open porosity	[-]